Energy Research and Development Division

FINAL PROJECT REPORT

Understanding and Reducing Barriers to Wind Energy Expansion in California

An Investigation of How Wind Resources Vary by Year and Are Impacted by Climate Change

California Energy Commission

Edmund G. Brown Jr., Governor

December 2018 | CEC-500-2018-035

PREPARED BY:

Primary Author(s):

Dev Millstein[1]
Paul Ullrich[2]
Meina Wang[2]
Craig Collier[3]
Joshua Solomon-Culp[1]

1 Lawrence Berkeley National Laboratory
Energy Technologies Area
One Cyclotron Road, Berkeley, CA 94720
Berkeley, CA 94720
Phone: (510)-486-4556 | Fax: (510)-486-5928
http://www.lbl.gov

2 University of California, Davis
Department of Land, Air and Water Resources
One Shields Ave.
Davis, CA 95616
http://www.caes.ucdavis.edu/

3 DNV GL
9665 Chesapeake Drive, Suite 435
San Diego, CA 92123

Contract Number: EPC-15-068

PREPARED FOR:

California Energy Commission

David Stoms
Project Manager

Aleecia Gutierrez
Office Manager
ENERGY GENERATION RESEARCH OFFICE

Laurie ten Hope
Deputy Director
ENERGY RESEARCH AND DEVELOPMENT DIVISION

Drew Bohan
Executive Director

ACKNOWLEDGEMENTS

The authors thank Chris Hayes and Daran Rife of DNV GL for helpful discussions. From Lawrence Berkeley National Laboratory, the authors thank Aditya Murthi for helping develop the study design of this research and Samir Touzani for helpful discussion about the methodological approach. This research used resources of the National Energy Research Scientific Computing Center (NERSC), a DOE Office of Science User Facility supported by the Office of Science of the U.S. Department of Energy under Contract No. DE-AC02-05CH11231. This project is further supported by the National Institute of Food and Agriculture, U.S. Department of Agriculture, Hatch Project under California Agricultural Experiment Station project CA-D-LAW-2203-H. Author Ullrich is supported by Department of Energy Office of Science Award Number DE-SC0016605, "An Integrated Evaluation of the Simulated Hydroclimate System of the Continental U.S."

PREFACE

The California Energy Commission's Energy Research and Development Division supports energy research and development programs to spur innovation in energy efficiency, renewable energy and advanced clean generation, energy-related environmental protection, energy transmission, and distribution and transportation.

In 2012, the California Public Utilities Commission established the Electric Program Investment Charge (EPIC) to fund public investments in research to create and advance new energy solution, foster regional innovation, and bring ideas from the lab to the marketplace. The California Energy Commission and the state's three largest investor-owned utilities – Pacific Gas and Electric Company, San Diego Gas & Electric Company, and Southern California Edison Company – were selected to administer the EPIC funds and advance novel technologies, tools, and strategies that provide benefits to their electric ratepayers.

The Energy Commission is committed to ensuring public participation in its research and development programs that promote greater reliability, lower costs, and increase safety for the California electric ratepayer and include:

- Providing societal benefits.
- Reducing greenhouse gas emission in the electricity sector at the lowest possible cost.
- Supporting California's loading order to meet energy needs first with energy efficiency and demand response, next with renewable energy (distributed generation and utility scale), and finally with clean conventional electricity supply.
- Supporting low-emission vehicles and transportation.
- Providing economic development.
- Using ratepayer funds efficiently.

Understanding and Reducing Barriers to Wind Energy Expansion in California is the final report for the Understanding and Mitigating Barriers to Wind Energy Expansion in California project (Grant Number EPC-15-068) conducted by Lawrence Berkeley National Laboratory. The information from this project contributes to the Energy Research and Development Division's EPIC Program.

For more information about the Energy Research and Development Division, please visit the Energy Commission's website at www.energy.ca.gov/research/ or contact the Energy Commission at 916-327-1551.

ABSTRACT

Accurately characterizing site-level wind energy variability is essential during wind project development. Understanding the features and probability of low-wind years is of interest to developers and financers. Numerous and varied wind observations makes these characterizations challenging, thus techniques to improve these characterizations are valuable. To improve resource characterization, this research links site-level, hub-height, wind resource variability to regional wind variability of meteorological patterns (for either the central or southern California region) to a-scale greater than 600 miles. The approach involves statistical clustering of high-resolution modeled wind data for California from 1980 to 2015. Application of these methods reveal unique meteorological patterns driving low and high wind years at five wind project sites. Correlations between climate modes (recurring large-scale climate patterns such as El Niño/La Niña) and the frequency of different regional wind patterns, a linkage valuable for wind resource characterization and forecasting, are identified. This approach can be applied across locations and may benefit many aspects of wind energy resource evaluation and forecasting. Researchers also focused on climate change impacts on California wind resources. First, the research team examined the 36-year historical high-resolution modeling for temporal trends, illuminating already-occurring wind regime changes that are consistent with global warming: anomalously hot summer days increased at half a day per year, and stagnant conditions increased at one-third of a day per year. Second, the Variable-Resolution Community Earth System Model was used to investigate climate change impacts on wind resources between a 1980-2000 period and a midcentury 2030-2050 period. These projections suggest that wind power generation capacity throughout California is expected to increase during the summer and decrease during fall and winter, based on significant changes at several wind farm sites. Large-scale seasonal patterns from these model simulations were investigated to understand the synoptic-scale impact on localized wind speed change.

Keywords: Wind energy, resource assessment, hub-height winds, climate change, climate modes, statistical clustering, variable-resolution climate modeling

Please use the following citation for this report:

Millstein, Dev, Paul Ullrich, Meina Wang, Craig Collier, and Joshua Solomon-Culp. Lawrence Berkeley National Laboratory, University of California, Davis, and DNV GL. 2018. *Understanding and Reducing Barriers to Wind Energy Expansion in California*. California Energy Commission. Publication Number: CEC-500-2018-035.

TABLE OF CONTENTS

Page

LIST OF FIGURES

Page

LIST OF TABLES

EXECUTIVE SUMMARY

Introduction

Wind power is an affordable and sustainable electricity generation source that helps reduce electric sector emissions of greenhouse gases and criteria air pollutants. To help realize these goals, this project aims to reduce barriers to wind energy expansion, namely by improving the description, or characterization, of how much the wind resource varies across time. "Wind resource" in this case is defined as the amount of wind energy that could be generated over a specific period. For example, a project might generate 20 percent more energy in one year compared to the previous year, and if this difference were due solely to differences in wind speeds, rather than maintenance or other operational issues, this difference would represent the change in wind resource.

The variability in wind resource is directly linked to project revenue streams and, thus, to project viability. However, it is challenging to predict the average level of the wind resource and the annual and seasonal variability of that resource at a particular project site. This challenge is partly due to a lack of long-term measurements of winds (particularly of measurements at heights above ground that are relevant for wind energy planning). The uncertainty regarding available wind resources translates into revenue risk, which translates into higher costs.

However, the challenges created by wind resource variability affect more than just estimates of long-term project revenue. Operational decisions for the electricity system must be made based on the predicted wind resource available across multiple locations over the course of the next several minutes, hours, and days. Errors in the forecasts and characterization of available wind resources on these time scales can increase the system-wide costs of providing electricity. Thus, the ability to understand and forecast wind resources at multiple time scales can not only help reduce project development costs, but also help smooth the integration of wind generation into the power grid.

Yet, there is still another reason to pursue research into wind resource variability: climate change may alter the wind patterns. Climate change could potentially increase or decrease the wind resources available at sites across California, and could do so over the next decades, which is within the expected lifetimes of new wind energy facilities. Moreover, improved turbine and tower technology may allow wind project developers to explore new locations and design projects for even longer lifetimes, potentially exposing new projects to additional resource variability, associated with climate change, that has been previously ignored or unexplored.

This project, therefore, aims to provide new insight into what meteorological phenomena are associated with periods of strong and weak wind resources, as well as how California wind resources might change over time.

Project Purpose

This project served two purposes, looking retrospectively at the recent past and prospectively at the near future. The first was to develop new methods to characterize variation in wind resources and use those methods to characterize historical wind resource variation at five major wind development sites in California, providing a new, publicly available record of resource variability at these locations. The research also determined the influence of climate modes (that is, recurring large-scale climate patterns such as El Niño/La Niña) on wind resources at five sites: Central California, which includes the Shiloh and Altamont Pass sites, and Southern California, which includes the Alta, San Gorgonio, and Ocotillo sites, and whether climate change is already influencing California wind resources.

With these new methods and data, scientists and wind project developers can refine the processes of site-level resource assessment and reduce risk and cost of wind development. Furthermore, the new methods could seed further research, leading to improved short-term wind resource forecasting.

The second purpose was to produce a new, state-of-the-art, high-resolution simulation of future wind resources across California, specifically at the five major wind development sites. New climate simulations, such as those described in this report, are necessary because typical climate models do not adequately account for the complexity of California's terrain, and other efforts to produce higher-resolution forecasts of wind power resources across California are not publicly available and are limited by expensive computational demands. The analyses were designed to provide new results about the sensitivity of California wind resources to climate change, and produce an understanding of larger-scale climate changes (that is, synoptic scale, which means greater than 1,000 kilometers, or 600 miles) in the climate system that drive local changes to wind resources. When combined with other independent wind resource simulations, these results will build confidence in the forecasts of future wind speeds and reduce risks to project development, thus reducing costs to ratepayers.

Project Approach

The Research Team

The project team was led by a research scientist at Lawrence Berkeley National Laboratory. The University of California Davis and Lawrence Berkeley National Laboratory led the climate modeling, and an industry partner, DNV GL, was the private source of "Virtual met" data and enhanced public and industry outreach. Dr. Ryan Wiser (Lawrence Berkeley National Laboratory) was a strategic advisor on the project.

Process to Analyze Historical Variability in California Wind Resources

The research team analyzed the historical variability in California wind resources during 1980 – 2015. This analysis was based on the Virtual met product, a proprietary meteorological model, which provided hourly hub-height wind fields, resolved to a 4-km resolution, for California. The Virtual met product was carefully evaluated against independent observations and compared to multiple reanalysis products, which are historical meteorological simulations based on a large set of archived observations. Reanalysis data are coarse (~50 kilometer grid cells) but have complete geographic coverage across many decades.

To develop new insight into historical variability patterns, the research team grouped and categorized days with similar wind regimes in the Virtual met product. This daily categorization allows for the identification of wind resources patterns that could not be seen by analyzing seasonal and annual trends.

For this analysis, California was split into two domains – one focused on Central California containing the northern, coastal wind resource areas (Shiloh and Altamont Pass) and one focused on Southern California with the major desert wind resource areas (Alta, San Gorgonio, and Ocotillo). The research team defined 10 typical daily wind regimes (a regional pattern of wind speeds and directions during a day) for each domain. The team analyzed synoptic-scale conditions as a function of each of the wind regimes. Moreover, at each of the five sites, the team analyzed the wind resource found under each of the wind regimes. The researchers used differences in wind resource under each wind regime to characterize what types of weather patterns drive wind energy generation at each site. Differences in the wind regime frequency (types of weather) and intensity (the speed of the winds given a specific wind regime), and in total wind resource (the electricity one could generate given the wind speeds at specific wind plant sites), were used to identify meteorological patterns associated with high and low wind resource years at each site. Finally, the team correlated the frequency of wind regimes with climate mode and analyzed it over time for signs of climate change.

Process to Analyze Climate Change and California Wind Resources

In this project, the research team used a state-of-the-art global climate model (Variable Resolution Community Earth System Model) to simulate midcentury changes to future wind resources in California. This model allows for a high-resolution representation of California (about 14 km) with a seamless connection to a coarser representation of the rest of the globe. This research is the first time such a model was used explicitly to examine the effects of climate change on California wind resources. The team carefully validated the historical output from this model against available observations, as well as reanalysis products and the Virtual met product.

Future changes to wind resources were analyzed at all five sites by comparing the simulation of 1980 – 2000 to the simulation of 2030 – 2050. The research team analyzed changes to resource variability across multiple time scales. Furthermore, the team identified synoptic-scale and localized drivers behind seasonal wind energy change.

Technical Advisory Committee

The research team formed a technical advisory committee to give advice and constructive criticism on the research approach and on making the study as useful as possible to energy investors, wind developers, and energy planners and regulators. The committee was composed of representatives from an energy investment firm, climate scientists, and the three state energy agencies—California Public Utility Commission, California Independent System Operator, and the California Energy Commission. The guidance from the committee led to changes in the set of wind energy sites studied as well as adding an analysis of how the supply would match demand throughout the day to show how consistent the wind resource is and will be in the future.

Project Results

Historical Variability in California Wind Resources

The researchers identified the types of meteorological patterns that drove wind energy production at each focus site. The wind resource was different under each wind regime and at each of the five wind sites. For example, only a few wind regimes generated most of the energy at some of the sites, while a diverse set of weather patterns was needed to produce annual energy generation at other sites. Identifying cluster types (wind regimes) permits an intuitive link between observable weather phenomena and site-level production patterns of wind energy.

Each of these wind regimes was associated with a distinct meteorological pattern at the synoptic scale. In addition, each wind regime was associated with distinct daily patterns at each of the five sites. Thus, the clustering method allowed direct links to be made from the synoptic-scale meteorological patterns to regional wind patterns to site-level daily wind cycles.

The research team used the clustering framework to compare the top (windiest) years to the bottom (calmest) years. At all sites, dramatic differences in total potential energy generation (and thus project level revenue) was found between the top and bottom year (with the least difference being found at Alta, where the best year was about 20 percent greater than the worst year, while the best year at Ocotillo, the site with the largest difference, was almost 50 percent greater than the worst year). At each site, unique changes to the frequency or the wind speed intensity or both of certain wind regimes were identified. This allowed the linkage of low and high wind years to patterns in regional and synoptic-scale meteorological patterns. This is the first step in developing a chain of causality describing why certain years provide low wind resources (that is, if one knows what synoptic-scale patterns occur more frequently in low wind years, one could investigate what causes those synoptic-scale patterns to occur). Thus, this is also the first step in developing the ability to forecast the likelihood of an upcoming strong or weak wind resource year for a particular site.

Finally, the research team analyzed the effect of climate mode on wind energy generation at each site. While climate mode indices were not correlated directly with total monthly wind generation, they were correlated with the frequency of certain wind regimes and, therefore, were correlated with the submonthly patterns of wind generation. Thus, predicting near-term wind resources could benefit from including the effects of climate mode on wind regimes. On longer time scales, accounting for changes to wind patterns associated with climate mode could benefit research on the effects of climate change, as climate change could potentially affect wind resources through multiple pathways, including through changing the frequency and intensity of climate modes.

Climate Change and California Wind Resources

Based on the historical record, California may already be seeing impacts of climate change on wind resources. Specifically, the number of days with hot summer conditions and non-summer dead (calm) days in Central California increased at a rate of roughly one-half and one-fourth day per year, respectively, from 1980–2015. The changes to the frequency of these regimes did not produce a detectable impact in the time series of total seasonal or annual generation. However, if the patterns of change continue, total electricity generation potential will likely be affected.

Looking forward with the variable resolution model, the research team found significant seasonal changes in the available wind resource at most sites, with an increase in summer and a decrease in fall and winter at all five sites, if greenhouse gas emissions continue at current rates. Synoptic-scale and localized drivers (such as changes to the surface pressure gradient between the Central Valley and the Mojave Desert) behind seasonal wind energy change were also identified, and suggested climate change may tend toward synoptic patterns that lead to higher wind speed during summer and lower wind speed during fall and winter.

This finding was particularly interesting in that all five sites indicated change in the same direction during certain seasons. This finding, combined with the explicit analysis of synoptic-scale patterns, suggested that the model simulations indicate climate change may alter the statewide patterns of ventilation (usually onshore flow) and impact wind generation across the state. A limitation here is that this simulation may not agree with forecasts produced by other models, although some initial comparisons to past work were included. By identifying the specific changes to future synoptic conditions, this work provides a useful starting point for comparisons across models that can provide more useful information than simply comparing the average changes to modeled future wind resources at individual locations.

Overall, this study improves the characterization of uncertainty around the magnitude and variability in space and time of California's wind resources in the near future, and enhances the understanding of the mechanisms related to the trends in wind resource variability. Most importantly, the simulation forecasts non-negligible changes to future wind resources, and thus highlights the need for future research on this topic, including comparison with other climate models. Some specific research directions include:

- Refining the method of correlating short-run site-level wind measurements to a nearby, longer-run record of wind speeds, as is often performed during the site evaluation stage of project development.
- Improving wind power forecasts of site-level resources from easily observed and predicted synoptic-scale meteorological patterns and climate modes.
- Testing whether the techniques in this study can help identify conditions that give rise to extreme wind events. This could also have applications in research related to air quality or wildfire forecasting.
- Improving projections of wind resources under climate change.

Project Outreach

The team presented this work at numerous conferences including the American Geophysical Union Fall Meeting, December 2017 and the annual Community Earth System Model meeting in 2017. Several journal articles have been published based on this study: Renewable Energy Journal (2018) https://www.sciencedirect.com/science/article/pii/S0960148118304397, Data in Brief (2018) https://www.sciencedirect.com/science/article/pii/S2352340918305341 and Climate Dynamics (2018) https://link.springer.com/article/10.1007%2Fs00382-018-4421-y.

Benefits to California

This project offers specific benefits to California, as well as more general advances in scientific methodology. The ability to readily, and intuitively, link site-level wind patterns to larger-scale wind and meteorological fields could be useful in many applications.

- This report provides a new and publicly available assessment of the historical wind resource variability at five important wind power development sites in California.
- This report provides new predictions of future changes to wind resource at the same five sites and assesses changes to larger-scale synoptic conditions, all based on a state-of-the-art, high-resolution climate model. Furthermore, the changes predicted here can provide necessary context for additional research on climate change impacts on wind resources.
- These clustering methods have great potential to help improve and contribute to the development of new applications that could be used to understand and forecast wind variability across a variety of temporal scales. For instance, this study could improve electricity supply forecasting for grid management or inform long-term energy planning by refining wind projections.
- This project developed new methods for assessing wind variability and for classifying wind patterns across California. These methods can be applied in all wind project locations. By reducing the uncertainty in wind energy projections, this approach can reduce risk to investors and lead to greater investment in this low-carbon energy source.
- The methods developed in this project may seed further research.

Overall, this work advances the scientific understanding of wind resource variability over many time scales. As the understanding of these topics is improved, the precision with which wind resources can be forecast will improve, which will lower the risk, and associated costs, of developing wind power. This cost reduction will benefit electricity consumers and developers and enable wind power to serve a greater portion of power generation needs within the state and elsewhere. Moreover, all of California will benefit from reduced emissions of local pollutants and greenhouse gases associated with this clean energy resource.

CHAPTER 1: Introduction

1.1 Background and Overview

The Fourth California Climate Change Assessment indicates that, in California, temperatures will rise significantly during this century, wildfire risks will increase, extremely hot days will likely become more prevalent, and other changes will likely occur that, together, will stress California's water and electricity systems and natural ecosystems, as well as potentially have major impacts on public health (Bedsworth et al. 2018). However, that report also indicates "warming will be significantly greater with higher emissions than with lower emissions." To help minimize emissions from the electricity sector, California, through Senate Bill 100 (De León, Chapter 312, Statutes of 2018), requires utilities to procure 60 percent of their electricity from renewable sources by December 31, 2030 and 100 percent from eligible renewable energy resources and zero-carbon resources by December 31, 2045.

Over the past decade or so, dramatic cost reductions have been seen in both solar and wind power generation (Barbose et al. 2017, Bolinger et al. 2017, Wiser et al. 2017). Recent U.S. wind power generation prices, in particular, compare very favorably to forecast prices of gas-fired generation (Wiser et al. 2017). Furthermore, wind and solar power generation are already contributing to air quality and climate goals nationally and within the state and have, for example, reduced air pollution-related mortalities by 3,000 to 12,700 across the United States during the nine-year period 2007 through 2015 (Millstein et al. 2017), where the wide range is based on varying epidemiological studies and varying estimates of pollutant transport.

Thus, wind energy is an affordable electricity generation technology that can help reduce electric sector emissions of greenhouse gases and criteria air pollutants. (Criteria air pollutants, such as sulfur dioxide, nitrogen oxides, and fine particulate matter, are linked to local and regional public health damages.) Although not the focus of this report, other renewable generation or energy efficiency strategies can also provide similar benefits.

To help support the above goals, this project aims to reduce barriers to wind energy expansion. Though the wind energy sector has rapidly expanded during recent years domestically and globally, many challenges remain that delay or prevent development in many situations. The U.S. Department of Energy's *Wind Vision* (DOE 2015) describes challenges and potential mitigating actions. Some of the most prominent challenges described within that document include reducing wind costs through improving technology, wind resource characterization, supply chain, and related logistics. While there are many potential avenues to reduce barriers to wind energy expansion, this project focuses on developing new techniques to assess wind energy resources across regions and at particular sites. This focus also fits well within the national *Wind Vision*, as improving wind resource characterization is listed as Action 1.1 in the roadmap of suggested actions within that document. The research has both a prospective and retrospective focus, aiming to help develop techniques to evaluate resource variability based on the historical record, as well as to assess the potential change to resources due to future climate change.

Estimating lifetime, site-level power generation for a project is a key input into many aspects of the decision-making process of a project. Accurate, site-level quantification of resource variability, especially characterization of low wind years, is essential information for project developers and financers (Tindal 2011, Bailey et al. 2015, Bolinger 2017). However, site-level resource assessment is challenging due to a lack of local long-term hub-height wind measurements, and many approaches attempt to overcome this limitation. For example, Carta et al. (2013) describes “measure-correlate-predict” approaches, which use short-run, site-level measurements combined with long-run reanalysis data, or nearest available long-run observations, to estimate long-run resource variability at a particular site. Also, during operations, understanding and forecasting short-term variability at the project level can help reduce grid-level challenges that arise with high levels of wind penetration (Albadi et al. 2010, Xie et al. 2011, Archer et al. 2017). Thus, improving the general understanding of wind resource variability can help support many aspects of wind power development and operations.

Looking forward improved turbine and tower technology may allow wind project developers to explore new locations and design projects for longer lifetimes, potentially exposing new projects to resource variability, associated with climate change, that has been previously ignored or unexplored. Like many other renewable energy technologies, wind energy is influenced by climate change through changes in global energy balance and the resulting atmospheric circulation (Hubbert 1971). Research efforts have examined climate impacts on wind resources at various regions around the globe (Pryor et al. 2011, Pryor et al. 2013, Goddard et al. 2015, Gross et al. 2016, Haupt et al. 2016, Ma et al. 2016, Karnauskas et al. 2017, McElroy et al. 2017). The few studies that have examined the impact of climate change on wind resources over California using global or regional climate models or both (Rasmussen et al. 2011, Duffy et al. 2014) have been inconclusive. These studies have shown sensitivity to model setup, including choice of physics scheme, downscaling method, and number of models used (Segal et al. 2001, Archer et al. 2003, Pryor et al. 2005, Sailor et al. 2008, Yu et al. 2015). Furthermore, the spatial variability of wind energy resources and related sensitivity to model settings emphasizes the benefit of higher-resolution models and the use of multiple models (Rasmussen et al. 2011).

1.2 Project Objectives

The goals in this research are to help reduce, over a 10- to 30-year horizon, wind energy development risks resulting from uncertainty in wind regimes by improving characterization of wind resource magnitude, variability, and operating conditions and to help convey this risk to stakeholders to help optimal planning and growth for the wind industry.

The objectives of this research are to define what drives annual variability in wind resources in California. Specifically, the aim of this project is to focus on major wind sites in California and to describe and characterize the historical variability in wind resources at these sites. This project will determine what specific meteorological patterns are seen during “good years” and during “bad years” and investigate the larger-scale patterns associated with the variability in annual wind resources. Of particular note, this report will assess how wind resources have varied with changes to the intensity in climate modes (such as El Niño/La Niña).

Looking forward, the report will investigate how climate change may affect wind energy resources out to midcentury. The report will investigate links to climate change impacts in the historical wind power record as well as use a variable-resolution global climate model to explore high-resolution predictions of wind resources in California

1.3 Report Organization

The investigation depends on the use of two main tools: The first is a retrospective high-resolution modeling product, “Virtual met,” produced by DNV GL. This product covers California at 4 km resolution from 1980 – 2015. The second is variable resolution global climate model, the Variable-Resolution Community Earth System Model (VR-CESM). VR-CESM was used to simulate two periods, 1980 – 2000 and 2030 – 2050. The research team set the VR-CESM to have a highly resolved regional representation of California (14 km) with a coarse representation of the rest of the globe. The team used the VR-CESM model to produce the forward-looking analysis of the sensitivity of wind resources to climate change.

The investigation of historical variability in wind resources is based on a statistical technique that can provide a deeper and intuitive understanding of the variability in wind resources. This approach is to group together days with similar meteorological, or other properties, using statistical clustering and related techniques. This approach can help link variation in wind seen at individual sites to meteorological patterns at larger geographic and multiple temporal scales, providing insight into the mechanisms for, and potentially predictability of, such variation. This approach is described within the Methods Section 2.1.4, and historical variability results are described in Chapter 3.

This investigation focuses specifically on five major California wind power sites – Shiloh, Altamont Pass, San Gorgonio, Alta, and Ocotillo. These sites were selected to show a variety of major wind power locations in the state, including locations with growth potential or upcoming repowering requirements.

The remaining sections are organized as follows: Within the Methods section, the models, observational and reanalysis data sets, and the statistical clustering technique are detailed. Moreover, a detailed model validation section is included within the Methods section. Chapter 3 describes results of the retrospective analysis of historical wind variability (3.1) and climate mode impacts on wind resource variability (3.2). Chapter 4 presents the prospective analysis of climate change impacts on wind resources. The analysis of climate change impacts includes a discussion of impacts that have already been observed, as well as a section on the modeled future impacts. The content of this report has also been published in the peer-reviewed literature, please see Millstein et. al. (2018) and Wang et al. (2018a).

CHAPTER 2:
Methods and Model Validation

2.1 Methods Overview

2.1.1 Selection of Five Sites of Interest

Within this study, California was divided into two primary subdomains: Central California (C) subdomain, which includes the Shiloh and Altamont Pass sites, and Southern California (S) subdomain, which includes the Alta, San Gorgonio, and Ocotillo sites. These five wind resource areas constitute a selection of wind farm sites currently at service and wind project sites slated for new or expanded development or repowering. Furthermore, these five wind represent the five largest wind resource areas of the state. (For additional description of California wind resource areas, see http://www.energy.ca.gov/maps/renewable/wind.html.) Figure 1 depicts this region, along with the five wind farms.

Figure 1: California Subdomains and Project Sites of Focus

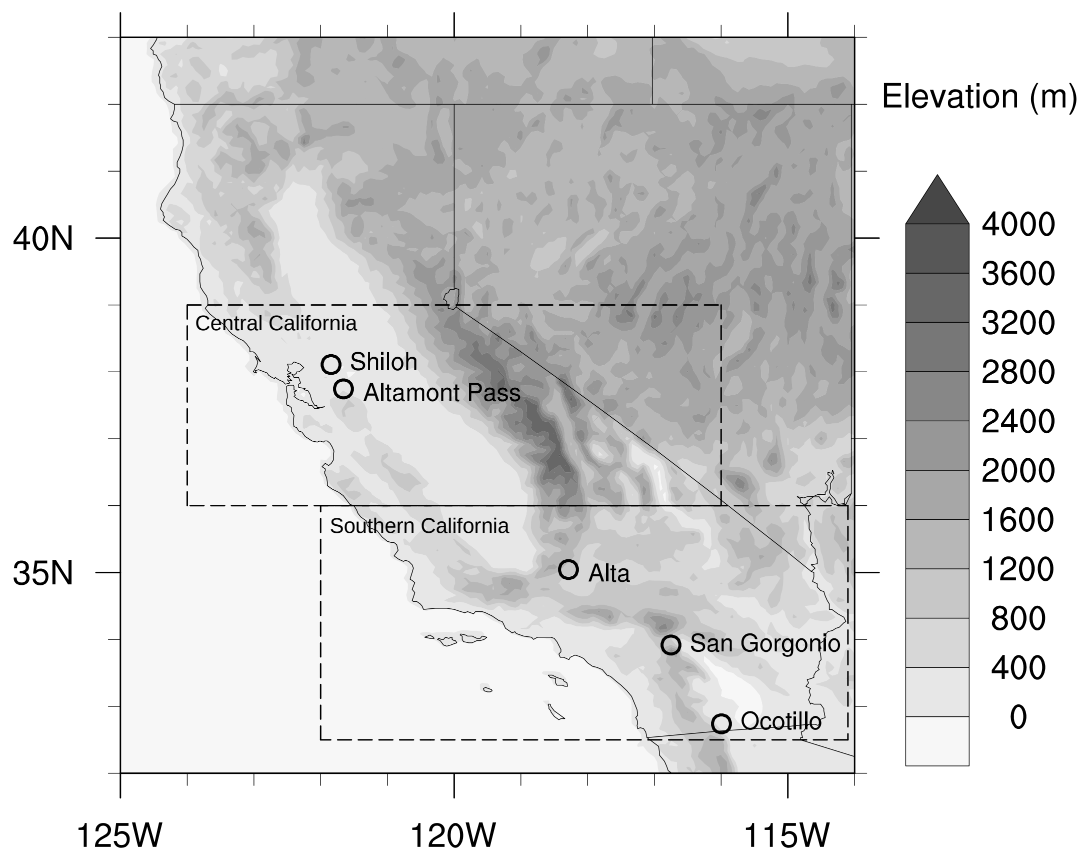

Source: Lawrence Berkeley National Laboratory

2.1.2 Fine-Scale Modeling of Wind Speeds and Wind Power

2.1.2.1 Virtual Meteorology Product from DNV GL (Virtual met)

DNV GL, or full name Det Norske Veritas Germanischer Lloyd, is a large energy consultancy firm that supports wind power development throughout the world. For this research, DNV GL provided its Virtual met product covering 1980 – 2015 focused on California. The Virtual met product is a dynamically downscaled regional model product based on Modern-Era Retrospective analysis for Research and Applications, Version 2 (MERRA-2) input data and is designed specifically to provide wind farm developers with accurate characterizations of wind power resources at existing and prospective project sites.

The downscaling is accomplished in two steps: First, the Weather Research and Forecasting (WRF) model is used to dynamically downscale MERRA to 20 km resolution across California; second, an analog-based ensemble downscaling method is used to refine the resolution to 4 km. To provide training data for the statistical model, a nested version of the same model is run at high resolution. The period over which the coarse and high-resolution runs overlap is called the *training period*, while the remaining portion is termed the *downscaling period*. To downscale the predictor data outside the training period, the best matching coarse estimates (termed "analogs") over the training period are found. The downscaled solution is then constructed from the set of high-resolution values that correspond to the best matching coarse analogs. This method is broadly based on work led by Delle Monache (Delle Monache et al. 2011, Delle Monache et al. 2013). The Virtual Met product provides wind speeds and directions at multiple heights, including 10 m and 100 m. In this work, the 100 m height was used to represent hub height and the 10 m height to represent surface winds. Separately, the 80 m height was used for general validation and comparisons to the VR-CESM, as well as other reanalysis products.

2.1.2.2 Variable Resolution Community Earth System Model (VR-CESM)

CESM Version 1.5.5, a fully coupled atmospheric, land, ocean, and sea ice model, was used for this study. All simulations used the F-component set (FAMPIC5), which prescribes sea surface temperatures and sea ice but dynamically evolves the atmosphere and land surface component models. The atmospheric component mode is the Community Atmosphere Model, Version 5.3 (CAM5) (Neale et al. 2010) with the spectral-element dynamical core (Dennis et al. 2012) in the variable-resolution (VR) configuration (Zarzycki et al. 2014). The VR model grid used for this study, depicted in Figure 2, was generated for use in CAM5 and the Community Land Model (CLM) with the open-source software package SQuadGen (Guba et al. 2014, Ullrich 2014). On this grid, the finest horizontal resolution is 0.125° (~14km), with a quasi-uniform 1° mesh over the remainder of the globe. Two simulations were conducted using this grid structure: First, the historical run covers the period from October 1, 1979, to December 31, 2000, with the first three months discarded as the spin-up period, for a total of 21 years outputted every three hours. This historical period was chosen to provide an adequate sampling of the interannual variability and to coincide with the period from the rest of the modeling and reanalysis datasets. For projections of future wind energy change, the midcentury simulation ran with the "business-as-usual" Representative Concentration Pathway 8.5 (RCP8.5) (Taylor et al. 2012) from October 1, 2029, to December 31, 2050, again discarding the first three months for a total of

21 years. The research team chose the future period to emphasize the midcentury focus of this study and avoid divergence in the predicted impacts among different RCPs. Greenhouse gas (GHG) and aerosol radiative forcings are prescribed based on historical or RCP8.5 concentrations for each simulation. More details on VR-CESM can be found in (Rhoades et al. 2016).

Previous studies (Huang et al. 2016a, Rhoades et al. 2016) using VR-CESM have demonstrated the competitiveness of the model in studying high-resolution regional climatology when compared to other regional climate models, especially when nonlocal processes have significant influence on the local climatology. VR-CESM has demonstrated a better representation of climatology within regions of complex topography, due to the relatively fine regional resolution compared with conventional GCM simulations (Zarzycki et al. 2015, Huang et al. 2016b, Rhoades et al. 2018).

Figure 2: The VR-CESM Grid

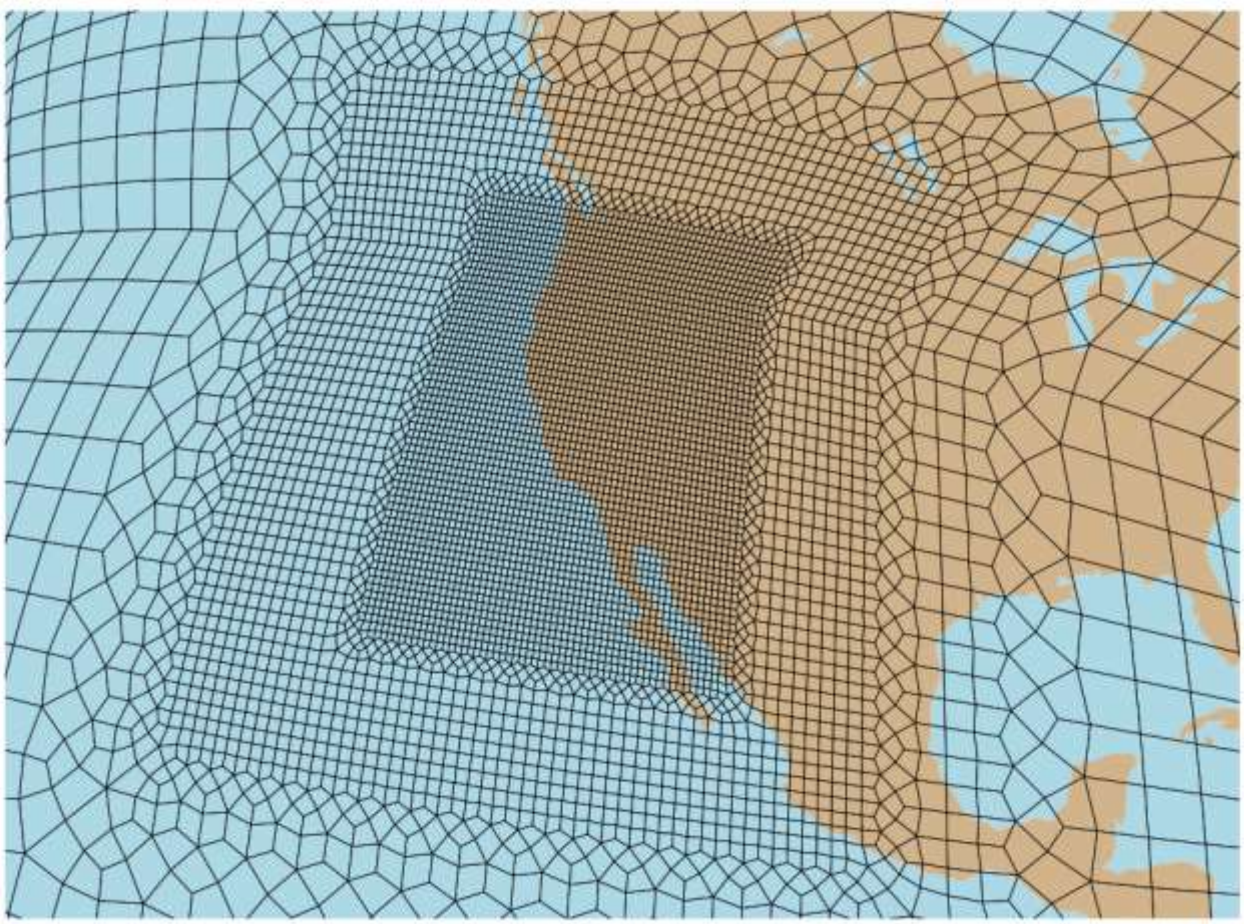

Constructed by Successively Refining a Cubed-Sphere Grid with a 1° (111km) Quasi-Uniform Resolution to a Resolution of 0.125° (~14km) Over the Western USA

Source: Lawrence Berkeley National Laboratory

2.1.2.3 Representation of Topography

Figure 3: Topographical Representation of California and Surrounding Regions

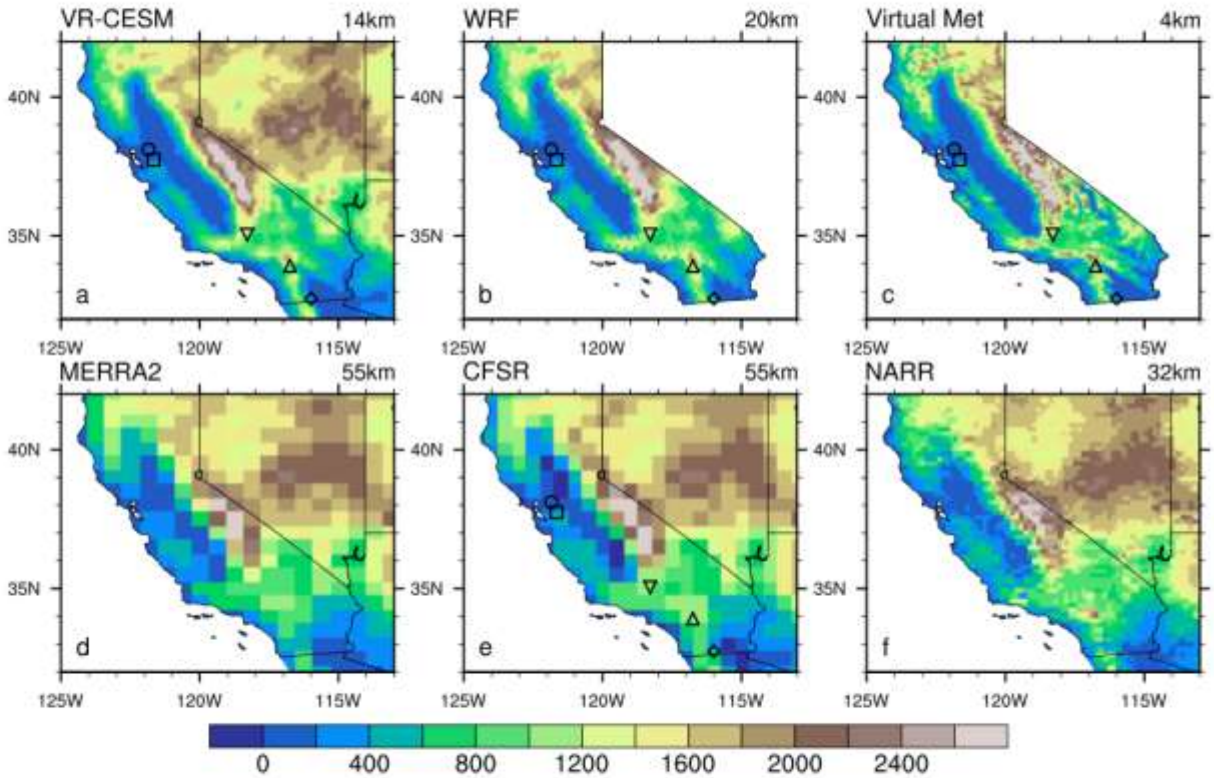

From model (top row) and reanalysis (bottom row) datasets. Note: The "WRF" data present in the top row represent the coarse DNV GL product before downscaling into the Virtual met product.

Source: Lawrence Berkeley National Laboratory

Local topography is important in representing the wind field, particularly in regions of significant topographic variability that tend to be well suited for wind power generation. Consequently, the importance of model resolution cannot be overstated. Topographic profiles from each of the models and reanalysis datasets are plotted in Figure 3. As can be seen here, DNV GL WRF model ran at 20 km resolution (b), which captures the dynamical wind field at this resolution, and then statistically downscaled to 4 km resolution (c). VR-CESM uses a relatively smooth topography by comparison, due to the slightly lower spatial resolution of 14 km (a). MERRA2, CFSR, and NARR (d-f) all have much more poorly refined topography, with a poor representation of the coastal ranges that are important for shaping the wind field. These differences also imply that each model has a different altitude for the wind farms and sounding stations used in this study.

2.1.3 Reanalysis Products and Associated Method

VR-CESM and the Virtual met products were compared to each other, and several reanalysis products (MERRA-2, CFSR, and NARR). The reanalysis products are described here.

***MERRA-2* (Reanalysis product).** MERRA-2 is a reanalysis product for the satellite era using the Goddard Earth Observing System Data Assimilation System Version 5 (GEOS-50) produced by Global Modeling and Assimilation Office (GMAO) at NASA (Gelaro et al. 2017). MERRA-2 integrates several improvements over the first version MERRA product, as described in (Rienecker et al. 2011). For the fields used in this study, the spatial resolution is ~55 km with 3-hour output frequency from 1980 to present. Vertical interpolation of MERRA-2 data, described below, was performed to calculate hub height wind speed at 80 m. Variables used in vertical interpolation were extracted from two subsets: 3-hour instantaneous pressure level assimilation (GES 2017b) and hourly instantaneous single-level assimilation (GES 2017a) (extracted every 3 hours).

***CFSR* (Reanalysis product).** The Climate Forecast System Reanalysis (CFSR) from the National Centers for Environmental Prediction (NCEP) is a global, coupled reanalysis that spans from 1979 to the present with ~55 km spatial resolution and 6-hour temporal resolution of relevant wind fields (Saha et al. 2010). Notably, this temporal resolution is relatively low compared to the other datasets. The analysis subset was used in this study, and vertical interpolation was performed every 6 hours.

***NARR* (Reanalysis product).** The North American Regional Reanalysis (NARR), another NCEP reanalysis product, features a slightly higher spatial resolution of ~32 km. It is a dynamically downscaled data product with spatial coverage over North America, with 3-hour temporal resolution from 1979 through present (Mesinger et al. 2006). Hub-height wind speeds from NARR were also calculated at this frequency.

The research team determined the wind speed at each wind farm location using nearest grid point values to each wind farm site. To obtain 80 m wind vectors for this study, vertical interpolation was performed on 3-hour VR-CESM, 3-hour MERRA-2, 6-hour CFSR, and 3-hour NARR products from 1980 to 2000. Eighty-meter wind output is available directly from the DNV GL Virtual met data product used in this study, so values are extracted directly from the output from 1980 to 2000. Vertical interpolation of VR-CESM data uses the 3D wind field on hybrid surfaces and 10 m altitude wind speed, which is computed from similarity theory. For VR-CESM data, the interpolation procedure is as follows:

(1) the CAM5 hybrid coordinates are first converted to pressure coordinates within the column being analyzed;
(2) the height of each pressure surface above ground level (AGL) is computed by subtracting the surface geopotential height from the geopotential height of the model level;
(3) two model levels that bound the desired interpolation altitude are selected or, if the interpolation altitude is below the lowest model level, the lowest model level and 10 m wind speed field are used;
(4) logarithmic interpolation is applied to obtain the wind speed at the desired interpolation altitude.

Specifically, the team performed the interpolation by fitting a log equation with the two levels bounding the altitude to be calculated, then interpolating the wind at desired altitude (Justus et al. 1976). Vertically interpolated wind speeds from MERRA-2, CFSR, NARR, and sounding observations were all obtained by a similar procedure and were calculated at three hub heights (50 m, 80 m, and 140 m). Further, wind speed at 80 m was logarithmically interpolated for all three sounding instrument locations and compared with the interpolated 80 m wind speed at each sounding location and model/reanalysis dataset.

The wind field enters into the maximum potential wind power P (W) via the expression $P = \frac{1}{2}\rho A U^3$, where ρ is air density (kilogram per cubic meter [kg/m^3]), A is the cross-section area of the turbine rotor (m^2), and U is wind speed at hub height (m/s). Given the cubic relationship between wind speed and wind energy potential, even a small change in wind speeds can change wind energy production substantially. The energy contribution of wind turbines to the electric power system is then computed as the total amount of usable energy supplied by the turbine per year (Fripp et al. 2008). The capacity factor (CF) is thus often defined as actual power output divided by the maximum wind power output that can be generated through the system. This wind speed and CF relationship is not continuous, since there are discontinuous minimum and maximum wind speeds required to begin and cease wind power production (the latter to avoid damage to the wind turbine under extreme wind conditions), and this relationship is represented with different power curves associated with each of the wind farm sites. For this study, the calculated CF at each wind farm site is based on different characteristic power curves specific to each site (Appendix A) and do not include electrical losses during power generation.

2.1.4 Clustering Approach

One approach to analyzing variability in wind speed and direction has been to group together days or hours with similar meteorological, or other properties, using statistical clustering or related techniques. This approach can help link variation in wind seen at individual sites to meteorological patterns at larger geographic and multiple temporal scales, providing insight into the mechanisms for, and potentially predictability of, such variation. For example, Berg et al. (2013) find a shift in the Southern California winter surface wind regimes during El Niño, and other works have aimed to improve regional descriptions of surface wind climatology (Zaremba et al. 1999, Ludwig et al. 2004, Conil et al. 2006, Seefeldt et al. 2007, Jiménez et al. 2009, Chadee et al. 2015). Clustering techniques are used to identify wind patterns associated with certain air pollution profiles (Darby 2005, Beaver et al. 2009, Jin et al. 2011). Although to date, clustering approaches have mainly been applied to surface-level wind fields, Clifton and Lundquist (Clifton et al. 2012) cluster speed and direction measurements observed at a tall tower in Colorado, finding links in wind resource characteristics to El Niño, and suggest the clustering technique might aid in site-level wind resource estimation. Also, Gibson and Cullen (Gibson et al. 2015) link wind measurements at a tower in southern New Zealand to typical synoptic-scale patterns.

This study extends and adapts clustering techniques to the analysis of hub-height wind resources to (1) directly link site-level wind regimes to synoptic-scale meteorological conditions, (2) illuminate the unique reasons for variation in annual generation potential at specific wind project sites, and (3) provide insight into the impacts of climate-mode intensity and the impacts of climate change on wind resources. The clustering technique is performed on the 100-meter wind fields from the DNV GL Virtual met product. While this demonstration focuses on California, the generalized approach can be applied in any location and shows potential to help improve wind resource assessment and benefit other aspects of wind energy operations and in other fields.

The approach taken here broadly builds on and extends previous clustering efforts (Ludwig et al. 2004, Darby 2005, Conil et al. 2006, Beaver et al. 2009, Jin et al. 2011, Berg et al. 2013). California was first split into two domains – one centered on Central California, including the Shiloh and Altamont Pass wind farms, and one centered on Southern California, including the Alta, San Gorgonio, and Ocotillo wind farms (Figure 1). The research team developed a separate, independent set of clusters for each domain. Clusters developed in the Central California domain are labeled "C," followed by an identifying number 1 – 10. Clusters developed in the Southern California domain are labeled "S" and followed by an independent identifying number 1 – 10. The identifying numbers are not used in this work for anything other than identification and are effectively arbitrary in order. Each 24-hour period (from January 1, 1980, through December 31, 2015) was classified as a cluster type. Thus, every day in the period was classified as one of 10 clusters in the Central California domain and one of 10 clusters in the Southern California domain.

The research team accomplished the clustering through a two-step process. First, the dimensionality of the problem was reduced using principal components analysis (PCA), and second, an agglomerative clustering algorithm was applied to the principal component multipliers (the "scores" or "weights" of the PCA). PCA allows spatial data, at any particular time, to be represented by a mean spatial pattern plus the sum of a limited number of weighted principal spatial patterns. Previous studies (Ludwig et al. 2004) and (Jin et al. 2011) provide useful explanations related to the application of PCA to wind fields. From PCA, the first 10 weights of the principal spatial patterns were saved, as these first 10 principal components accounted for greater than 80% of the total variance in wind regimes within each domain, and additional weights would have added less than 1% to the explanation of the variance. Thus, the dimensionality of each hour was reduced from 2-component (u and v) modeled wind outputs at hub height across all grid cells (~8,500 in each domain) to 10 PCA weights. The PCA weights were then grouped together by 24-hour periods to form the input for the agglomerative clustering. Thus, each day, for each domain, is categorized as a particular cluster based on a set of (24×10) 240 PCA scores that describe the regime of wind speed and direction throughout the day and across the domain.

The research team performed the cluster analysis using a hierarchical clustering technique, specifically agglomerative clustering using Ward's method (Ward Jr 1963). Agglomerative clustering begins with each "observation," in this case, each day, classified as a cluster, and observations are then merged together into larger groups based on minimizing a criterion (Ward's method minimizes the variance of the clusters being merged) until the predetermined number of total clusters is reached. The "right" total number of clusters varies by application and, in this case, was determined by inspecting the regional wind regimes (similar to Figure 11) after repeatedly running the clustering algorithm while varying the targeted number of clusters. For example, in this case, the use of 5 clusters did not portray the full range of patterns found with 10 clusters, and the set of 15 clusters contained clusters with wind regimes similar to each other. In other words, using 15 clusters identified differences among clusters that were subtler than needed for this application. While this approach was sufficient for this analysis, it may be desirable to optimize iteratively the number of total clusters for specific applications, such as short-term forecasting.

The PCA included developing and processing an extremely large matrix, including columns representing 315,552 hours and rows representing ~8,500 grid cells. (The total cells differed slightly between the Central and Southern California domains.) Therefore, the large memory nodes on the Haswell computer within the U.S. Department of Energy National Energy Research Scientific Computing Center (NERSC) were used. The research team implemented the PCA and agglomerative clustering methods using the publicly available Scikit-learn algorithms (Pedregosa et al. 2011).

2.2 Model Comparisons and Validation

2.2.1 Comparison to Reanalysis Products

Figure 4 depicts the 80 m wind speed fields (vertically interpolated values except for Virtual met) from each of the datasets in the Central California domain. Wind fields shown are seasonal mean values for all March-April-May (MAM), June-July-August (JJA), September-October-November (SON), December-January-February (DJF) seasons in the historical period 1980-2000. To better match the wind speeds predicted in the virtual met product, the research team applied a multiplier of 1.30 to the VR-CESM results to produce a bias-corrected VR-CESM (BC VR-CESM) prediction. The value of this multiplier is determined by the mean wind speed difference between VR-CESM and the Virtual met. As can be seen in Figure 4 and Figure 5, the wind magnitudes are more comparable to Virtual met; the latter still produces more spatial variation as compared to BC VR-CESM. Because of the high spatial resolution of Virtual met (4 km), more topographic features are apparent in the wind field, whereas the MERRA-2, CFSR, and NARR wind fields show almost no topographic features due to the relatively coarse resolution. Comparing VR-CESM to Virtual met, the overall pattern is similar, although VR-CESM exhibits lower mean wind speeds overall. This difference will be further assessed as part of the wind farm site comparisons in Section 3.2. Figure 5 depicts mean winds for the Southern California domain. Again, the patterns remain similar between VR-CESM and Virtual met but with a reduced wind magnitude.

Figure 4: Seasonal Average of Interpolated 80 m Wind Speed from Each Dataset for the Historical Period 1980-2000 in the Central California Domain

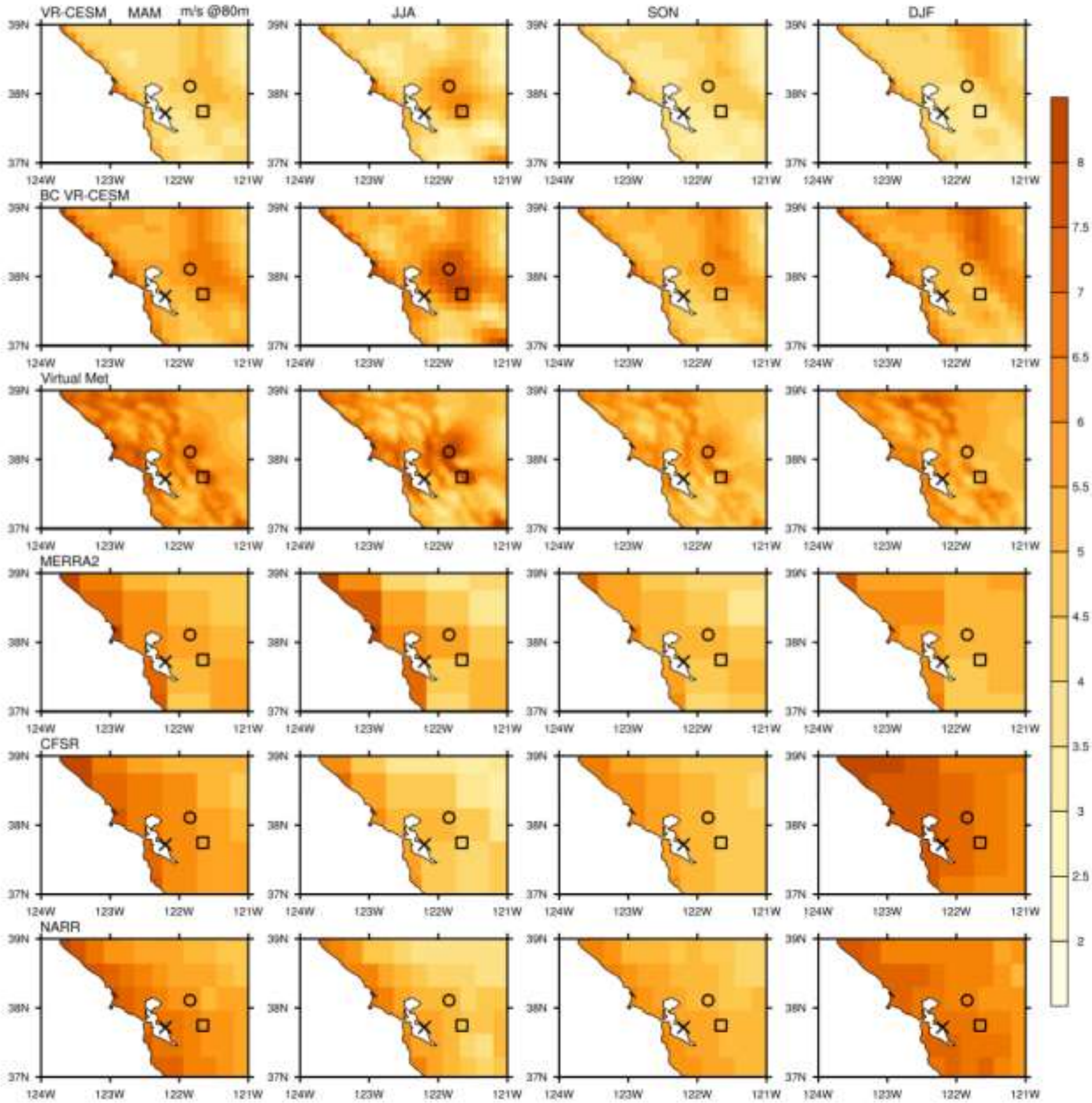

Symbols represent the Shiloh (circle) and Altamont (square) wind energy sites. X represents the Oakland observation site.

Source: Lawrence Berkeley National Laboratory

Figure 5: Seasonal Average of Interpolated 80 m Wind Speed from Each Dataset for the Historical Period 1980-2000 in the Southern California Domain

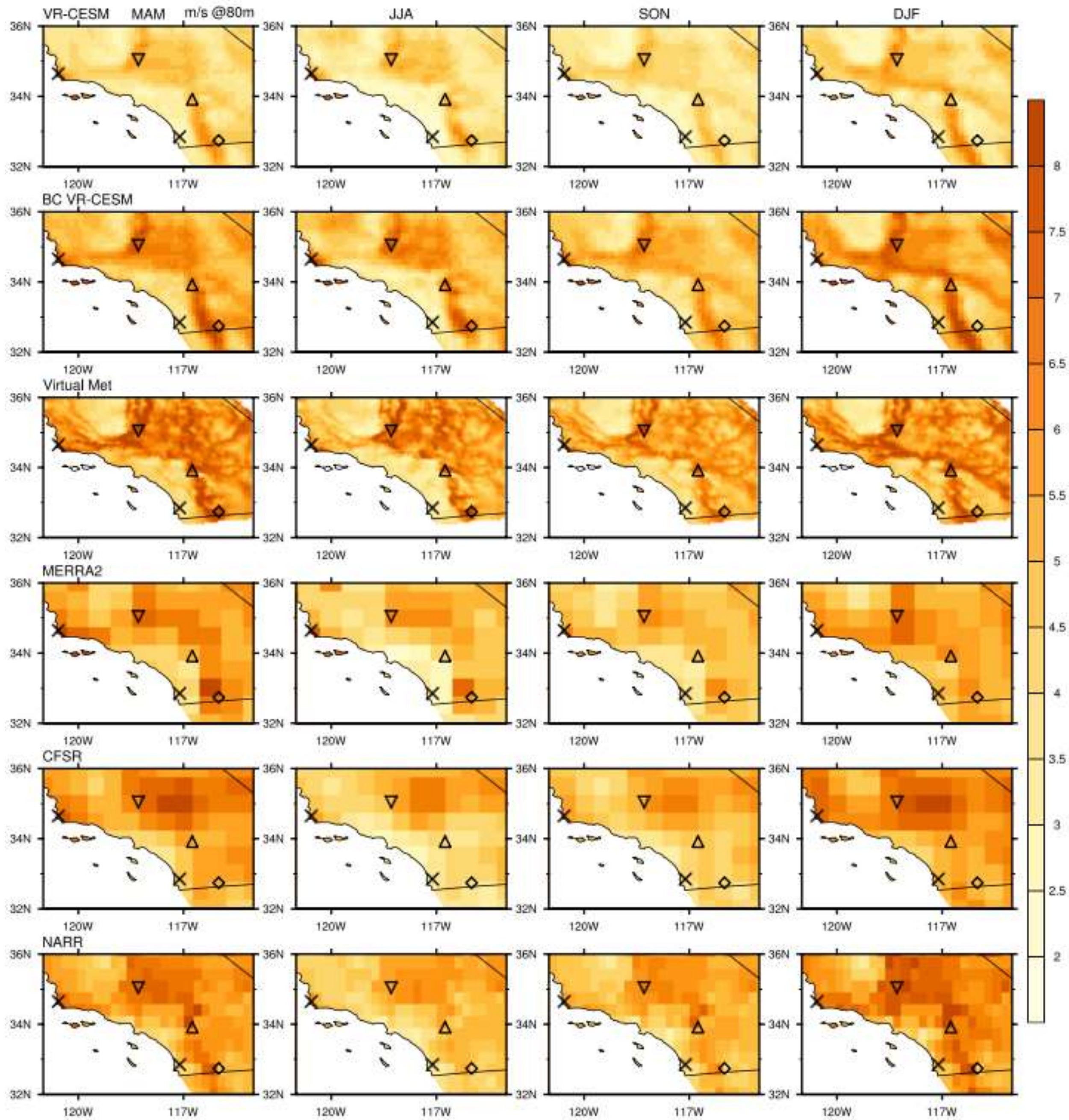

Symbols represent the Alta (inverted triangle), San Gorgonio (triangle), and Ocotillo (diamond) wind energy sites. X represents the Vandenberg and Miramar observational sounding sites.

Source: Lawrence Berkeley National Laboratory

Quantitatively, the VR-CESM and Virtual met product outputs are highly correlated (~ 0.69), which suggests that the underlying physical mechanisms responsible for determining wind speed are similar between these two products. The slow wind speeds in VR-CESM are likely a consequence of excessive diffusion in the lowest model levels and further hypothesized to be connected to a boundary layer parameterization in CESM that is not tuned for the high resolutions employed in this study.

Monthly climatological mean wind speeds at each wind farm site are depicted in Figure 7. As observed in Figures 4 and 5, Virtual met tends to produce the highest overall wind speeds. Whereas VR-CESM exhibits a lower wind speed magnitude than Virtual met, both datasets produce similar spatial patterns that are different from the other three reanalysis datasets. In particular, the coarser resolution reanalysis data tend to exhibit a weak seasonal cycle. Computing the correlation across monthly mean wind speeds between each dataset with Virtual met, VR-CESM has the highest correlation (on average ~0.87 over all five wind farm sites), followed by MERRA-2 (~0.55), and CFSR (~0.37). NARR (~0.17) exhibiting the weakest correlation. To further quantify the spatial correlations between datasets, the research team calculated the centered Pearson pattern correlation (Figure 6) for seasonal mean 80 m wind speeds from all the datasets, with the domains masked to include only California, matching the domain from Virtual met. As observed in Figure 6, VR-CESM produces the highest pattern correlation (~0.69) with Virtual met, followed by MERRA-2 (~0.58). Therefore, the temporal and spatial correlation comparisons suggest VR-CESM produces the most similar wind speed climatology (both temporally and spatially) to Virtual met, followed by MERRA-2. NARR produces the lowest correlation in space and time – in fact, discrepancies in the spatial structure of the NARR wind climatology likely indicate potentially significant errors in representation of wind speeds (David Pierce, personal communication).

The frequencies of instantaneous 80 m wind speeds from each dataset are shown in Figure 8. Wind speeds in almost all locations appear to follow a Rayleigh distribution, as is typical for wind speeds where the velocity in each coordinate direction is normally distributed. However, the Virtual met data diverge from the Rayleigh distribution at several locations, which may indicate physical processes that are uniquely captured by this product at high spatial resolution. Specifically, Virtual met produces higher wind speeds at a higher frequency than other datasets in many cases, leading to a greater spread among the wind speed bins. Frequencies from BC VR-CESM are closer to Virtual met compared to VR-CESM due to increased wind speed, although there remains a mismatch in the shape of the distribution. Unfortunately, the authors are unaware of any publicly available hub-height wind speed datasets that would allow direct validation of these results against observations. As can be seen in Figure 9, the histograms of wind speed from BC VR-CESM are closer to WRF 20 km, although the further downscaled Virtual met results exhibit much higher frequencies over the highest wind speed bins at all locations except San Gorgonio. For wind speed fields at the other two analyzed hub heights (50 m and 140 m), see Appendix A. In general, higher hub heights tend to produce larger wind speeds, although the patterns remain similar.

Figure 6: Averaged Pearson Pattern Correlations Between Each Pair of Datasets as Obtained from the Seasonal Mean 80 m Wind Speed from 1980 to 2000

VR-CESM					
Virtual Met	0.69				
MERRA-2	0.61	0.58			
CFSR	0.45	0.53	0.58		
NARR	0.45	0.52	0.51	0.77	
Model name	VR-CESM	Virtual Met	MERRA-2	CFSR	NARR

Source: Lawrence Berkeley National Laboratory

Figure 7: Monthly Mean 80 m Wind Speed (Color-Coded Lines on Left) and Mean CF (Blue Lines on Right) at Each Wind Farm Site from All Datasets During Historical Period 1980-2000

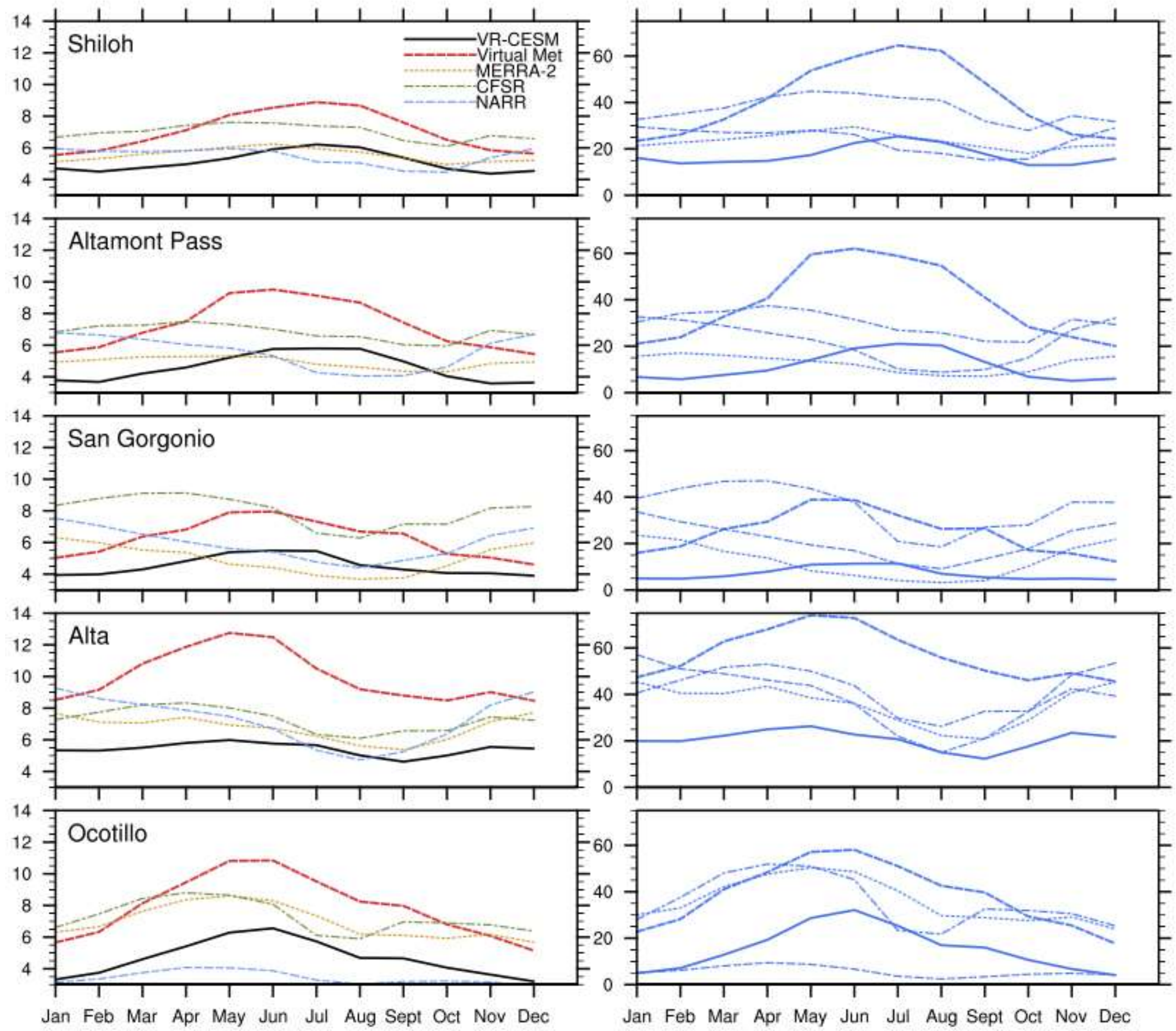

Source: Lawrence Berkeley National Laboratory

Figure 8: Frequencies for Instantaneous 80 m Wind Speeds from All Datasets at Each Wind Farm Location for the Historical Period 1980-2000 by Season

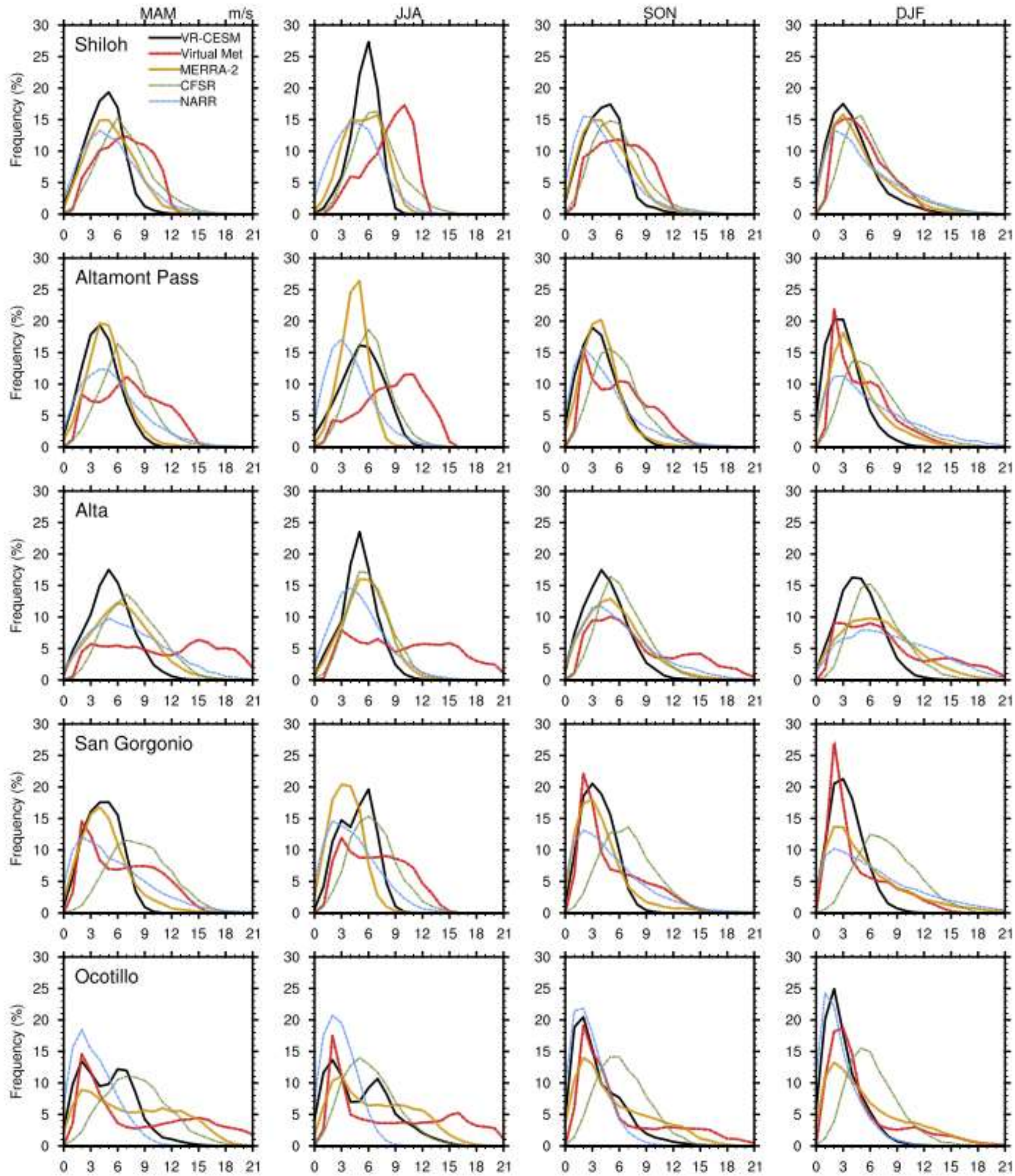

The bin width is 1m/s and covers the range from 0m/s to 21m/s.

Source: Lawrence Berkeley National Laboratory

Figure 9: Frequencies for Instantaneous 80 m Wind Speed from Bias-Corrected VR-CESM (BC VR-CESM) and 20 km WRF Compared to VR-CESM and Virtual Met at Each Wind Farm Location for the Historical Period 1980-2000

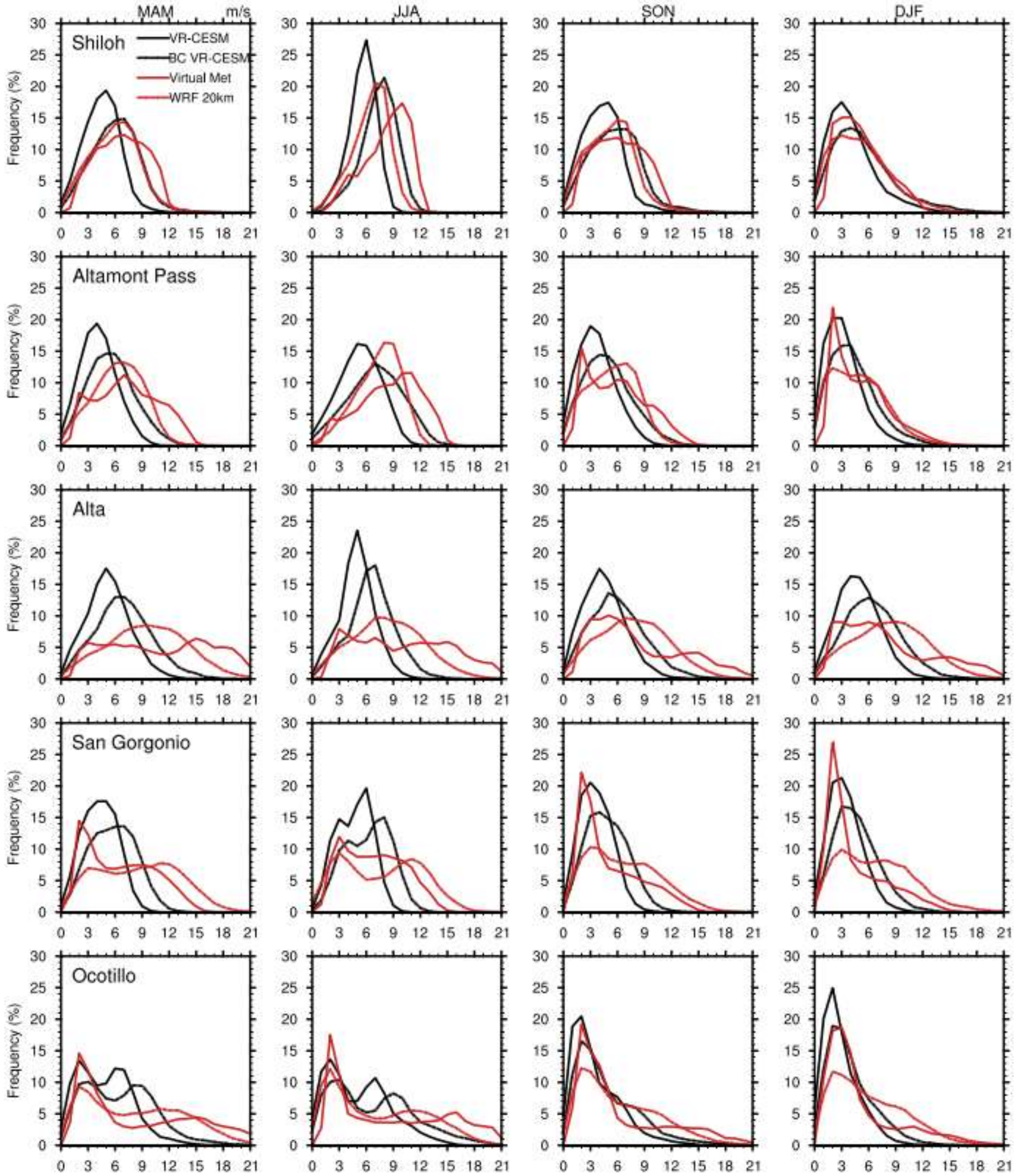

The bin width is 1m/s and covers the range from 0m/s to 21m/s.

Source: Lawrence Berkeley National Laboratory

2.2.2 Comparison to Point Observations

The performance of VR-CESM and Virtual met was then assessed against the 10 m hourly Integrated Surface Database (ISD). Although ISD incorporates hundreds of observation stations across California, many of these stations do not provide consistent observations over the relevant historical period (1980-2000). To maximize the number of available stations each year and ensure sure each year has complete data coverage, the research team calculated validation metrics (Table 1) separately for each year between 1980 and 2000. Also, to avoid issues with near-surface coastal flow, only inland observation stations were selected for comparison. After imposing these restrictions, the team used an average of 100 inland stations from each year.

Table 1 provides the averaged seasonal bias and root-mean-square error (RMSE) at 10 m altitude from the five datasets against ISD observations from 1980 to 2000. Here, a negative (positive) bias indicates that the wind speed is lower (higher) than observations. As observed, VR-CESM tends to produce lower wind speeds than observation, whereas the Virtual met produces overall higher wind speeds. MERRA-2 and Virtual met exhibit similar differences, as MERRA-2 provides the boundary conditions for the WRF model; nonetheless, Virtual met does produce higher mean wind speeds than MERRA-2, likely due to a positive wind bias that appears consistently in the WRF model (Shimada et al. 2011, Carvalho et al. 2014). CFSR exhibits lower wind speeds for most of the year except the DJF season, whereas NARR produces higher wind speeds in all seasons. For MAM and JJA seasons, Virtual met is very close to observations – namely, it shows a relatively small bias, whereas VR-CESM has strong negative biases in both seasons. In the SON and DJF seasons, VR-CESM is closer to observations compared to Virtual met, particularly during the DJF season (and closer to observations than all other datasets). As VR-CESM also obtains 10 m wind using the lowest model level wind plus similarity theory, the biases in 10 m wind have the potential to be conveyed to higher elevations during the calculation. So, this 10 m wind speed comparison with observation also provides some insight into the possible biases for wind speed at 80 m.

Table 1: Bias and RMSE for 10 m Wind Speed from All Five Datasets to Inland ISD Observational Stations from 1980 to 2000

Model Name	Stats	MAM	JJA	SON	DJF	Annual Average Bias
VR-CESM	Bias	0.80	-0.52	0.32	-0.16	-0.45
	RMSE	1.23	1.06	0.88	0.85	
BC VR-CESM	Bias	-0.04	0.21	0.28	0.52	0.24
	RMSE	1.10	1.10	1.00	1.17	
Virtual Met	Bias	0.02	-0.03	0.4	0.56	0.24
	RMSE	0.97	1.02	0.94	1.02	
MERRA-2	Bias	-0.14	-0.13	0.23	0.52	0.12
	RMSE	0.87	0.92	0.78	0.91	

CFSR	Bias	-0.48	-0.50	-0.14	0.23	-0.22
	RMSE	1.11	1.11	0.83	0.88	
NARR	Bias	0.11	0.16	0.52	0.67	0.37
	RMSE	1.34	1.17	1.25	1.49	

Bias and RMSE both have units of m/s. MAM = spring; JJA = summer; SON = fall; DJF = winter.

Source: Lawrence Berkeley National Laboratory

A note on comparisons of wind speeds at hub-height: Hub-height wind data in California are often produced through private investment and, hence, a closely guarded trade secret confidential to project owners. Consequently, for validation of the modeled hub-height wind speed data against observation, the assessment is limited to a select number of vertical sounding sites across California (shown in Figures 4 and 5) for comparison of higher-level wind speeds, and all of the three soundings are at airports near the coast with complex local topographies. The coarse resolution of these models requires them to average inland and offshore wind speeds, leading to skewed results. Also, the sounding observations are only measured twice daily. These factors have to be taken into account when interpolating to calculate 80 m wind from sounding observations and from model and reanalysis dataset at these sounding locations. In comparison, the three lower resolutions reanalysis datasets all project higher-than-observation wind speeds. At the Oakland site (airport code OAK), wind speed projected from VR-CESM is the closest (bias = 0.95m/s) to observations in terms of wind magnitude, though Virtual met captures monthly variation better (correlation = 0.62). However, at Vandenberg (airport code VBG) and Miramar (airport code NKX), none of the model datasets could be said to capture the values and seasonal variation particularly well, even though VR-CESM and Virtual met are the closest among all.

2.2.3 Comparison Between VR-CESM and Virtual Met

To investigate further the difference in wind field between VR-CESM and Virtual met, the Virtual met product was regridded to the VR-CESM grid and the difference taken. Figure 10 shows 1980-2000 seasonal mean wind speed difference from Virtual met minus VR-CESM, with positive values indicating Virtual met has higher wind speeds than VR-CESM. The difference is not spatially uniform – in particular, when comparing Figure 10 alongside Figure 3, Virtual met projected higher wind speed over higher altitudes and lower wind speed at lower altitudes. The five wind farm sites all sit at relatively high topography regions, and consequently, Virtual met projects higher values at all five locations from Figure 10, consistent with Figure 7.

Figure 10: Comparison Between DNV GL Virtual Met 4 km and VR-CESM (Virtual Met Minus VR-CESM) of Interpolated 80 m Wind Speed Between 1980-2000 for Central, Southern, and California Domains

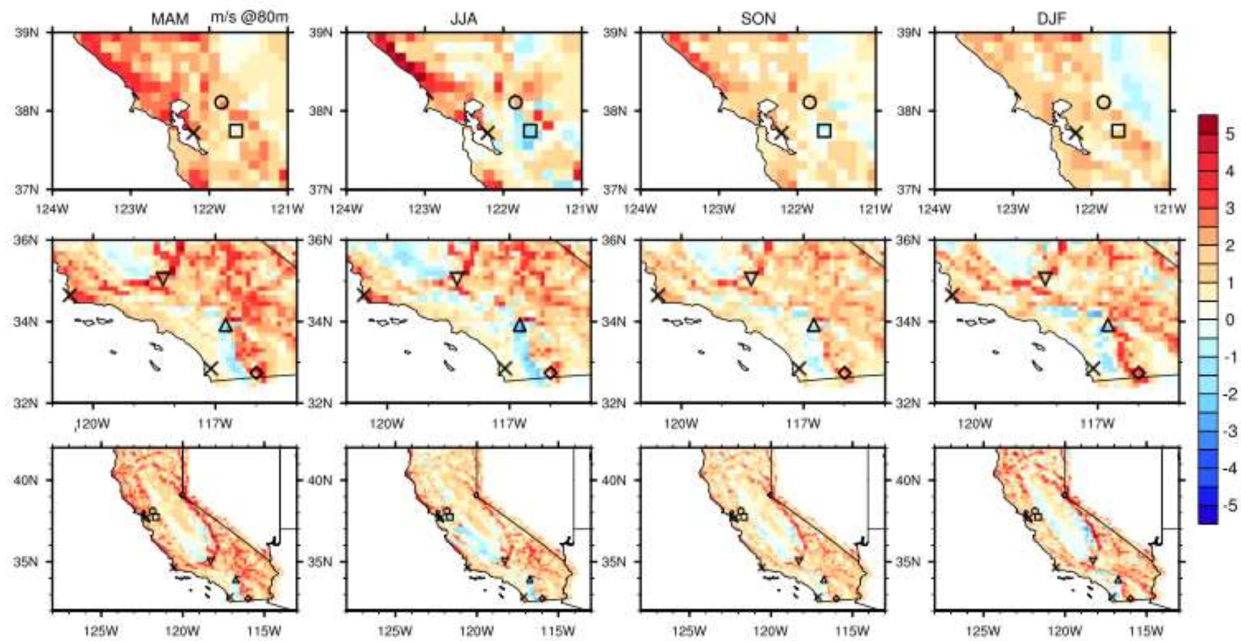

Symbols represent the Shiloh (circle), Altamont (square), Alta (inverted triangle), San Gorgonio (triangle), and Ocotillo (diamond) wind energy sites. X represents the sounding sites at Oakland, Vandenberg, and Miramar.

Source: Lawrence Berkeley National Laboratory

2.3 Methods for Climate Modes

The research team tested the correlation between the frequency of the clusters and the occurrence of major climate modes. Because the clusters are based solely on the DNV GL Virtual met product, this test is of the correlation between the observed historical intensity of climate modes and the wind regimes modeled within the DNV GL Virtual met product. This test is not related to the VR-CESM model and does not include any test of future conditions.

For each season, each cluster was correlated with the seasonal indices of five climate modes, the El Niño Southern Oscillation (ENSO), the Pacific North American (PNA) pattern, the North Atlantic Oscillation (NAO), the Arctic Oscillation (AO), and the Pacific Decadal Oscillation (PDO), (NOAA 2017a, NOAA 2017b, NOAA 2017c, NOAA 2017d, NOAA 2017e). Climate mode indices are available on a monthly basis and were averaged over each season to create a seasonal index time series of for each climate mode. For each climate mode, the index values are centered on 0.0 and range, mostly, between -1.0 and 1.0, although some months have values of larger magnitude than 1.0. A value of zero means the climate mode is in a neutral state. A value of 1.0 or larger represents a strong climate mode event, and a value of -1.0 represents a strong event of the opposite form. For example, during the winter of 2015 – 2016, the ENSO index ranged from 2.0 – 2.3, representing strong El Niño conditions. During the following winter, 2016 – 2017, the ENSO index ranged from -0.8 – -0.4, representing weak La Niña conditions.

CHAPTER 3: Historical Variability in California Wind Resources

A key concept describing wind resources is capacity factor (hereafter, CF). For a particular period, CF is the ratio (expressed here in percentage) of energy generated by a turbine to the energy that same turbine could have generated had it been running at this rated capacity continuously. In this chapter, CFs are calculated over various periods (i.e., monthly, seasonal, or annual) and for each of the specific clusters (i.e., for the set of days classified as a particular cluster). A second metric, not to be confused with CF, but also in percentage terms, is the percentage of total potential annual generation during a season or within a single cluster.

The CF is calculated without adjusting for any potential losses, such as electrical resistance losses or wake losses, based on using a power curve to estimate hourly generation as a function of wind speed. The research team converted wind speeds output from the Virtual met product to wind energy generation potential using idealized power curves. This generation potential represents a lossless potential and does not account for wake or electrical loses. Wind speeds were transformed at each location and at each hour using the normalized power curves presented in the Wind Integration National Dataset (WIND) Toolkit (Draxl et al. 2015) developed at the National Renewable Energy Laboratory. Specifically, International Electrotechnical Commission (IEC) Classes 3, 2, 3, 2, and 1 turbine curves were applied to Shiloh, Altamont Pass, Alta, San Gorgonio, and Ocotillo, respectively. Please see Section 2.1.4 for a review of the motivations, methods, and prior literature related to the following discussion.

3.1 What Is the Historical Pattern of Wind Resource Variability?

Across the five focus sites, there is large variation in resource potential. At each site, there is also important variation across the years. Average CFs range from 57% at Alta to 31% at San Gorgonio, with the other sites falling within that range. CFs varied by season and were higher in summer overall. This seasonality gives rise to 33% to 37% of annual generation occurring during July and August, across all the sites. An exception is at Alta, where only 28% of the total annual generation occurred during summer.

Variation in annual wind resource at each site is noteworthy. The ratio of the top year CF to the bottom year CF ranged from 1.19 at Alta to 1.47 at Ocotillo. Thus, in the most extreme case, the best year at Ocotillo would have produced almost 50% more energy than the worst year. More generally, the average annual resource variability ranged from 3.9% at Shiloh to 7.8% at San Gorgonio (and 4.2% at Alta and 7.4% at Ocotillo), where this is quantified as the ratio of the standard deviation of the annual CF to the average annual CF and multiplied by 100%.

The research team correlated wind resources among sites. For example, the coefficient of determination comparing the annual CFs of the three Southern California sites ranged from

0.48 to 0.66. The Central California sites – Shiloh and Altamont – had lower correlation, with the corresponding coefficient of determination equaling 0.28. The Southern California sites showed little correlation with the Central California sites. Finally, there was no evidence of temporal trends in annual or seasonal CFs at any of the sites from 1980 – 2015. Additional details related to site-specific resource variability are included in Appendix B.

3.1.1 Characterization of Historical Daily Wind Regimes

To better understand what drives the important level of temporal variation described above, the clustering technique is used to classify wind regimes and connect wind regimes and temporal patterns to synoptic-scale patterns and climate modes. This section provides an overview of the different wind regimes found in Central and Southern California.

Ten clusters were identified for each domain. (See Figure 1 for a map of the domains.) Each cluster describes a unique wind regime (a regional pattern of wind speeds and directions over a day). To identify each cluster, the labels "C" and "S" are used for Central and Southern California, respectively, followed by an arbitrarily ordered cluster number 1 – 10. See the Methods for details about the clustering algorithm. Clusters are not linked between domains, e.g. C1 is not related to S1. The uniqueness of each cluster can be seen in the sample of four Central California clusters shown in Figure 11. One can see a striking difference, for example, in both the wind resources available and the general regional wind regime when comparing the two summer clusters (C1 and C7) showing typical marine air penetration (Wang et al. 2018b) conditions to the nonsummer clusters showing flow from the north and east (C4) and showing typical conditions of a stagnant day (C9).

Although the clusters were developed based only on hub-height wind speed and direction, additional meteorological properties emerge that further distinguish and characterize each cluster. In Figure 11, for example, C1 and C7 represent different flow conditions typical during the summer but are differentiated by a temperature anomaly, as C7 corresponds to days with relatively higher temperatures than C1. Across the Central and Southern California domains there were distinct clusters associated with rainy storms, with stagnant days, and with cool or warm dry days. Of particular interest in Southern California, there were two clusters (S5 and S6) that showed the distinct offshore flow associated with Santa Ana wind conditions. The Venn diagrams in Figure 12 summarize these differences across the 10 clusters in each domain. Further details are provided in Appendix C.

Each cluster is associated with distinct synoptic-scale patterns. Synoptic-scale in meteorology is defined as a horizontal scale on the order of 1,000 km or more. The seasonal mean anomaly fields associated with each cluster were analyzed. The analyzed fields include 700 hectopascal (hPa) geopotential height, which is defined as the height of 700hPa isobar surfaces above mean sea level, as well as the surface pressure, and temperature at 2 meters above the surface. The geopotential height field was chosen at 700hPa since it reflects the general circulation pattern: wind flow at this pressure level is largely geostrophic and, hence, follows constant geopotential contours. The surface pressure field also affects local wind speeds due to pressure gradient, which is closely associated with surface temperature changes. Three steps were used to find the seasonal anomaly for each cluster. First, the monthly mean geopotential height, surface pressure, and 2-meter temperature were calculated across the full period. Second, the anomaly fields on days categorized as the particular cluster of interest were calculated by subtracting the long-term monthly mean fields from the daily mean values. Finally, the research team calculated the average over all the anomaly values within the cluster and season of interest across the full period to find the seasonal averaged anomaly fields.

Figure 13 shows the anomaly from each monthly mean field in geopotential height at 700hPa, surface pressure, and surface temperature for the same group of clusters shown in Figure 11. The synoptic-scale patterns represent the average anomaly across all days associated with each cluster and are calculated separately by season. Each of the four clusters in Figure 13 shows distinct synoptic-scale patterns. The two summer clusters, C1 and C7, which have relatively similar regional wind regimes, show almost opposite synoptic trends: the anomalies of geopotential height, surface pressure, and surface temperature show the same spatial distribution but with opposites signs. C1 is associated with a negative anomaly in geopotential height centered off the Oregon coast, which enhances the flow of marine air into Central California, cooling inland temperatures. By contrast, the positive geopotential height anomaly field in C7 slightly suppresses onshore flow, leading to overall weaker marine air penetration, as shown in Figure 11. This example demonstrates how the clustering technique can illuminate meaningful differences between wind regimes even if those regimes share some similarities, such as the inflow patterns in C1 and C7.

It was demonstrated above that wind speed regimes at specific wind project locations (the diurnal regime inlays in Figure 11) can be linked to regional wind patterns (Figure 11), as well as to synoptic-scale conditions (Figure 13). This linkage provides a useful framework with which to investigate variability in wind power resource – the focus of the next sections.

Figure 11: Average Wind Vectors for a Sample of the Central California Clusters

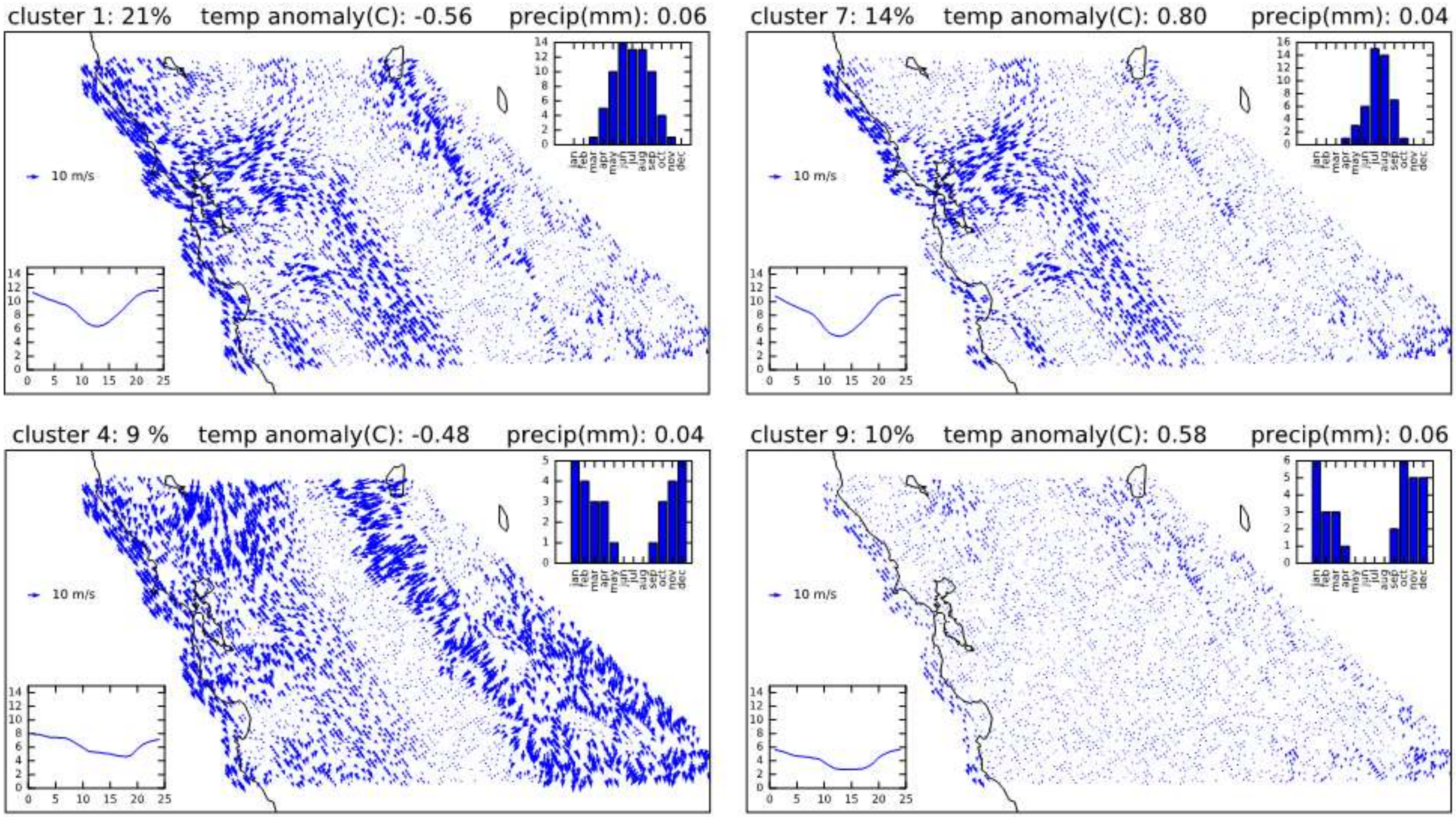

The upper right corner inlay the average number of days per month the cluster is found. The lower left corner inlay shows the average diurnal pattern of wind speed (m s-1) at the grid cells centered on the Altamont Pass and Shiloh wind farms. The information across the top of each panel includes the cluster number, the percentage of the year each cluster is found, the average temperature anomaly at the Altamont Pass and Shiloh wind farms (with the anomaly taken separately for each month and then averaged over the full-time span), and finally, the average daily precipitation.

Source: Lawrence Berkeley National Laboratory

Figure 12: Qualitative Description of Central (a) and Southern (b) California Wind Regimes

a

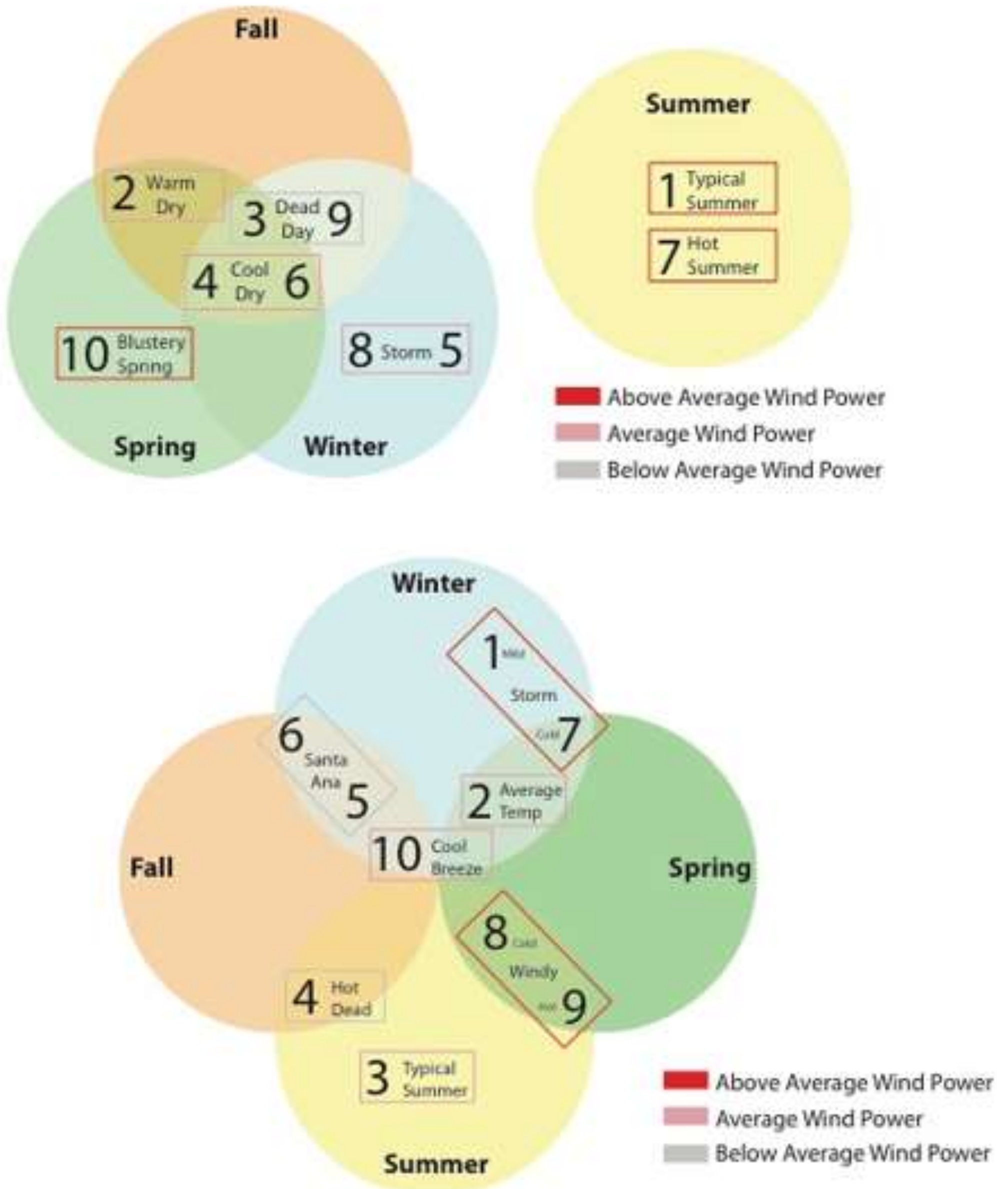

b

Cluster numbers have no relationship between regions, e.g. C1 has no relationship to S1. The color of each box indicates relative energy potential of each regime based on the average energy potential of Shiloh and Altamont Pass for Central California and Alta, San Gorgonio, and Ocotillo for Southern California. Seasonal designations were chosen to indicate the time of year each cluster occurred most frequently, although most clusters were observed to occur (although less frequently) outside the designated seasons.

Source: Lawrence Berkeley National Laboratory

Figure 13: Seasonal Average Synoptic-Scale Anomalies for 700 hPa Geopotential Height, Surface Pressure, and 2-Meter Temperature by Central California Cluster

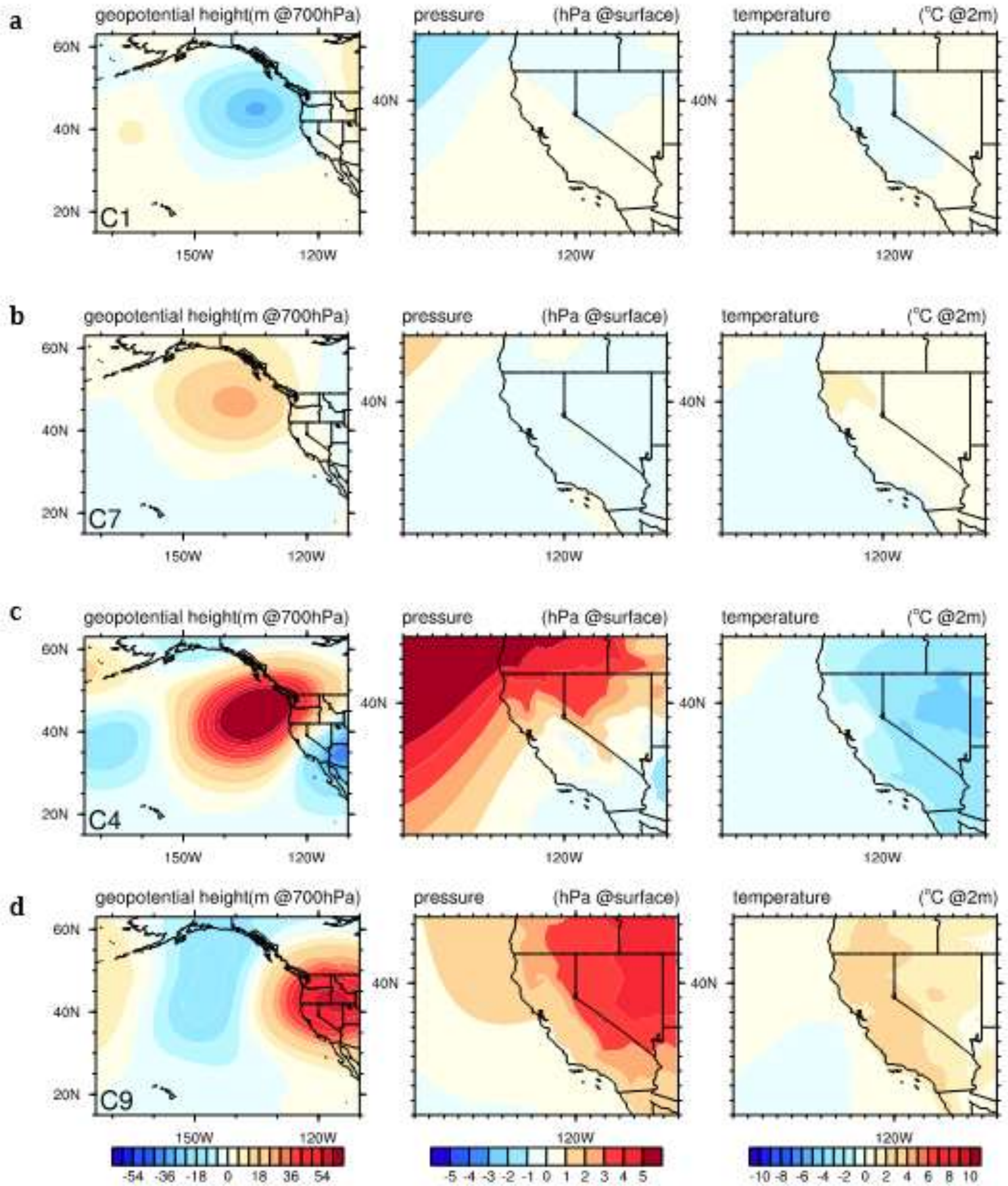

a, Cluster 1 averaged over June, July, and August. b, Cluster 7 averaged over June, July, and August. c, Cluster 4 averaged over September, October, and November. d, Cluster 9 averaged over September, October, and November.

Source: Lawrence Berkeley National Laboratory

3.1.2 Historical Wind Resource Variability, Top vs. Bottom Years

This section describes why some years produce more power generation and some years produce less. To provide context, the average CFs of each cluster and the percentage of total annual generation potential from each cluster are found (Figure 14). Most noticeable, the Central California sites (Shiloh and Altamont Pass) depend on only two clusters (C1 + C7, see the top row of Figure 11) for about half of the associated potential energy resource. These clusters represent two typical types of summertime marine air penetration wind patterns. The rest of the energy potential at the Central California sites is split among storms (C5 + C8), warm fall and spring days (C2), and dead days (C3 + C9), each accounting for ~10%, with cool and dry winter and spring like days (C4 + C6) accounting for ~15%. While generation potential at the two Central California sites is similarly divided between the weather regimes, correlation between the annual CFs at the sites is not particularly strong ($r^2 = 0.28$), thus the factors that drive interannual variability differ across these sites.

At the Southern California sites, specifically, San Gorgonio and Ocotillo, windy spring weather (S8 + S9) accounts for ~35% of total generation. Storms (S1 + S7) account for ~25% of total generation, and typical summer weather (S3) accounts for ~20% of annual generation. Santa Ana-type weather (S5 + S6) and dead days (S4) combined account for only ~10% of total generation but 35% of total days. At Alta, also in the Southern California domain, the distribution of generation across the clusters is similar to San Gorgonio and Ocotillo, although one sees some differences for certain clusters (e.g., S2, S5, S8).

Most of the clusters spanned more than a single season, and in Southern and Central California, each season was made up of multiple clusters. Thus, analyzing resource variability by cluster allows one to investigate changes in weather patterns that might be obscured when looking at resource variability on a seasonal basis.

To understand what drives variation between the top wind years and the bottom wind years, the cluster frequency and cluster CFs found during the highest wind years are compared to those found during the lowest wind years. This comparison is made at each site and across the top five to the bottom five wind resource years. Through this comparison, the clusters most responsible for differences in wind resource are identified, and the influence caused by changes to the frequency of the cluster and the influence caused by changes to the within-cluster wind intensity (indicated by the cluster CF) are isolated. The source of resource variability differs strongly at each site.

At Altamont Pass, 38% more energy is produced on C1 days during top years versus bottom years. Some of this increased energy production during C1 was due to an increase to within-cluster wind speeds (at Altamont Pass: CF_{C1}-top/CF_{C1}-bottom = 1.08). Also, there were 19 additional C1 days, on average, per top year. Correspondingly, there were 17 fewer C7 days per top year. This switch is notable as both C1 and C7 represent typical summer conditions but are associated with different regional and synoptic-scale characteristics (Figure 3). In particular, C7 represents hotter conditions compared to the cooler C1. There are other differences as well – 33% more energy was generated during stormy weather (C5 + C8), much of which is due to an additional 12 days of storms during top years. To a lesser degree, other clusters changed in frequency as well (e.g., C9, “dead days” occurred six fewer times during top years than bottom years, a 16% reduction in frequency). Moreover, the average wind intensity within 8 of the 10 clusters was stronger during top years. Differences between top and bottom years are summarized in Tables 2 and 3, with additional details provided in Appendix B.

A step toward isolating the effect of top-bottom variation from within-cluster wind intensity, or from cluster frequency, is to calculate hypothetical site-level annual capacity factors. The actual average top year CF (CF-top) is equal to the sum across clusters of CF_i-top * AF_i-top (where AF is the annual fraction, $days_i$/days per year, of each cluster, the subscript i referring to cluster number). Instead, to isolate the effect of changing within-cluster wind intensity (hereafter CF-wind), one would sum CF_i-bottom * AF_i-top. Likewise, summing CF_i-top * AF_i-bottom isolates the effect of changing cluster frequency (hereafter CF-freq). These calculations are simplistic as they ignore interaction between cluster frequency and CF change, but they do give a general idea of the relative importance of frequency versus intensity. At Altamont Pass, both CF-wind and CF-freq fall roughly in the middle between CF-top and CF-bottom (Table 3), indicating that both frequency changes and within-cluster wind intensity changes play important roles in driving the difference between top and bottom years. To summarize, at Altamont Pass, the primary difference between top years and bottom years is an increased frequency of cooler typical summer conditions at the expense of hotter summer conditions. Furthermore, top years had a greater frequency of stormy days and a reduced frequency of dead days. Of roughly equal importance, there is an increase in within-cluster wind speed across most of the clusters.

Shiloh, on the other hand, is almost entirely sensitive to changes to within-cluster wind speed: the CF-freq is only 1% smaller than CF-top, whereas CF-wind and CF-bottom are 10% and 11% smaller than CF-top, respectively (Table 3). The largest factor in the difference between top and bottom wind years derives from an increase to wind speeds within C1 (CF_{C1}-top/CF_{C1}-bottom = 1.23). Thus, the primary factor driving top years at Shiloh is the intensity of the typical summertime marine air penetration conditions (the regional and synoptic-scale structure that is represented by C1). Of secondary importance is an increase to wind speeds in the C4, C6, and C10 clusters that represent typical springtime conditions but not stormy conditions. Unlike Altamont Pass, at Shiloh the ratio of CF-top to CF-bottom is insensitive to frequency of storms (C5 and C8) or stagnation ‘dead’ days (C3 and C9).

There are differences between top and bottom years at the other three sites as well, which, for brevity, will be described more qualitatively below. Alta is more sensitive to the frequency of clusters than the within-cluster wind speeds. Specifically, top years at Alta have 26 more storm days (S1 and S7) and 10 additional hot windy spring days (S9). These come at the expense of dead days (S4) and Santa Ana wind days (S5 and S6), which combined account for 43 fewer days on top years. The largest change to within cluster wind intensity is to storm cluster S1: CF_{S1}-top/CF_{S1}-bottom = 1.12. Unlike Altamont Pass and Shiloh, Alta sees little difference in either frequency or intensity of the typical summer conditions (S3) between top and bottom years.

San Gorgonio and Ocotillo have similar differences between top and bottom years. They are roughly equally sensitive to cluster frequency and within-cluster wind intensity changes. During top years, San Gorgonio and Ocotillo each have ~20 additional storm days (S1 and S7) and ~10 additional cold windy spring days (S8). These come at the expense of dead days (S4), Santa Ana wind days (S5 and S6), and hot, windy spring days (S9). Moreover, the typical summer cluster (S3) is more frequent and has more intense wind speeds during top years at these sites.

Figure 14: Average Capacity Factor and Percentage of Total Wind Resource Potential

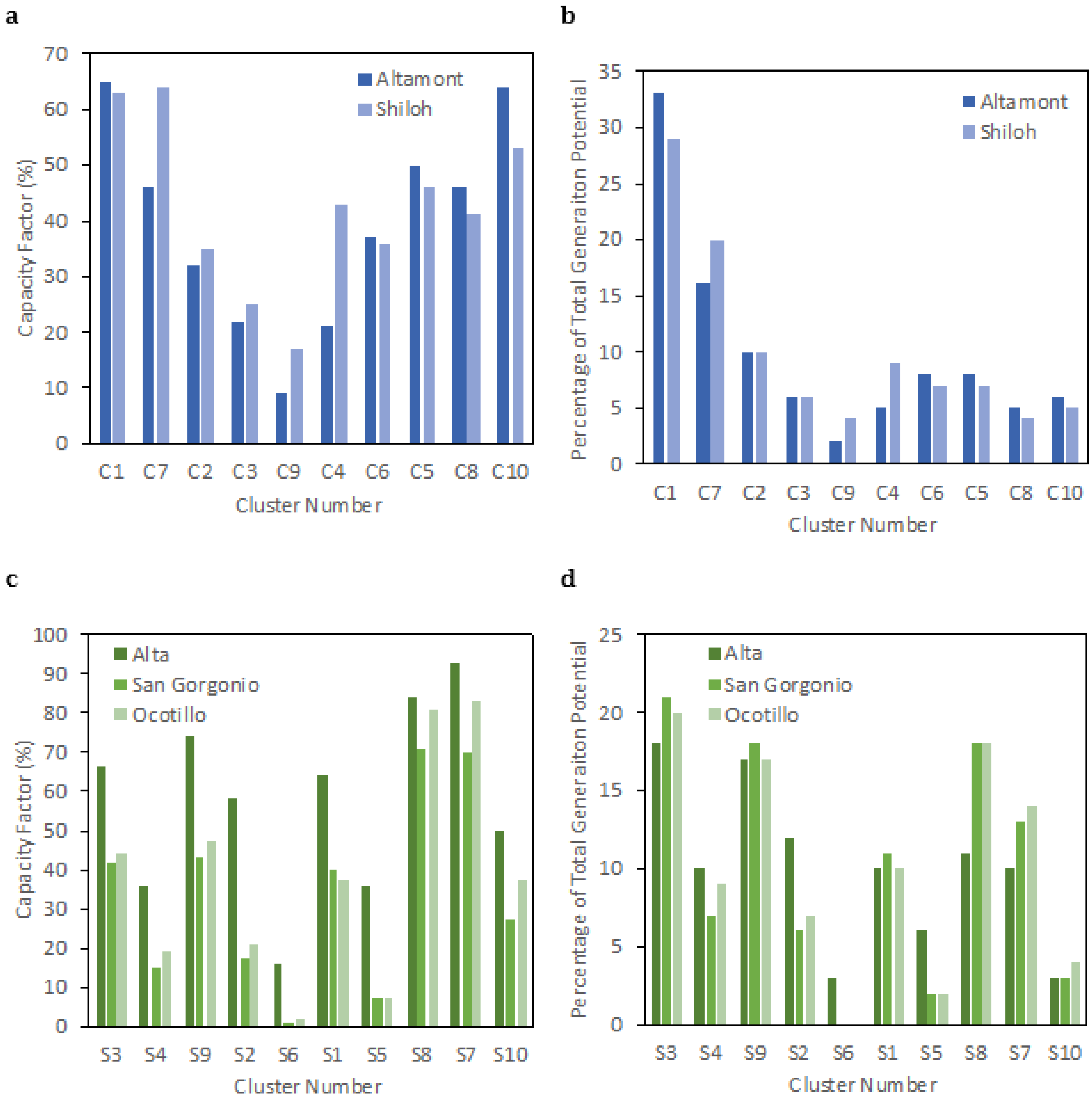

a and c, Capacity Factor by Cluster. b and d, Percentage of Total Generation Potential by Cluster. a and b, Central California Sites. c and d, Southern California Sites. Note: Clusters are shown in descending order, left to right, of the frequency of occurrence.

Source: Lawrence Berkeley National Laboratory

Table 2: Average Differences, in Total Days and in Capacity Factor, Between the Top Five and Bottom Five Wind Years at Each Site

	Central California					
	Shiloh			Altamont Pass		
	Δ Days	Δ CF (%)	% of top-years energy	Δ Days	Δ CF (%)	% of top-years energy
C1 or S1	11.0	3.7	30.0	19.2	5.0	37.9
C2 or S2	-8.0	2.3	9.2	-11.4	6.0	9.0
C3 or S3	-7.2	4.7	6.2	-0.4	0.1	5.9
C4 or S4	6.2	6.4	9.5	-8.8	3.3	4.1
C5 or S5	-3.8	9.6	5.9	6.2	4.4	9.0
C6 or S6	4.0	5.7	7.6	8.0	-2.1	7.2
C7 or S7	-4.0	3.9	18.5	-17.2	2.5	10.7
C8 or S8	-2.4	5.8	4.1	6.2	3.7	6.8
C9 or S9	2.8	1.3	4.1	-6.2	6.9	2.6
C10 or S10	2.0	11.5	4.9	4.2	4.3	6.9

	Southern California								
	Alta			San Gorgonio			Ocotillo		
	Δ Days	Δ CF (%)	% of top-years energy	Δ Days	Δ CF (%)	% of top-years energy	Δ Days	Δ CF (%)	% of top-years energy
C1 or S1	15.0	11.7	13.1	13.2	13.3	15.3	9.4	13.5	12.5
C2 or S2	8.4	-0.3	13.4	0.6	-0.6	5.2	-6.4	-2.3	5.6
C3 or S3	-0.6	2.3	17.8	6.8	7.5	18.7	5.2	7.2	19.2
C4 or S4	-20.8	-0.6	7.6	-16.4	2.6	6.4	-13.6	3.0	7.9
C5 or S5	-10.8	-1.1	4.2	-6.2	-0.5	1.4	-8.8	-0.6	1.2
C6 or S6	-11.2	-2.8	1.4	-3.6	-0.3	0.2	0.8	-0.7	0.3
C7 or S7	11.4	1.7	11.5	10.4	6.4	17.5	10.8	1.2	16.7
C8 or S8	4.0	1.4	11.2	7.8	2.6	17.3	10.2	3.7	17.5
C9 or S9	10.2	6.6	17.2	-9.8	9.9	15.3	-7.8	10.3	15.8
C10 or S10	-5.4	2.8	2.5	-3.2	3.0	2.7	-0.4	5.8	3.4

Differences are taken as the average top year value minus corresponding bottom year value. The '% of top-years energy' is provided for context and is not a differenced quantity but simply the average percentage of total annual potential generation at each site corresponding to each cluster.

Source: Lawrence Berkeley National Laboratory

Table 3: Average Annual Capacity Factors and the Influence of Changes to Wind Regime Frequency and Intensity on Annual Capacity Factor During Top Five and Bottom Five Wind Years at Each Site

	CF-top (%)	CF-wind (%)	CF-freq (%)	CF-bottom (%)
Shiloh	47.0	42.4	46.4	41.9
Altamont Pass	43.2	39.6	40.4	36.7
Alta	60.6	58.1	54.8	53.0
San Gorgonio	36.0	31.0	32.2	27.7
Ocotillo	39.3	34.7	35.1	30.9

Source: Lawrence Berkeley National Laboratory

3.1.3 Conclusions Related to Historical Wind Resource Variability

Using the above methods, the research team isolated the weather patterns that are associated with high and low generation years. The direct connection between cluster and synoptic-scale conditions provides a ready starting point for future efforts to investigate the causes of, and develop the ability to predict, such variability. More generally, several applications within the wind industry could use the clustering framework developed here , as well as other fields or research, such as atmospheric science and air quality. Atmospheric scientists could use the framework to help explain the causes for particularly anomalous wind resource periods. Wind developers could include it in the early stages of site-level wind resource assessment, possibly as a refinement of the measure-correlate-predict process. Grid operators may find the synoptic-scale link useful for short-term wind resource forecasting and the links to climate modes useful in medium-term wind resource forecasting. (See the next section.) Most generally, the framework allows for an accounting of wind resource variability that is not bound artificially to seasonal or monthly periods, directly links local wind patterns to regional and synoptic-scale patterns, and is intuitive and accessible, yet quantitative and repeatable in any location.

3.2 Climate Modes and Historical Wind Resources

3.2.1 Relationships of Wind Resources to Climate Modes

Climate modes are identifiable, large-scale climate patterns that affect regional weather. Prior studies have linked wind resource variation to climate mode at regions around the world (Li et al. 2010, Clifton et al. 2012, Berg et al. 2013, Yu et al. 2016, McElroy et al. 2017).

In the results presented here, although there was no evidence of correlation between seasonal average CF and climate modes, there was evidence that the frequency of a number of clusters in both Central and Southern California were linked to climate mode indices. The correlation is based on a simple variable, linear regression between season average cluster frequencies, and seasonal average climate indices. Additional measures and techniques may bear insight into possible links between climate variability and wind resource variability. For example, this study does not consider correlations on subseasonal timescales, the possibility of lagged responses, interactions between multiple climate modes and cluster frequency, nor the intercorrelation of climate modes themselves. However, the results presented here demonstrate at a high level the connections between cluster frequency and climate mode, while more complex analysis should be considered when developing explicit forecasting approaches.

Reported here is the percentage increase to seasonal frequency of clusters in response to a shift from -1.0 to +1.0 in the associated climate mode index. All values reported are statistically significant at the 95% level unless otherwise stated. For each season, the correlations between each cluster and the monthly indices of five climate modes – the El Niño Southern Oscillation (ENSO), the Pacific/North American (PNA) pattern, the North Atlantic Oscillation (NAO), the Arctic Oscillation (AO), and the Pacific Decadal Oscillation (PDO) – were tested. As expected, storm clusters C8 and S1 increased in frequency by 45% and 30% during winter with ENSO (although the S1 trend was not statistically significant with a p-value of 0.052). C8 also increased by 74% during winter with PNA. Interestingly, storm clusters C5 and S7 were not correlated with ENSO, indicating that perhaps the clusters are picking out storms with different origins. S1 represents the storm type most common in Southern California. S7 occurs less frequently and is distinctly colder than S1, having a temperature anomaly of -3.5° versus 0.2 °C. S7 is correlated with NAO decreasing by 45% in the spring. The distinction between C5 and C8 is not immediately obvious.

Additional teleconnections were found in both Central and Southern California domains, however, unlike the correlations between storms and ENSO and PNA, there is no a priori reasons to expect these additional teleconnections. Therefore, due to issues of multiplicity, one cannot assume these correlations are statistically significant despite test p-values below 0.05. Still, these correlations may provide useful context for further research and are thus reported here. In Central California, additional teleconnections include dead days (C3 and C9) and hot summer days (C7). During the fall, C3 increased by 40% with PNA and C9 increased by 35% with NAO. During the spring, C7 increased by ~70% with both AO and NAO. In Southern California, typical warm summer days, S3, increased by 50% with ENSO during the spring. There was no evidence of teleconnections between climate modes and the Central or Southern California clusters during the summer.

3.2.2 Conclusions Related to Climate Modes and Wind Resources

These results show that while climate mode indices were not correlated directly with total monthly wind generation, climate modes are correlated with the frequency of certain weather patterns (clusters) and, therefore, were correlated with the submonthly patterns of wind generation. Thus, near-term predictions of wind resources by grid operators could benefit from including the impacts of climate mode on weather patterns. On a longer timescale, climate change impacts research could also benefit by accounting for changes to wind patterns associated with climate mode, as climate change could potentially impact wind resources through multiple pathways, including through changing the frequency and intensity of climate modes.

CHAPTER 4: Climate Change and California Wind Resources

4.1 Climate Change May Already Be Impacting Wind Resources

This section begins by analyzing climate change impacts from the historical perspective (36-year record from DNV GL). Although total annual wind resources have not been changing with climate, there are strong correlations with climate change, cluster frequency, and wind intensity within clusters. While there was no evidence of temporal trends in energy resources at the seasonal or annual level, there was evidence of trends in cluster frequency. Specifically, the frequencies of C7, hot summer conditions, and C9, nonsummer dead days increased at a rate of roughly one-half and one-fourth day per year (Figure 15), respectively. The trend for C7 and C9 was found to be significant at the 95% level. The increased frequency of C7 and C9 came at the expense of all other clusters, which declined in frequency over time except C3, but these results were not statistically significant. Despite the result of statistical significance for C7 and C9, this time-series analysis is based only on 36 data points (1 per year) and thus potentially influenced by decadal or multidecadal climate modes; so conclusions should be treated cautiously. There was not strong evidence of temporal trends in cluster frequency in Southern California.

If this pattern is maintained, it represents an important change to weather patterns in Central California. Increasing at half a day per year, C7 occurs ~18 days more per year at the end of the period than the beginning, and this change is focused on a narrow portion of the year, as C7 occurs mostly during summer months. The roughly nine-day increase in C9 during this period is also important and focused on nonsummer months. The increase in C9 dead days may have important implications for air quality (Mickley et al. 2004, Leung et al. 2005, Dawson et al. 2014, Sun et al. 2017). The changes to C7 and C9 are generally consistent with a signal of global warming: Stagnant conditions (i.e. C9) are forecast to increase across the western United States throughout the 21st century (Jacob et al. 2009, Horton et al. 2014), and C7 and C9 are associated with warmer-than-average temperatures having positive temperature anomalies of 0.79 ˚C and 0.58 ˚C, respectively. However, since temperature was not involved in generating the clusters, this suggests that shifts in wind patterns may be an additional impact due to climate change beyond temperature increases.

Figure 15: Frequency of C7 and C9 Over Time

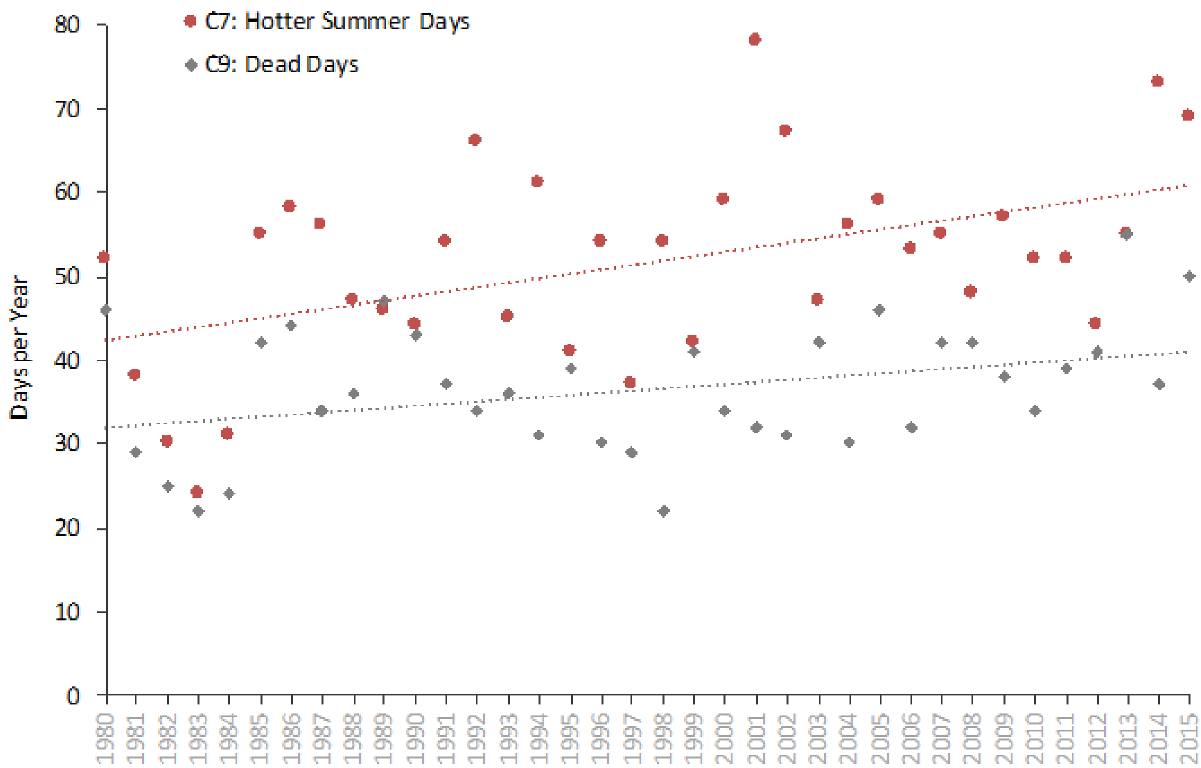

Source: Lawrence Berkeley National Laboratory

What are the implications of these changes for wind energy? C7 has the highest wind generation potential of any cluster at Shiloh and is ranked 5 out of 10 at Altamont Pass. Thus, one might expect some positive change in resource potential at Shiloh and little change at Altamont. However, there was not a significant signal in average summer CF at Shiloh. Perhaps this is because C7 and C1 have similar CFs at Shiloh, and some of the increased C7 comes at the expense of C1. Furthermore, while one might expect the increase in C9 days to lead to a decreased nonsummer energy potential, there was not a significant signal in the average nonsummer seasonal CFs. As the additional C9 days are spread across three seasons, the change within a single season is small compared to the variability of the season. Of course, if these trends continue, a change to seasonal power generation may be seen in the future. For example, some climate models show increasing spring or summer wind resources in California, with decreasing wind resources during other times of year (Duffy et al. 2014). Karnauskas et al. (2017) show decreasing future resources during the winter.

One note about statistical significance, autocorrelation of the errors in an ordinary least squares estimation can lead to an underestimation of the standard errors. A significant trend in clusters C7 and C9 was described above. The partial autocorrelation function (shown in Appendix D) was examined for C7 and C9, and C7 exhibited significant autocorrelation at lag 1. To account for the autocorrelation, the research team used the Cochrane-Orcutt procedure (Cochrane et al. 1949) to calculate a new p-value for the slope of C7. The Cochrane-Orcutt procedure removes the influence of lag 1 correlation and produces correct standard errors. The original p-value of the C7 slope was 0.003, and the p-value for the slope after applying the Cochrane-Orcutt procedure was 0.012. Thus, after correcting for autocorrelation, the slope of C7 was still found to be significant. The slope of C9 was also found to be significant at the 95% confidence level, having a p-value of 0.039. Given that no lag was found to have significant autocorrelation for C9, the p-value was not adjusted with the Cochrane-Orcutt procedure.

4.2 Modeled Future Changes to Wind Resources

This section focuses on future projections of wind energy from VR-CESM midcentury simulation under the RCP8.5 "business-as-usual" scenario. In this section, seasonal wind power changes are first quantified from the midcentury projection, then understood in terms of the synoptic-scale meteorological shifts associated with these changes at each wind farm site.

4.2.1 Projected Changes

Figure 16 compares the seasonal 80m wind speed change between midcentury and historical periods (2030-2050 minus 1980-2000). These results indicate the SON, DJF, and MAM seasons exhibit decreases in wind speed for all seasons across most areas except for parts of the Central Valley. However, JJA winds were projected to increase in magnitude throughout most of California, particularly through the Southern California domain.

Figure 16: Comparison of VR-CESM Seasonal Averaged 80 m Wind Speed Between Historical 1980-2000 and Midcentury 2030-2050 (Mid-Century Minus Historical) for Central California, Southern California, and California Domains

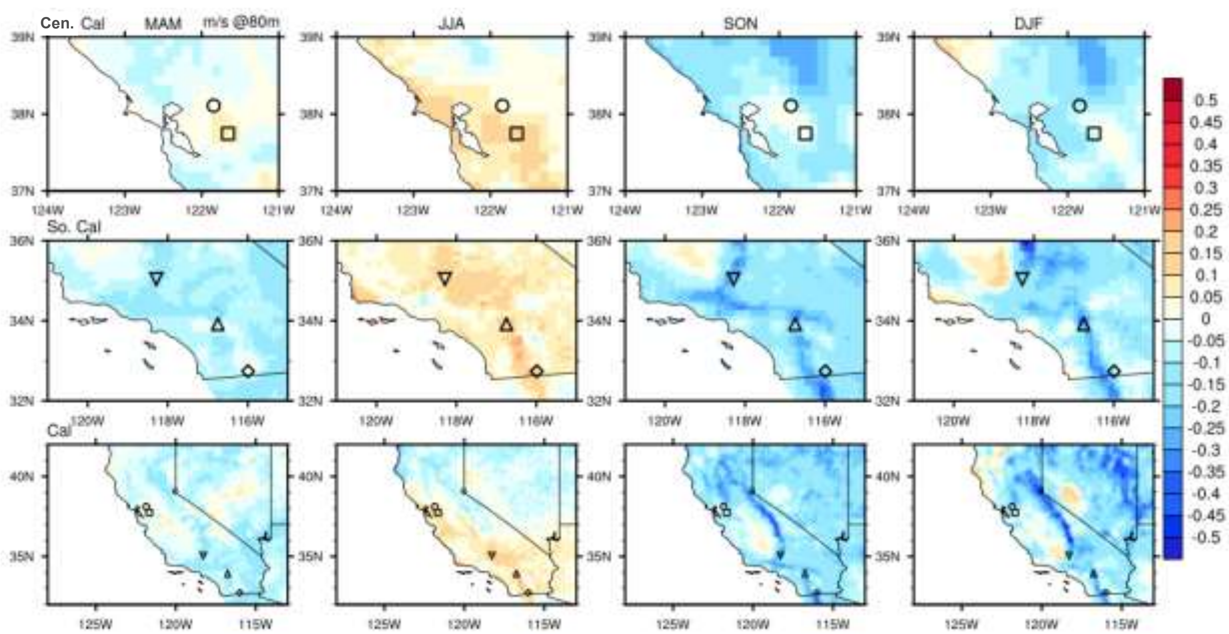

Symbols represent the Shiloh (circle), Altamont (square), Alta (inverted triangle), San Gorgonio (triangle), and Ocotillo (diamond) wind energy sites.

Source: Lawrence Berkeley National Laboratory

Comparing historical and future simulations, the seasonal pattern of CF and wind speed at each site was similar, with overall higher wind speeds during summer months and lower wind speeds during winter months (Figure 17). All wind farm sites exhibit a net increase in wind speed and CF during the summer months (JJA) and decrease during the winter months (DJF). Annual wind energy production decreases at all sites except Altamont Pass (Table 4). Consistent with Figure 17, JJA at all wind farm sites is associated with an increase in CF, while SON and DJF seasons lead to a decrease in CF. The SON CF decrease is consistent with results from (Duffy et al. 2014), which analyzed possible future trends at the Tehachapi wind farm site (at a similar location to Alta) and projected a significant decrease in wind speed throughout midcentury fall months, and little change in spring and summer.

Figure 17: Comparison of 80m Wind Speed and Capacity Factor Between Historical and Midcentury at Each Wind Farm Site

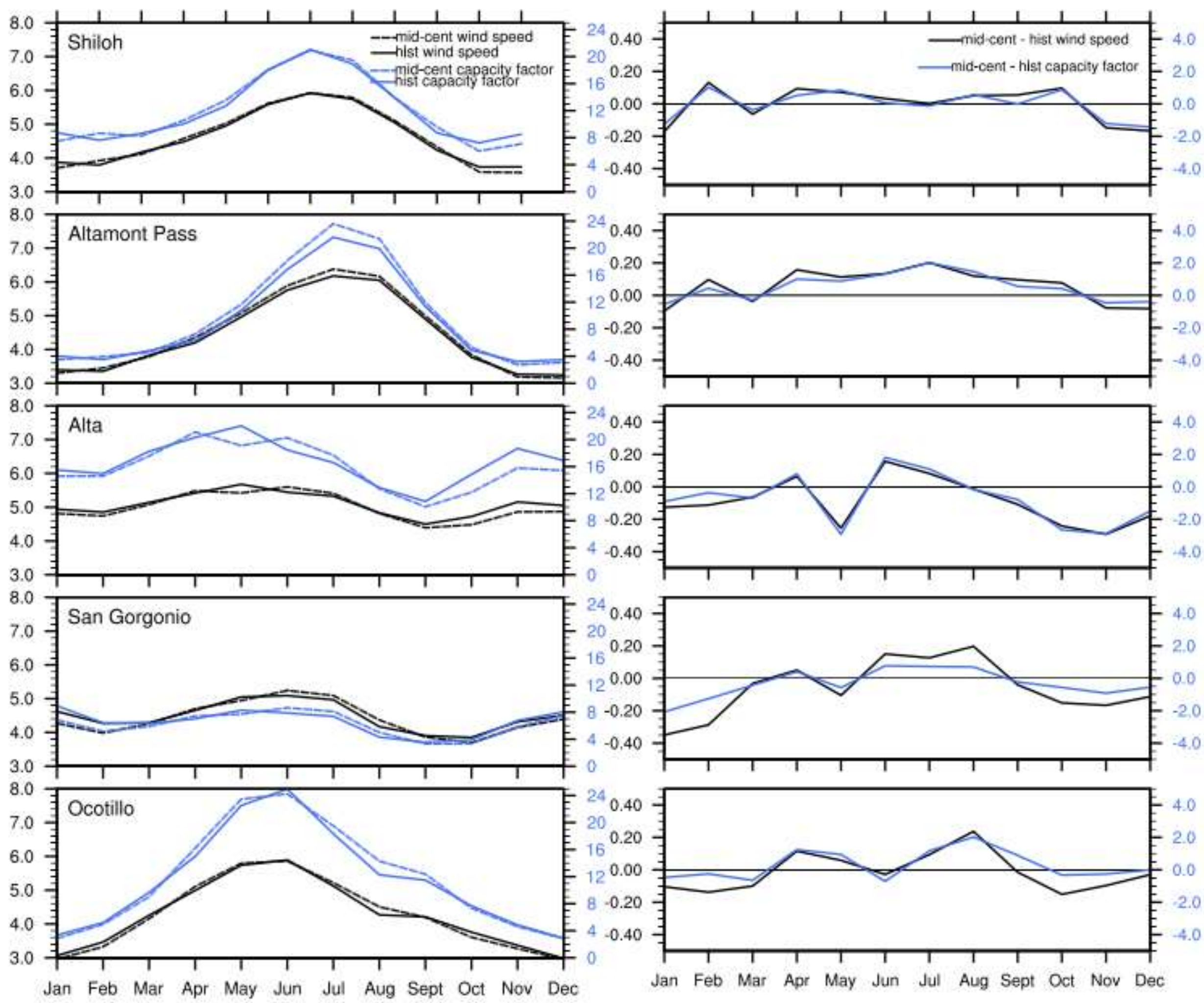

The left column shows the absolute values by month; the right column shows the change in values from the historical period by month.

Source: Lawrence Berkeley National Laboratory

An increase in the frequency of lower wind speeds during SON and DJF seasons indicates the decreasing trend in wind speed through these two seasons. A decrease in the frequency of lower wind speeds during JJA and an increase in the frequency of higher wind speeds indicate the increasing trend in wind speed during this season. Figure 18 depicts the differences in frequency between seasonal 80 m wind speeds over the historical and midcentury periods from VR-CESM. The bold lines in Figure 18 correspond to the seasons with significant CF changes from Table 4.

Table 4: Seasonal and Annual Capacity Factor Changes at Each Wind Farm Under Midcentury 2030-2050 Compared to Historical 1980-2000

Wind Farm	MAM	JJA	SON	DJF	Annual
Shiloh	+ 0.2%	+ 0.4%	− 7.7%	− 5.8%	− 3.2%
Altamont Pass	+ 4.2%	**+ 7.5%**	− 4.5%	− 0.9%	+ 1.6%
Alta	− 5.1%	+ 8.3%	**− 13.3%**	− 7.3%	− 4.4%
San Gorgonio	− 2.4%	**+ 9.7%**	**− 10.9%**	**− 16.9%**	− 5.1%
Ocotillo	+ 1.6%	+ 5.6%	− 2.0%	− 9.0%	− 1.0%

Mid-Century CF Minus Historical CF, divided by Historical CF, and written as a percentage at each wind farm site. Bold face indicates a percentage change above the 95% significance level.

Source: Lawrence Berkeley National Laboratory

4.2.2 Synoptic-Scale Drivers

As mentioned earlier, synoptic-scale fields are associated with horizontal scales on the order of 1,000 km or more. To identify the synoptic-scale drivers that could influence the historical and midcentury wind climatology, the research team analyzed the mean meteorological fields from the VR-CESM simulations for seasons with significant CF changes (JJA in Figure 19, SON in Figure 20, DJF in Figure 21). In particular, the analysis focuses on the 700hPa geopotential height field, which is defined as the height of 700hPa isobar surfaces above mean sea level, as well as surface pressure, surface temperature, and hub-height wind field at 80m. In particular, the 700hPa geopotential height field was analyzed as it reflects the general circulation, with wind flow at this level largely following constant geopotential contours. The surface pressure field also impacts local wind speeds and is closely associated with surface temperature changes. Synoptic-scale fields during the MAM season were not investigated, as there was no significant CF change detected over this period (Table 4).

Figure 18: Differences in Frequencies Between Midcentury 2030-2050 and Historical 1980-2000 at Each Wind Farm Location

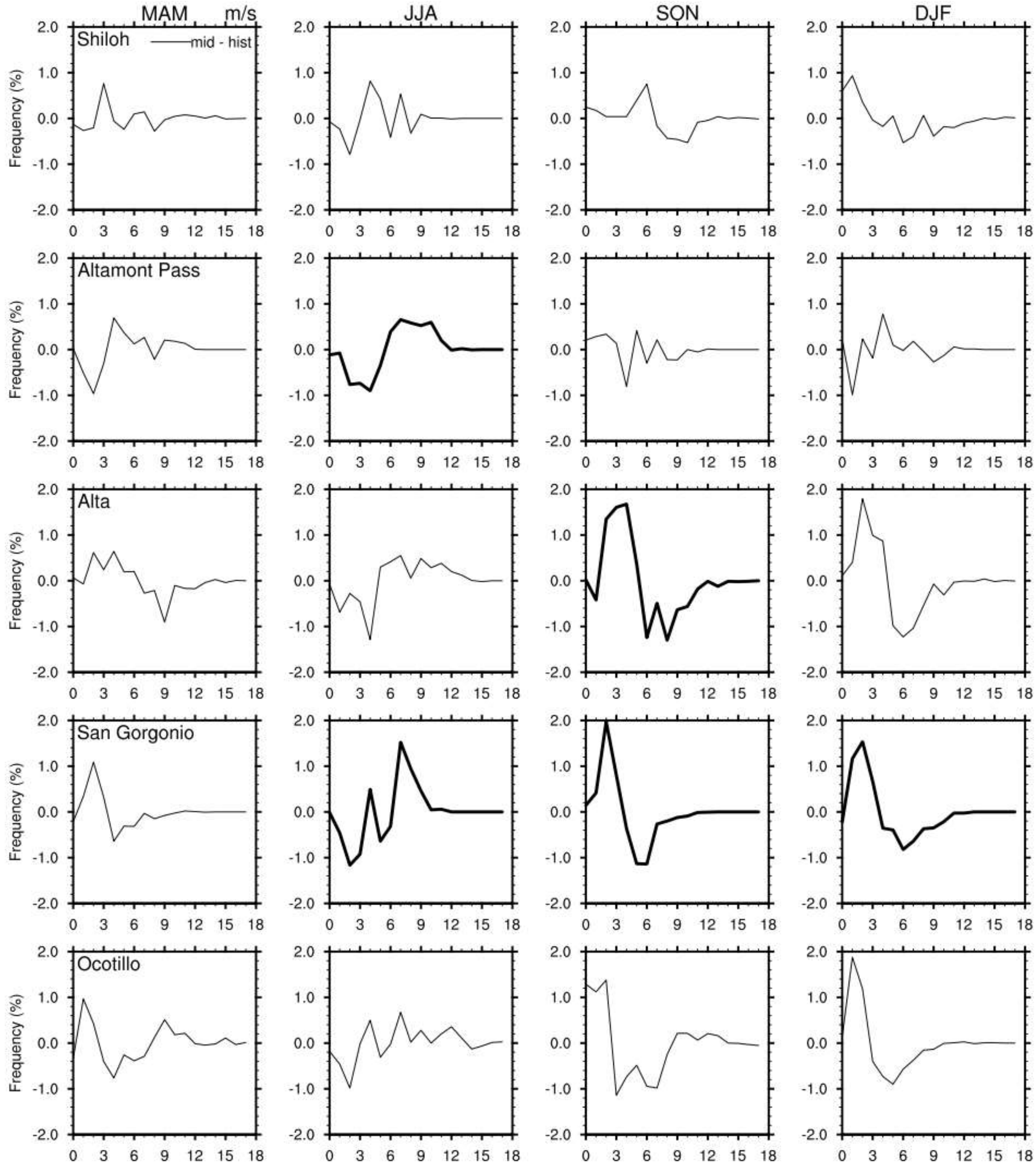

Midcentury Minus Historical for seasonal Averaged 80 m wind speed from VR-CESM at each wind farm location. Bold lines correspond to significant changes from Table 4. The x-axis is in units of m s^{-1}.

Source: Lawrence Berkeley National Laboratory

Through JJA (Figure 19), the 700hPa geopotential height field features an offshore trough and geopotential height contour lines perpendicular to coast. This pattern indicates a typical summertime marine air penetration condition (Fosberg et al. 1966, Beaver et al. 2006, Wang et al. 2018b) and is driven by the offshore trough modifying the geopotential height contour lines to be perpendicular to the coastline, allowing cool and moist marine air to penetrate inland. The location of the offshore trough is directly responsible for driving marine air through the San Francisco Bay Delta. Relative to the historical period, the magnitude of the 700hPa geopotential height field under the midcentury increases (as a direct consequence of low-level warming). However, this increase is less pronounced over the Northern Pacific, which drives a weakening of the typically northerly wind pattern that traces the coastline in Northern and Central California, and an increase in the onshore flow pattern driven by the general circulation. This in turn leads to an increase in wind speeds through the San Francisco Delta region (Shiloh and Altamont Pass in the Central California domain). A shift in this synoptic-scale pattern also drives increased ventilation in the Southern California domain.

Surface pressure in JJA is also observed to increase more rapidly at higher altitudes; consequently, the surface pressure in the Mojave Desert increases more rapidly than the Central Valley and leads to a weaker pressure gradient between the Central Valley and the Mojave Desert. A similar observation was made by (Miller et al. 2006) to explain a projected decrease in Santa Ana wind events in this region during the fall. Although this is a potential driver for wind speed decrease at Alta in Southern California, the impact of a reduced pressure gradient is counterbalanced by the changes to the large-scale geopotential height field, which enhances westerly winds throughout California.

Figure 19: JJA Season

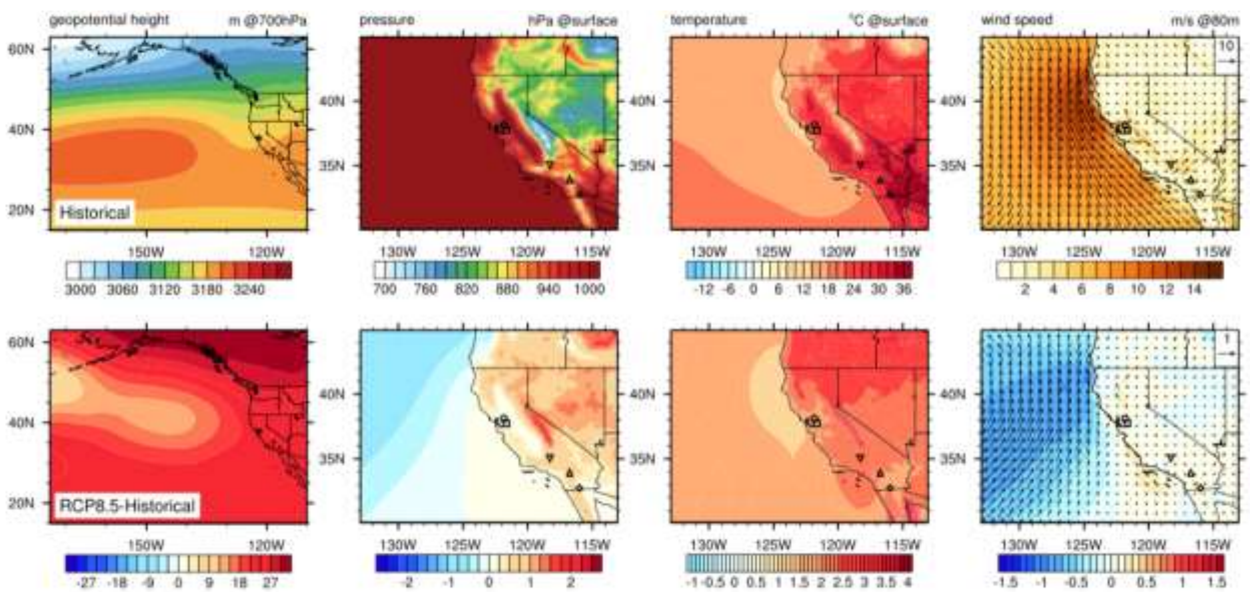

Season Seasonal Mean 700hpa Geopotential Height, Surface Pressure, Surface Temperature, and 80 m Wind Fields on Historical 1980-2000 (Top Row), and the Corresponding Anomaly Fields on Midcentury 2030-2050 (Bottom Row) During JJA Season. Anomaly values (bottom row) were calculated from subtracting mean historical fields (top row) from mean midcentury fields.

Source: Lawrence Berkeley National Laboratory

Figure 20: SON Season

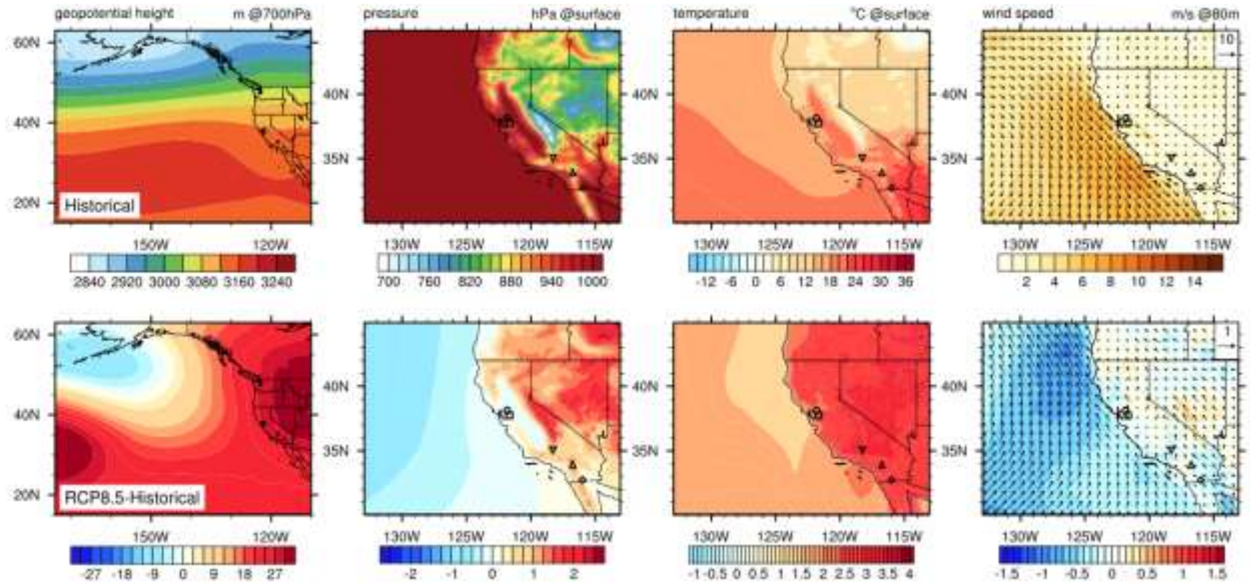

Seasonal Mean 700hpa Geopotential Height, Surface Pressure, Surface Temperature, and 80 m Wind Fields on Historical 1980-2000 (Top Row) and the Corresponding Anomaly Fields on Midcentury 2030-2050 (Bottom Row) During SON Season

Source: Lawrence Berkeley National Laboratory

Figure 21: DJF Season

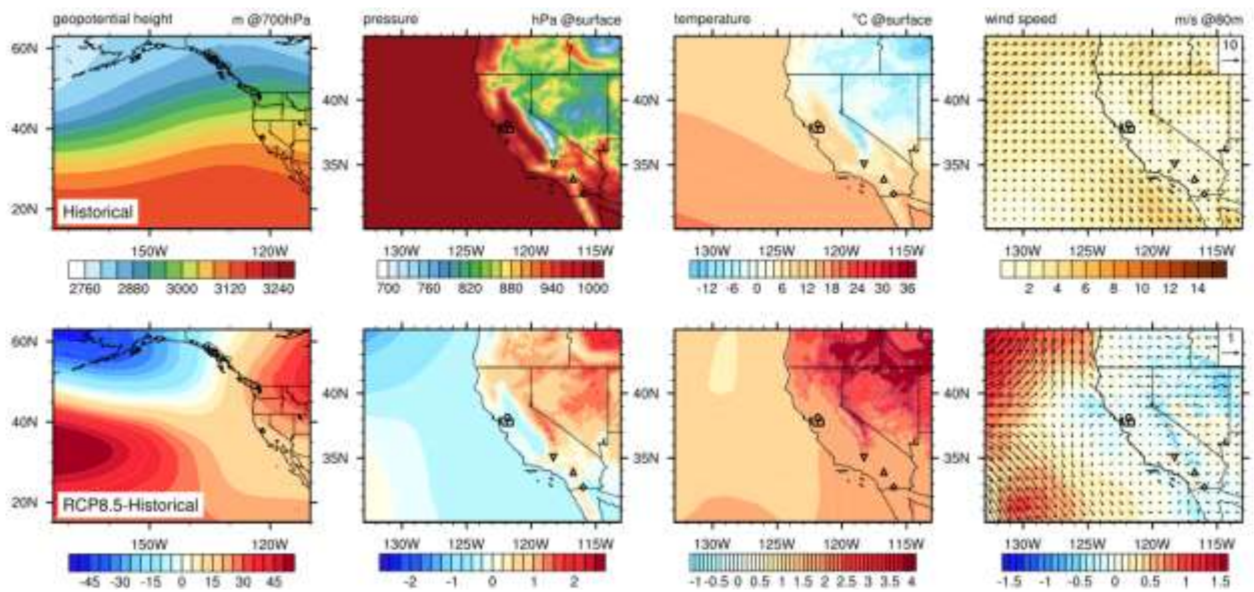

Seasonal Mean 700hpa Geopotential Height, Surface Pressure, Surface Temperature, and 80 m Wind Fields on Historical 1980-2000 (Top Row) and the Corresponding Anomaly Fields on Midcentury 2030-2050 (Bottom Row) During DJF Season

Source: Lawrence Berkeley National Laboratory

Across both periods, SON wind speeds are generally reduced compared to JJA, partly due to the decrease in land-sea temperature contrast and associated reduction to marine air penetration.

Comparing the 700hPa geopotential height field between historical and midcentury during SON (Figure 20), the entire California coast is under the influence of the weakening of wind flow parallel to the coast, driven by the negative geopotential anomaly south of Alaska and accompanied by a positive geopotential height anomaly over the continent. Through the Southern California domain, a weakening pressure gradient drives a decrease in the wind speed at Alta and San Gorgonio. This observation is in agreement with the observations of (Duffy et al. 2014), and leads to a projected 10-15% power potential decrease during the fall in midcentury near Tehachapi.

Through DJF (Figure 21), increased geopotential height over the subtropical western Pacific and the North American continent leads to a weaker northerly flow parallel to the coast and a reduced onshore flow. Further, with surface pressure decreases in the Central Valley, the surface-level pressure gradient between the Central Valley and the Mojave Desert decreases, which would, in turn be expected to drive lower wind speeds at the Alta wind farm site. The surface pressure gradient also decreases between the inland area and the ocean near the San Gorgonio wind farm site, which enhances the wind speed decrease.

The seasonal meteorological patterns under the midcentury RCP8.5 scenario provide further evidence that future changes of wind energy in California will be influenced by both the synoptic-scale and local changes. Overall, the synoptic analysis suggests that the climate through midcentury will be conducive to higher wind speeds across California during JJA (5-10% at four of the five sites examined) and lower wind speeds during SON (particularly at Alta and San Gorgonio, each of which exhibited a > 10% decrease) and DJF (with a 17% decrease at San Gorgonio). The changes to the surface pressure gradient between the Central Valley and the Mojave Desert appear robust across seasons and are a primary driver of wind speed decreases in the Southern California domain. To ensure the synoptic-scale climatology of VR-CESM was not an outlier, the research team also examined synoptic-scale geopotential height fields across CMIP5 models over the same period, and similar trends were observed.

4.3 Conclusions Related to Climate Change Impact on Wind Resources

Based on the historical record, California may already be seeing impacts of climate change on wind resources. Specifically, the frequencies of certain wind regimes over the period 1980 - 2015, specifically those associated hot summer conditions and nonsummer dead days, were increasing at a rate of roughly one-half and one-fourth day per year (Figure 15), respectively. The changes to the frequencies of these regimes did not produce a detectable impact in the time series of total seasonal or annual generation. However, if the patterns of change continue, total generation potential will likely be affected.

Looking forward with the VR-CESM model, the research team found significant seasonal changes in the available wind resource at most sites, with an increase in summertime (JJA) resources and a decrease in fall (SON) and winter (DJF) under RCP8.5 at all five sites (Table 4). The team also identified synoptic-scale and localized drivers behind seasonal wind energy change, suggesting that climate change may favor synoptic patterns that lead to higher wind speed during JJA and lower wind speed during SON and DJF. Overall, this study improves the characterization of uncertainty around the magnitude and variability in space and time of California’s wind resources in the near future, and enhances the general understanding of the physical mechanisms related to the trends in wind resource variability.

CHAPTER 5: Conclusions and Recommended Future Actions and Research

Wind energy resources vary across all time scales. Understanding how wind resources may vary across the life of a particular wind project is critical to supporting wind development and wind integration. The research team designed this project to provide new insight into how wind resources vary from season to season and year to year. This project examined the longer-term drivers of wind variability, such as climate mode impacts at seasonal time scales and climate change impacts at decadal periods. Moreover, the project investigated daily variations in wind patterns in the historical record and examined what differentiated high wind resource years from low wind resource years.

The project was designed with two broad goals: to provide new information about wind energy variation at five specific locations across California and to develop new methods and techniques that can enhance the understanding of wind resource variability everywhere.

5.1 Key Findings and Implications for Wind Energy Investment Risk

5.1.1 Historical Variability in California Wind Resources

The research team analyzed the historical variability in California wind resources over the period 1980 – 2015. This analysis was based on the Virtual met product, which provided hourly hub-height wind fields, resolved to a 4-km resolution, across California.

To develop new insight into historical variability patterns, the research team grouped together and categorized days with similar wind regimes. This daily categorization allowed for the identification of wind resources patterns that could not be seen by analyzing bulk seasonal and annual trends. The team achieved this categorization by extending and adapting statistical clustering techniques described in previous literature and discussed in Chapter 2, and applying the techniques to the Virtual met product. As will be outlined in Section 5.2, these clustering methods have great potential to help improve and contribute to the development of new applications that could be used by grid operators, planners, and project developers to understand and forecast wind variability across a variety of temporal scales.

For this analysis, California was split into two domains – one focused on Central California and one focused on Southern California. Ten typical daily wind regimes were defined for each domain using the clustering technique mentioned above. Each of these wind regimes was found to be associated with a distinct meteorological pattern at the synoptic scale (horizontal scale of >1,000 km). Also, each wind regime was found to be associated with distinct diurnal patterns at each of the five sites of focus. Thus, the clustering method allowed direct links to be made from the synoptic-scale meteorological patterns to regional wind patterns and to site-level diurnal wind cycles. The ability to readily, and intuitively, link site-level wind patterns to larger-scale wind and meteorological fields could be useful in many applications, as will be detailed in Section 5.2.

Although 10 wind regimes were identified at each domain, the amount of potential wind energy was different under each regime and at each of the five sites of focus. For example, some of the sites depended on only a few wind regimes for most of the energy generation, while other sites depended on a larger set for most of the energy generation. The report describes differences among sites. The identification of cluster types (wind regimes) allows for this type of characterization in general and for the development of an intuitive link between observable weather phenomena and site-level wind energy production patterns.

The clustering framework was used to compare the top wind years to the bottom wind years. At multiple sites, dramatic differences in total potential energy generation (and thus project-level revenue) were found between top and bottom years (with the least difference being found at Alta, where the best year was ~20 percent greater than the worst year, while the best year at Ocotillo, the site with the largest difference, was almost 50 percent greater than the worst year). The research team investigated the drivers of these differences by examining changes to the frequency of the wind regimes during the top and bottom years. The team also analyzed within-cluster wind speed differences between top and bottom years. At each focus site, the team identified unique changes to the frequency and/or the wind speed intensity of certain wind regimes. This identification allowed the linkage of low and high wind years to patterns in regional and synoptic-scale meteorological patterns. This is the first step in developing a chain of causality describing why certain years provide low wind resources (e.g., if one knows what synoptic-scale patterns occur more frequently in low wind years, one could investigate what causes those synoptic scale patterns to occur). Thus, this is also the first step in developing the ability to forecast the likelihood of an upcoming strong or weak wind resource year for a particular site.

Finally, the research team analyzed the impact of climate mode on wind energy generation at each site of focus. While climate mode indices were not correlated directly with total monthly wind generation, climate modes were correlated with the frequency of certain wind regimes and, therefore, were correlated with the submonthly patterns of wind generation. Thus, near-term prediction of wind resources by grid operators could benefit from including the impacts of climate mode on wind regimes. On longer time scales, research of climate change impacts could also benefit by accounting for changes to wind patterns associated with climate mode, as climate change could potentially affect wind resources through multiple pathways, including through changing the frequency and intensity of climate modes.

5.1.2 Climate Change and California Wind Resources

The research team analyzed climate change impacts on California wind resources using two methods. The first method was to examine long-term trends in the historical wind records within Virtual met. The second approach was to develop a high-resolution global climate simulation to simulate midcentury changes to future wind resources in California. This simulation was achieved using the state-of-the-art VR-CESM model. This model allows for a high-resolution representation of California (~14 km) with a seamless connection to coarser representation of the globe (1°). This research is the first time such a model was used explicitly to examine climate change impacts to California wind resources.

Based on the historical record, California may already be seeing impacts of climate change on wind resources. Specifically, the frequency of certain wind regimes in Central California, those associated with hot summer conditions and nonsummer dead days, were increasing at a rate of roughly one-half and one-fourth day per year, respectively. The changes to the frequency of these regimes did not produce a detectable impact in the time series of total seasonal or annual generation. However, if the patterns of change continue, total generation potential will likely be affected.

Looking forward with the VR-CESM model, significant seasonal changes were found in the available wind resource at most sites, with an increase in summertime (JJA) resources and a decrease in fall (SON) and winter (DJF) under RCP8.5 at all five sites (Table 4). Synoptic-scale and localized drivers behind season wind energy change were also identified, and suggested climate change may favor synoptic patterns that lead to higher wind speed during JJA and lower wind speed during SON and DJF.

This finding (directly above) was particularly interesting in that all the focus sites indicated change in the same direction during certain seasons. This finding, combined with the explicit analysis of synoptic-scale patterns, suggested that the VR-CESM simulations indicate climate change may alter the statewide patterns of ventilation (usually onshore flow) and impact wind generation across the state. A limitation here is that this simulation may not agree with forecasts produced by other models. However, by identifying the specific changes to future synoptic conditions, this work provides a useful starting point for comparisons across models that can provide more useful information than simply comparing the average changes to modeled future wind resources at individual locations. (See Section 5.2 for additional discussion.)

Overall, this study improves the characterization of uncertainty around the magnitude and variability in space and time of California's wind resources in the near future and enhances the understanding of the physical mechanisms related to the trends in wind resource variability. Most importantly, the simulation forecasts non-negligible changes to future wind resources and, thus, highlights the need for future research on this topic.

5.2 Future Research Directions

The results and methods presented in this report suggest applications and research directions that could be developed or improved.

First, researchers could refine the general practice of measure-correlate-predict (MCP) with clustering methods. Analysts perform MCP during the site evaluation of project development by linking short-run site-level wind measurements to an available, hopefully nearby, longer-run record of wind speeds. Researchers could refine MCP using information from the clustering methods described here, with the first step being to test whether developing separate relationships between the time-series during each cluster can improve the accuracy of MCP.

Related to MCP is the more general technique of statistical downscaling (estimating local meteorological conditions based on large-scaler observations or modeled conditions). Researchers could adapt portions of the methods described here and test them for the ability to refine downscaling techniques.

Second, researchers could develop wind power forecasts based on the link between large-scale meteorological fields, cluster type, and site-level wind resources. To the extent that synoptic-scale meteorological patterns can be easily observed and predicted, this approach could allow for low-cost wind power forecasts. Additional machine-learning techniques could be applied to refine the forecasting approach. Information regarding climate mode could also be integrated into these approaches.

Third, researchers could test whether the clustering techniques described here can help identify conditions that give rise to extreme wind events, significant ramp events, or other types of operational or system wide stress events. Beyond these wind power-focused events, scientists could apply these techniques to efforts that maximize transmission capacity dynamically based on line cooling by wind, or to research related to air quality or wildfire forecasting.

Finally, researchers could improve projections of wind resources under climate change. Additional, independent high-resolution modeling could be developed to assess future resource change, and specifically, synoptic-scale patterns could be analyzed to determine what type of large-scale changes are predicted across modeling platforms. Clustering of climate forecasts could also be used to determine what types of changes are expected to regional wind regimes.

5.3 Benefits to California

This project offers several specific benefits to California, as well as more general advances in scientific methodology.

- This report provides a new, and publicly available, assessment of the historical wind resource variability at five important wind power development sites in California—Shiloh and Altamont Pass in the north and Alta, San Gorgonio, and Ocotillo in the south.
- This report provides new predictions of changes to wind resource at the same five sites and provides analysis of changes to larger-scale synoptic conditions, all based on a state-of-the-art, high-resolution climate model. Energy planners, wind energy developers, and investors can all benefit from this information. Moreover, the changes predicted here can provide needed context for additional research on climate change impacts on wind resources.
- These clustering methods have great potential to help improve and contribute to the development of new applications that could be used to understand and forecast wind variability across a variety of temporal scales. For instance, this study could improve electricity supply forecasting for grid management or inform long-term energy planning by refining wind projections.

- This project developed new methods for assessing wind variability and for classifying wind patterns across California. These methods can be applied in all wind project locations. By reducing the uncertainty in wind energy projections, this approach can reduce risk to investors and lead to greater investment in this low-carbon energy source.
- The methods developed in this project may seed further research to continue improving wind forecasting and longer-term projections as described in section 5.2.

Overall, this work furthers the scientific understanding of wind resource variability over many time scales. As the science and understanding of these topics are improved, the precision with which wind resources can be forecast will improve, which will lower the risk, and associated costs, of developing wind power. This cost reduction will benefit electricity consumers and developers. Furthermore, as these lower costs allow wind power to serve a greater portion of power generation needs within the state and elsewhere, all of California would benefit from reduced emissions of local pollutants and greenhouse gases.

ACRONYMS AND ABBREVIATIONS

Term	Definition
EPIC	Electric Program Investment Charge
AF	Annual fraction, $days_i$/days-per-year, of cluster i
AGL	Above ground level
AO	Arctic Oscillation
BC VR-CESM	bias-corrected VR-CESM
C (as in C1 or C7)	Indicates the Central California domain and the associated cluster number
CAM5	Community Atmosphere Model, Version 5.3
CF	Capacity factor
CF (and –top, -bottom, -freq, and –wind	Capacity factor
CF-bottom	The average CF at a site during the bottom five windiest years
CF-freq	The hypothetical CF based on the wind intensity of the top five years but the cluster distribution of the bottom five years
CF-top	The average CF at a site during the top five windiest years
CF-wind	The hypothetical CF based on the cluster distribution of the top five years but the wind intensity of the bottom five years
CFSR	Climate Forecast System Reanalysis
CLM	Community Land Model
DNV GL	Det Norske Veritas Germanischer Lloyd
ENSO	El Niño Southern Oscillation
FAMPIC5	Within the VR-CESM simulations, FAMPIC5 is the F-component set, which prescribes sea surface temperatures and sea ice but dynamically evolves the atmosphere and land surface component models
GEOS-50	Goddard Earth Observing System Data Assimilation System Version 5
GHG	Greenhouse gas
GMAO	Global Modeling and Assimilation Office at NASA

hPA	Hectopascals (hPa) unit, equal to 100 pascals or 1 millibar
IEC	International Electrotechnical Commission
ISD	Integrated Surface Database
MAM, JJA, SON, and DJF	March-April-May, June-July-August, September-October-November, and December-January-February
MCP	Measure-correlate-predict
MERRA-2	Modern-Era Retrospective Analysis for Research and Applications, Version 2
NAO	North Atlantic Oscillation
NARR	North American Regional Reanalysis
NASA	National Aeronautics and Space Administration
NCEP	National Centers for Environmental Prediction
NERSC	U.S. Department of Energy National Energy Research Scientific Computing Center
NKX	Miramar (airport code NKX)
OAK	Oakland (airport code OAK)
PCA	Principal components analysis
PDO	Pacific Decadal Oscillation
PNA	Pacific North American pattern
RCP8.5	Representative Concentration Pathway 8.5 -- a "business-as-usual" scenario
RMSE	Root-mean-squared error
S (as in S1 or S7)	Indicates the Southern California domain and the associated cluster number
SB 350	California Senate Bill 350: Clean Energy and Pollution Reduction Act
VBG	Vandenberg (airport code VBG)
VR-CESM	Variable-Resolution Community Earth System Model
WIND	Wind Integration National Dataset
WRF	Weather Research and Forecasting model

REFERENCES

Albadi, M. and E. El-Saadany (2010). "Overview of Wind Power Intermittency Impacts on Power Systems." *Electric Power Systems Research* **80**(6): 627-632.

Archer, C. L. and M. Z. Jacobson (2003). "Spatial and Temporal Distributions of U.S. Winds and Wind Power at 80 m Derived from Measurements." *Journal of Geophysical Research: Atmospheres* **108**(D9).

Archer, C. L., H. P. Simão, W. Kempton, W. B. Powell and M. J. Dvorak (2017). "The Challenge of Integrating Offshore Wind Power in the U.S. Electric Grid. Part I: Wind Forecast Error." *Renewable Energy* **103**(Supplement C): 346-360.

Bailey, B. and J. Kunkel (2015). "The Financial Implications of Resource Assessment Uncertainty." *North American Windpower*. **12**.

Barbose, G. L., N. R. Darghouth, D. Millstein, K. LaCommare, N. DiSanti and R. Widiss (2017). *Tracking the Sun 10: The Installed Price of Residential and Non-Residential Photovoltaic Systems in the United States.*

Beaver, S. and A. Palazoglu (2006). "Cluster Analysis of Hourly Wind Measurements to Reveal Synoptic Regimes Affecting Air Quality." *Journal of Applied Meteorology and Climatology* **45**(12): 1710-1726.

Beaver, S. and A. Palazoglu (2009). "Influence of Synoptic and Mesoscale Meteorology on Ozone Pollution Potential for San Joaquin Valley of California." *Atmospheric Environment* **43**(10): 1779-1788.

Bedsworth, L., D. Cayan, G. Franco, L. Fisher, and S. Ziaja. (2018). *California's Fourth Climate Change Assessment. Statewide Summary Report.* California Governor's Office of Planning and Research, Scripps Institution of Oceanography, California Energy Commission, California Public Utilities Commission. SUM-CCCA4-2018-013.

Berg, N., A. Hall, S. B. Capps and M. Hughes (2013). "El Niño-Southern Oscillation Impacts on Winter Winds Over Southern California." *Climate Dynamics* **40**(1-2): 109-121.

Bolinger, M. (2017). *Using Probability of Exceedance to Compare the Resource Risk of Renewable and Gas-Fired Generation.*

Bolinger, M., J. Seel and K. H. LaCommare (2017). Utility-Scale Solar 2016: *An Empirical Analysis of Project Cost, Performance, and Pricing Trends in the United States*. Lawrence Berkeley National Lab.(LBNL), Berkeley, CA (United States).

Carta, J. A., S. Velázquez and P. Cabrera (2013). "A Review of Measure-Correlate-Predict (MCP) Methods Used to Estimate Long-Term Wind Characteristics at a Target Site." *Renewable and Sustainable Energy Reviews* **27**: 362-400.

Carvalho, D., A. Rocha, M. Gómez-Gesteira and C. S. Santos (2014). "WRF Wind Simulation and Wind Energy Production Estimates Forced by Different Reanalyses: Comparison With Observed Data for Portugal." *Applied Energy* **117**: 116-126.

Chadee, X. T. and R. M. Clarke (2015). "Daily Near-Surface Large-Scale Atmospheric Circulation Patterns Over the Wider Caribbean." *Climate Dynamics* **44**(11-12): 2927-2946.

Clifton, A. and J. K. Lundquist (2012). "Data Clustering Reveals Climate Impacts on Local Wind Phenomena." *Journal of Applied Meteorology and Climatology* **51**(8): 1547-1557.

Cochrane, D. and G. H. Orcutt (1949). "Application of Least Squares Regression to Relationships Containing Auto-Correlated Error Terms." *Journal of the American Statistical Association* **44**(245): 32-61.

Conil, S. and A. Hall (2006). "Local Regimes of Atmospheric Variability: A Case Study of Southern California." *Journal of Climate* **19**(17): 4308-4325.

Darby, L. S. (2005). "Cluster Analysis of Surface Winds in Houston, Texas, and the Impact of Wind Patterns on Ozone." *Journal of Applied Meteorology* **44**(12): 1788-1806.

Dawson, J. P., B. J. Bloomer, D. A. Winner and C. P. Weaver (2014). "Understanding the Meteorological Drivers of U.S. Particulate Matter Concentrations in a Changing Climate." *Bulletin of the American Meteorological Society* **95**(4): 521-532.

Delle Monache, L., F. A. Eckel, D. L. Rife, B. Nagarajan and K. Searight (2013). "Probabilistic Weather Prediction With an Analog Ensemble." *Monthly Weather Review* **141**(10): 3498-3516.

Delle Monache, L., T. Nipen, Y. Liu, G. Roux and R. Stull (2011). "Kalman Filter and Analog Schemes to Postprocess Numerical Weather Predictions." *Monthly Weather Review* **139**(11): 3554-3570.

Dennis, J. M., J. Edwards, K. J. Evans, O. Guba, P. H. Lauritzen, A. A. Mirin, A. St-Cyr, M. A. Taylor and P. H. Worley (2012). "CAM-SE: A Scalable Spectral Element Dynamical Core for the Community Atmosphere Model." *The International Journal of High Performance Computing Applications* **26**(1): 74-89.

DOE (2015). *Wind Vision: A New Era for Wind Power in the United States*. DOE/GO-102015-4557. U.S. Department of Energy, Washington, DC.

Draxl, C., A. Clifton, B.-M. Hodge and J. McCaa (2015). "The Wind Integration National Dataset (WIND) Toolkit." *Applied Energy* **151**: 355-366.

Duffy, P. B., J. Bartlett, J. Dracup, J. Freedman, K. Madani and K. Waight (2014). *Climate Change Impacts on Generation of Wind, Solar, and Hydropower in California*. Publication # CEC-500-2014-111. California Energy Commission.

Fosberg, M. A. and M. J. Schroeder (1966). "Marine Air Penetration in Central California." *Journal of Applied Meteorology* **5**(5): 573-589.

Fripp, M. and R. H. Wiser (2008). "Effects of Temporal Wind Patterns on the Value of Wind-Generated Electricity in California and the Northwest." *IEEE Transactions on Power Systems* **23**(2): 477-485.

Gelaro, R., W. McCarty, M. J. Suárez, R. Todling, A. Molod, L. Takacs, C. A. Randles, A. Darmenov, M. G. Bosilovich and R. Reichle (2017). "The Modern-Era Retrospective Analysis for Research and Applications, Version 2 (MERRA-2)." *Journal of Climate* **30**(14): 5419-5454.

GES (2017a). Goddard Earth Sciences Data and Information Services Center. MERRA-2 inst1_2d_asm_Nx: 2d,1-hourly, instantaneous, single-level, assimilation, single-level diagnostics v5.12.4. DOI: 10.5067/ 3Z173KIE2TPD.

GES (2017b). Goddard Earth Sciences Data and Information Services Center. MERRA-2 inst3 3d asm Np: 3d,3-Hourly,Instantaneous,Pressure- Level,Assimilation,Assimilated Meteorological Fields V5.12.4. DOI: 10.5067/QBZ6MG944HW0.

Gibson, P. B. and N. J. Cullen (2015). "Synoptic and Sub-Synoptic Circulation Effects on Wind Resource Variability–A Case Study from a Coastal Terrain Setting in New Zealand." *Renewable Energy* **78**: 253-263.

Goddard, S. D., M. G. Genton, A. S. Hering and S. R. Sain (2015). "Evaluating the Impacts of Climate Change on Diurnal Wind Power Cycles Using Multiple Regional Climate Models." *Environmetrics* **26**(3): 192-201.

Gross, M. and V. Magar (2016). "Offshore Wind Energy Climate Projection Using UPSCALE Climate Data Under the RCP8. 5 Emission Scenario." *PloS one* **11**(10): e0165423.

Guba, O., M. Taylor, P. Ullrich, J. Overfelt and M. Levy (2014). "The Spectral Element Method on Variable Resolution Grids: Evaluating Grid Sensitivity and Resolution-Aware Numerical Viscosity." *Geosci. Model Dev. Discuss* **7**: 4081-4117.

Haupt, S. E., J. Copeland, W. Y. Cheng, Y. Zhang, C. Ammann and P. Sullivan (2016). "A Method to Assess the Wind and Solar Resource and to Quantify Interannual Variability Over the United States Under Current and Projected Future Climate." *Journal of Applied Meteorology and Climatology* **55**(2): 345-363.

Horton, D. E., C. B. Skinner, D. Singh and N. S. Diffenbaugh (2014). "Occurrence and Persistence of Future Atmospheric Stagnation Events." *Nature Climate Change* **4**(8): 698-703.

Huang, X., A. M. Rhoades, P. A. Ullrich and C. M. Zarzycki (2016a). "An Evaluation of the Variable ‐ Resolution CESM for Modeling California's Climate." *Journal of Advances in Modeling Earth Systems* **8**(1): 345-369.

Huang, X. and P. A. Ullrich (2016b). "Irrigation Impacts on California's Climate With the Variable ‐ Resolution CESM." *Journal of Advances in Modeling Earth Systems* **8**(3): 1151-1163.

Hubbert, M. K. (1971). "The Energy Resources of the Earth." *Scientific American* **225**(3): 60-73.

Jacob, D. J. and D. A. Winner (2009). "Effect of Climate Change on Air Quality." *Atmospheric Environment* **43**(1): 51-63.

Jiménez, P. A., J. F. González ‐ Rouco, J. P. Montávez, E. García ‐ Bustamante and J. Navarro (2009). "Climatology of Wind Patterns in the Northeast of the Iberian Peninsula." *International Journal of Climatology* **29**(4): 501-525.

Jin, L., R. A. Harley and N. J. Brown (2011). "Ozone Pollution Regimes Modeled for a Summer Season in California’s San Joaquin Valley: A Cluster Analysis." *Atmospheric Environment* **45**(27): 4707-4718.

Justus, C. and A. Mikhail (1976). "Height Variation of Wind Speed and Wind Distributions Statistics." *Geophysical Research Letters* **3**(5): 261-264.

Karnauskas, K. B., J. K. Lundquist and L. Zhang (2017). "Southward Shift of the Global Wind Energy Resource Under High Carbon Dioxide Emissions." *Nature Geoscience*.

Leung, L. R. and W. I. Gustafson (2005). "Potential Regional Climate Change and Implications to U.S. Air Quality." *Geophysical Research Letters* **32**(16).

Li, X., S. Zhong, X. Bian and W. Heilman (2010). "Climate and Climate Variability of the Wind Power Resources in the Great Lakes Region of the United States." *Journal of Geophysical Research: Atmospheres* **115**(D18).

Ludwig, F. L., J. Horel and C. D. Whiteman (2004). "Using EOF Analysis to Identify Important Surface Wind Patterns in Mountain Valleys." *Journal of Applied Meteorology* **43**(7): 969-983.

Ma, J., G. R. Foltz, B. J. Soden, G. Huang, J. He and C. Dong (2016). "Will Surface Winds Weaken in Response to Global Warming?" *Environmental Research Letters* **11**(12): 124012.

McElroy, M. B., P. Sherman and X. Chen (2017). "Wind-Generated Electricity in China: Decreasing Potential, Inter-Annual Variability and Association With Changing Climate." *Scientific Reports* **7**(1): 16294.

Mesinger, F., G. DiMego, E. Kalnay, K. Mitchell, P. C. Shafran, W. Ebisuzaki, D. Jović, J. Woollen, E. Rogers and E. H. Berbery (2006). "North American Regional Reanalysis." *Bulletin of the American Meteorological Society* **87**(3): 343-360.

Mickley, L. J., D. J. Jacob, B. Field and D. Rind (2004). "Effects of Future Climate Change on Regional Air Pollution Episodes in the United States." *Geophysical Research Letters* **31**(24).

Miller, N. L. and N. J. Schlegel (2006). "Climate Change Projected Fire Weather Sensitivity: California Santa Ana Wind Occurrence." *Geophysical Research Letters* **33**(15).

Millstein, D., R. Wiser, M. Bolinger and G. Barbose (2017). "The Climate and Air-Quality Benefits of Wind and Solar Power in the United States." *Nature Energy* **2**(9): 17134.

Millstein, D., Solomon-Culp, J., Wang, M., Ullrich, P. and C. Collier, (2018) "Wind energy variability and links to regional and synoptic scale weather." *Climate Dynamics*. https://doi.org/10.1007/s00382-018-4421-y.

Neale, R. B., C.-C. Chen, A. Gettelman, P. H. Lauritzen, S. Park, D. L. Williamson, A. J. Conley, R. Garcia, D. Kinnison and J.-F. Lamarque (2010). "Description of the NCAR Community Atmosphere Model (CAM 5.0)." *NCAR Tech. Note NCAR/TN-486+ STR* **1**(1): 1-12.

NOAA. (2017a, 08/08/2017). "Arctic Oscillation (AO)." from https://www.ncdc.noaa.gov/teleconnections/ao/.

NOAA. (2017b, 08/08/2017). "Historical El Niño/La Niña Episodes (1950-present) ", from http://origin.cpc.ncep.noaa.gov/products/analysis_monitoring/ensostuff/ONI_v5.php.

NOAA. (2017c, 08/08/2017). "North Atlantic Oscillation (NAO)." from https://www.ncdc.noaa.gov/teleconnections/nao/.

NOAA. (2017d, 08/08/2017). "Pacific Decadal Oscillation (PDO)." from https://www.ncdc.noaa.gov/teleconnections/pdo/.

NOAA. (2017e, 08/08/2017). "Pacific-North American (PNA)." from https://www.ncdc.noaa.gov/teleconnections/pna/.

Pedregosa, F., G. Varoquaux, A. Gramfort, V. Michel, B. Thirion, O. Grisel, M. Blondel, P. Prettenhofer, R. Weiss and V. Dubourg (2011). "Scikit-Learn: Machine Learning in Python." *Journal of Machine Learning Research* **12**(Oct): 2825-2830.

Pryor, S. and R. Barthelmie (2011). "Assessing Climate Change Impacts on the Near-Term Stability of the Wind Energy Resource Over the United States." *Proceedings of the National Academy of Sciences* **108**(20): 8167-8171.

Pryor, S. and R. Barthelmie (2013). "Assessing the Vulnerability of Wind Energy to Climate Change and Extreme Events." *Climatic Change* **121**(1): 79-91.

Pryor, S., R. Barthelmie and E. Kjellström (2005). "Potential Climate Change Impact on Wind Energy Resources in Northern Europe: Analyses Using a Regional Climate Model." *Climate Dynamics* **25**(7-8): 815-835.

Rasmussen, D., T. Holloway and G. Nemet (2011). "Opportunities and Challenges in Assessing Climate Change Impacts on Wind Energy—A Critical Comparison of Wind Speed Projections in California." *Environmental Research Letters* **6**(2): 024008.

Rhoades, A. M., X. Huang, P. A. Ullrich and C. M. Zarzycki (2016). "Characterizing Sierra Nevada Snowpack Using Variable-Resolution CESM." *Journal of Applied Meteorology and Climatology* **55**(1): 173-196.

Rhoades, A. M., P. A. Ullrich and C. M. Zarzycki (2018). "Projecting 21st Century Snowpack Trends in Western USA Mountains Using Variable-Resolution CESM." *Climate Dynamics* **50**(1-2): 261-288.

Rienecker, M. M., M. J. Suarez, R. Gelaro, R. Todling, J. Bacmeister, E. Liu, M. G. Bosilovich, S. D. Schubert, L. Takacs and G.-K. Kim (2011). "MERRA: NASA's Modern-Era Retrospective Analysis for Research and Applications." *Journal of Climate* **24**(14): 3624-3648.

Saha, S., S. Moorthi, H. Pan, X. Wu, J. Wang, S. Nadiga, P. Tripp, R. Kistler, J. Woollen and D. Behringer (2010). "NCEP Climate Forecast System Reanalysis (CFSR) 6-Hourly Products, January 1979 to December 2010." *Research Data Archive at the National Center for Atmospheric Research, Computational and Information Systems Laboratory, Boulder, CO.*

Sailor, D. J., M. Smith and M. Hart (2008). "Climate Change Implications for Wind Power Resources in the Northwest United States." *Renewable Energy* **33**(11): 2393-2406.

Seefeldt, M. W., J. J. Cassano and T. R. Parish (2007). "Dominant Regimes of the Ross Ice Shelf Surface Wind Field During Austral Autumn 2005." *Journal of Applied Meteorology and Climatology* **46**(11): 1933-1955.

Segal, M., Z. Pan, R. W. Arritt and E. S. Takle (2001). "On the Potential Change in Wind Power Over the U.S. due to Increases of Atmospheric Greenhouse Gases." *Renewable Energy* **24**(2): 235-243.

Shimada, S., T. Ohsawa, S. Chikaoka and K. Kozai (2011). "Accuracy of the Wind Speed Profile in the Lower PBL as Simulated by the WRF Model." *Sola* **7**: 109-112.

Sun, W., P. Hess and C. Liu (2017). "The Impact of Meteorological Persistence on the Distribution and Extremes of Ozone." *Geophysical Research Letters* **44**(3): 1545-1553.

Taylor, K. E., R. J. Stouffer and G. A. Meehl (2012). "An Overview of CMIP5 and the Experiment Design." *Bulletin of the American Meteorological Society* **93**(4): 485-498.

Tindal, A. (2011). *Financing Wind Farms and the Impacts of P90 and P50 Yields*. EWEA Wind Resource Assessment Workshop.

Ullrich, P. (2014). "SQuadGen: Spherical Quadrilateral Grid Generator." from http://climate.ucdavis.edu/squadgen.php.

Wang, M., Ullrich, P. and D. Millstein (2018a) "The future of wind energy in California: Future projections with the Variable-Resolution CESM." *Renewable Energy* **127**: 242-257.

Wang, M. and P. Ullrich (2018b). "Marine Air Penetration in California's Central Valley: Meteorological Drivers and the Impact of Climate Change." *Journal of Applied Meteorology and Climatology* **57**: 137 - 154.

Ward Jr, J. H. (1963). "Hierarchical Grouping to Optimize an Objective Function." *Journal of the American Statistical Association* **58**(301): 236-244.

Wiser, R., M. Bolinger, G. Barbose, N. Darghouth, B. Hoen, A. Mills, J. Rand, D. Millstein, K. Porter, R. Widiss, N. Disanti, F. Oteri and S. Tegen (2017). *2016 Wind Technologies Market Report,* U.S. Department of Energy.

Xie, L., P. M. Carvalho, L. A. Ferreira, J. Liu, B. H. Krogh, N. Popli and M. D. Ilic (2011). "Wind Integration in Power Systems: Operational Challenges and Possible Solutions." *Proceedings of the IEEE* **99**(1): 214-232.

Yu, L., S. Zhong, X. Bian and W. E. Heilman (2015). "Temporal and Spatial Variability of Wind Resources in the United States as Derived from the Climate Forecast System Reanalysis." *Journal of Climate* **28**(3): 1166-1183.

Yu, L., S. Zhong, X. Bian and W. E. Heilman (2016). "Climatology and Trend of Wind Power Resources in China and Its Surrounding Regions: A Revisit Using Climate Forecast System Reanalysis Data." *International Journal of Climatology* **36**(5): 2173-2188.

Zaremba, L. L. and J. J. Carroll (1999). "Summer Wind Flow Regimes Over the Sacramento Valley." *Journal of Applied Meteorology* **38**(10): 1463-1473.

Zarzycki, C. M., C. Jablonowski, D. R. Thatcher and M. A. Taylor (2015). "Effects of Localized Grid Refinement on the General Circulation and Climatology in the Community Atmosphere Model." *Journal of Climate* **28**(7): 2777-2803.

Zarzycki, C. M., M. N. Levy, C. Jablonowski, J. R. Overfelt, M. A. Taylor and P. A. Ullrich (2014). "Aquaplanet Experiments Using CAM's Variable-Resolution Dynamical Core." *Journal of Climate* **27**(14): 5481-5503.

APPENDIX A: Data in Brief (VR-CESM).

This appendix includes the description of data information for hub-height wind-speed comparisons at multiple major wind farms across California. Datasets from the Variable-Resolution CESM, DNV GL Virtual met, MERRA-2, CFSR, NARR, ISD surface observations, and upper air sounding observations were used for calculating hub-height wind speed. Information on hub-height wind speed interpolation and power curves at each wind farm sites is also presented.

Data

The dataset reported in this article contains hub-height wind fields, with special focus on wind farms in California. Two modeling products, three reanalysis datasets, and two observational data are described in the article. The interpolation method for calculating hub-height wind speed is also presented in the article and can be applied to other studies. Power curves used for calculating wind energy capacity factors at each wind farm location are also provided.

Experimental Design, Materials, and Methods

VR-CESM (Global Climate Model Product)

Data provided in this article include two simulations using the Variable-Resolution CESM (VR-CESM) model. The CESM Version 1.5.5, a fully coupled atmospheric, land, ocean, and sea ice model, was utilized. Both simulations used the F-component set, which prescribes sea-surface temperatures and sea ice but dynamically evolves the atmosphere and land surface component models. The atmospheric component model is the Community Atmosphere Model, Version 5.3 (CAM5) (Neale et al. 2010) with the spectral-element (SE) dynamical core (Dennis et al. 2012) in the variable-resolution (VR) configuration. The VR model grid used for this study was generated for use in CAM and CLM with the open-source software package SQuadGen (Guba et al. 2014, Ullrich 2014). On this grid, the finest horizontal resolution is 0.125° (~14km), with a quasi-uniform 1° mesh over the remainder of the globe. Two simulations were conducted using this grid structure: First, the historical run covers the period from October 1, 1979, to December 31, 2000, with first three months discarded as the spin-up period, for a total of 21 years. This historical period was chosen to provide an adequate sampling of interannual variability, to coincide with the period from the rest of the modeling and reanalysis datasets, and because observed sea surface temperatures (which acted as boundary conditions for the simulation) were available only through 2005. For projecting future wind energy change, the research team's midcentury simulation ran with the "business-as-usual" Representative Concentration Pathway 8.5 (RCP8.5) (Taylor et al. 2012) from October 1, 2029, to December 31, 2050, again discarding the first three months for a total of 21 years. Greenhouse gas (GHG) and aerosol forcings are prescribed based on historical or RCP8.5 concentrations for each simulation. More details on VR-CESM can be found in Huang et al. (2016a) and Rhoades et al. (2016), and the model has been applied to previous studies (Rhoades et al. 2018, Wang et al. 2018b).

DNV GL Virtual Met (Dynamically downscaled Regional Model Product)

The DNV GL Virtual met product is derived from a hybrid dynamical-statistical downscaling system based upon the Weather Research and Forecasting (WRF) model and an analog-based ensemble downscaling method. A coarse resolution WRF simulation is run for the entire period to be downscaled, while for only a subset of that period, a nested version of the same model is run at high resolution. The period over which the coarse and high-resolution runs overlap is called the training period, while the remaining portion is termed downscaling period. For each time of the latter, the best matching coarse estimates (termed "analogs") over the training period are found. The downscaled solution is then constructed from the set of high-resolution values that correspond to the best matching coarse analogs. This method is based upon Delle Monache et al. (2011, 2013).

The WRF simulation used telescoping, one-way interacting computational grids. The respective horizontal grid increments are 20 km and 4 km, with the 4-km grid centered over California. The initial and lateral boundary conditions are specified using MERRA-2. The 20-km grid was run for the entire January 1, 1980 - December 31, 2015, period and generated output every hourly, while the nested 4 km grid was run only during the last year of the full simulation (January 1, 2015 to December 31, 2015). The high-resolution downscaled dataset is constructed for the entire 36-year period using the 4 km resolution training data and the 20-km simulation (both from the same WRF model configuration). The result is an hourly time series at each 4-km grid point for January 1, 1980, to December 31, 2015. Wind speed and direction at hub heights, including 50m, 80m, 140m, are output. DNV GL served solely as a data provider and is not responsible for any results from this data.

MERRA-2 (Reanalysis Product)

The Modern-Era Retrospective analysis for Research and Applications, Version 2 (MERRA-2) is a reanalysis product for the satellite era using the Goddard Earth Observing System Data Assimilation System Version 5 (GEOS-50) produced by Global Modeling and Assimilation Office (GMAO) at NASA (Gelaro et al. 2017). MERRA-2 integrates several improvements over the first version MERRA product (Rienecker et al. 2011). For the fields used in this study, the spatial resolution is ~55 km with 3-hourly output frequency from 1980 to present. Vertical interpolation of MERRA-2 data was performed to calculate hub-height wind speed. Variables used in vertical interpolation were extracted from two subsets: 3-hourly instantaneous pressure level assimilation (GES 2017b) and hourly instantaneous single-level assimilation (GES 2017a) (extracted at 3-hourly frequency).

CFSR (Reanalysis Product)

The Climate Forecast System Reanalysis (CFSR) from NCEP (National Centers for Environmental Prediction) is a global, coupled reanalysis that spans from 1979 to present, with ~55km spatial resolution and 6-hourly temporal resolution of relevant wind fields (Saha et al. 2010). Notably, this temporal resolution is the lowest out of the five datasets used. The analysis subset was chosen for vertical interpolation at 6-hourly frequency.

NARR (Reanalysis Product)

The North American Regional Reanalysis (NARR), another NCEP reanalysis product, features a slightly higher spatial resolution of ~32km. It is a dynamically downscaled data product with spatial coverage over North America, with 3-hourly temporal resolution from 1979 through present (Mesinger et al. 2006). Hub-height wind speeds from NARR were also calculated at this frequency.

ISD (In-Situ Observations)

The Integrated Surface Database (ISD) from NOAA's National Centers for Environmental Information (NCEI) was used for assessing hourly 10m wind speed from model and reanalysis. The ISD observational stations are distributed globally, with the highest concentration of stations found in North America. Stations across California that provide full-year data were selected. Because not all stations had continuous temporal coverage between 1980 and 2000, each year was calculated separately to maximize the number of available stations. To compare 10m wind speeds from model and reanalysis datasets to ISD, the nearest grid point values to each of the ISD stations were used. Coastal stations were neglected in the analysis of 10m winds due to coastal biases that tend to occur in near-surface coarse-resolution reanalysis. These biases tend to emerge because similarity theory is typically employed to extract 10m wind speeds, which produces different results over the ocean and land surface.

Upper Air Soundings (In-Situ Observations)

Upper air soundings (vertical wind profiles) from all the available locations across California are incorporated into the comparison (University of Wyoming, Department of Atmospheric Science (http://weather.uwyo.edu/upperair/sounding.html). The three available sounding locations in California are OAK at Oakland airport (station number 72493), VBG at Vandenberg Air Force Base (72393), and NKX at San Diego (72293). The period from the first two stations spans 1980 to 2000. NKX only has data available starting from September 1989, so only the full years 1990-2000 were assessed. Soundings were collected every 12 hours at 00Z and 12Z, and logarithmic vertical interpolation was performed to calculate hub-height wind at each sounding location. However, this logarithmic interpolation from sparsely sampled profile data could introduce uncertainties into the calculation.

Wind Speed Interpolation Method

The wind speed at each wind farm location was determined using nearest grid point values to each wind farm site. To obtain hub-height wind vectors, vertical interpolation was performed on 3-hourly VR-CESM, 3-hourly MERRA-2, 6-hourly CFSR, and 3-hourly NARR products from 1980 to 2000. As mentioned above, hub-height wind output is available directly from the DNV GL Virtual met data product. Vertical interpolation of VR-CESM data uses the 3D wind field on hybrid surfaces and 10m altitude wind speed, which is computed from similarity theory. For VR-CESM data, the interpolation procedure is as follows: (1) the CAM5 hybrid coordinates are first converted to pressure coordinates within the column being analyzed, (2) the height of each pressure surface above ground level (AGL) is computed by subtracting the surface geopotential height from the geopotential height of the model level, (3) two model levels that bound the desired interpolation altitude are selected or, if the interpolation altitude is below the lowest model level, the lowest model level and 10m wind speed field are used, and (4) logarithmic interpolation is applied to obtain the wind speed at the desired interpolation altitude. The interpolation was done by fitting a log equation with the two levels bounding the altitude to be calculated, then with the log profile, interpolating the wind at desired altitude (Justus et al. 1976). Vertically interpolated wind speed from MERRA-2, CFSR, NARR, and sounding observations all followed a similar procedure and were calculated at three hub heights (50m, 80m, and 140m). Figures A1 to A4 show the interpolated hub-height wind speed at 50m and 140m at the Central and Southern California domains.

Wind turbines can contribute to energy via the electric power system. This contribution is the total amount of usable energy supplied by the turbine per year (Fripp et al. 2008). The capacity factor (CF) is often defined as actual power output divided by the maximum amount of wind power that can be generated through the system. This wind speed and CF relationship is not continuous since there is a discontinuous minimum and maximum wind speed required to begin and cease wind power production (the latter to avoid damage to the wind turbine under extreme wind conditions), and this is represented with different power curves associated with each of the wind farm sites. The calculated CF at each wind farm site is based on different characteristic power curves at that site and do not include electrical losses during power generation. The normalized power curves at each wind farm sites, with each value corresponding to a 1m/s wind speed bin increment starting from 0m/s, are listed in Table A-1 and are derived from Draxl et al. (2015). To calculate the CF, wind speed is multiplied with the corresponding power curve value from the corresponding wind speed bin, and then times 100 to convert the percentage values. For details on the CF analysis, please refer to (Saha et al. 2010).

Table A-1: Power Curves for Wind Farms Across California. Each Value Corresponds to a 1m/S Wind Speed Bin Increment Starting from 0m/S

Wind farm	Power curve
San Gorgonio	IECclass1 = (0, 0, 0, 0.0043, 0.0323, 0.0771, 0.1426, 0.2329, 0.3528, 0.5024, 0.6732, 0.8287, 0.9264, 0.9774, 0.9946, 0.999, 0.9999, 1, 1, 1, 1, 1, 1, 1, 1, 1)
Altamont Pass, Ocotillo	IECclass2 = (0, 0, 0, 0.0052, 0.0423, 0.1031, 0.1909, 0.3127, 0.4731, 0.6693, 0.8554, 0.9641, 0.9942, 0.9994, 1, 1, 1, 1, 1, 1, 1, 1, 1, 1, 1, 1)
Alta, Shiloh	IECclass3 = (0, 0, 0, 0.0054, 0.053, 0.1351, 0.2508, 0.4033, 0.5952, 0.7849, 0.9178, 0.9796, 1, 1, 1, 1, 1, 1, 1, 1, 1, 1)

Source: Lawrence Berkeley National Laboratory

Figure A-1: Seasonal Average of Interpolated 50m Wind Speed from Each Datasets for Historical Period 1980-2000 in the Central California Domain

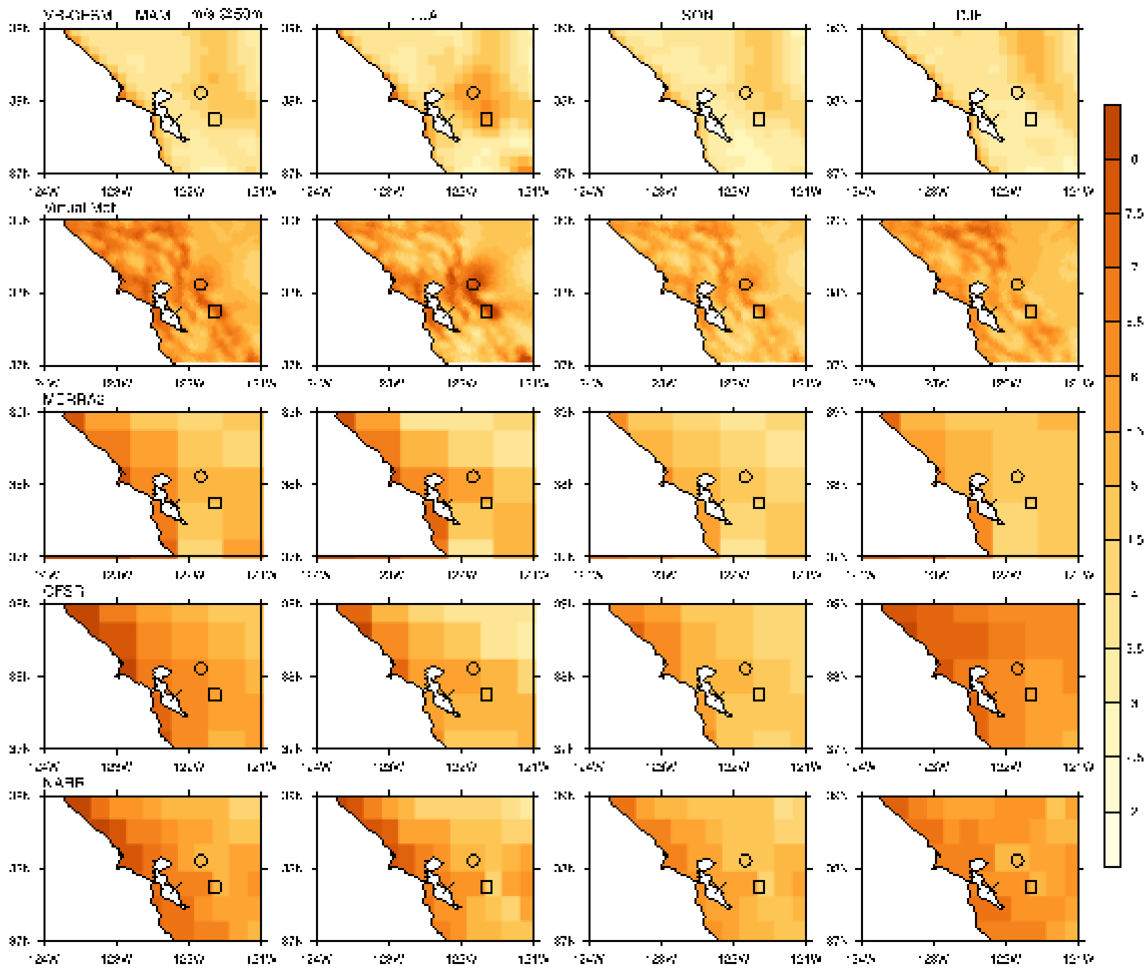

Source: Lawrence Berkeley National Laboratory

Figure A-2: Seasonal Average of Interpolated 50m Wind Speed from Each Datasets for Historical Period 1980-2000 in the Southern California Domain

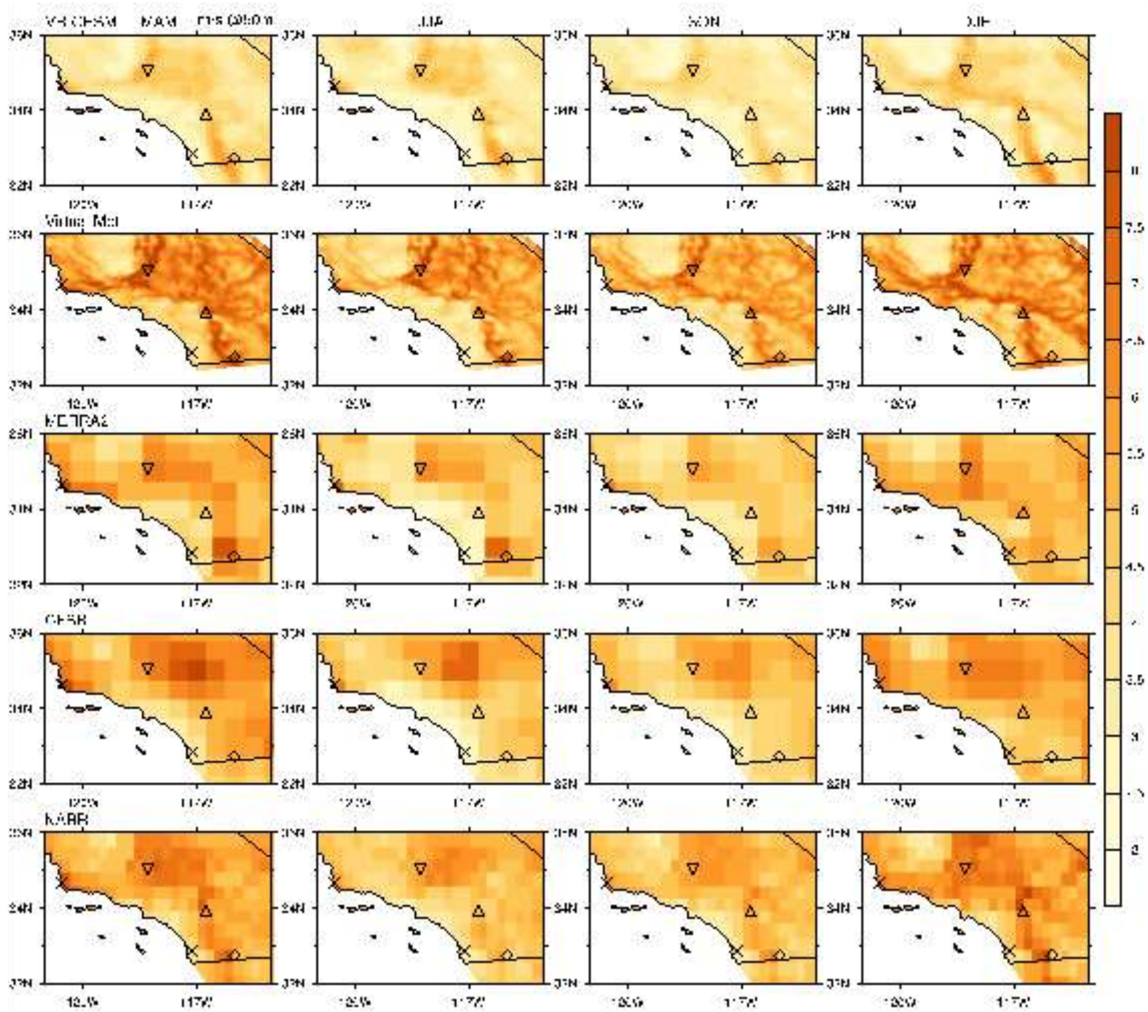

Source: Lawrence Berkeley National Laboratory

Figure A-3: Seasonal Average of Interpolated 140m Wind Speed from Each Datasets for Historical Period 1980-2000 in the Central California Domain

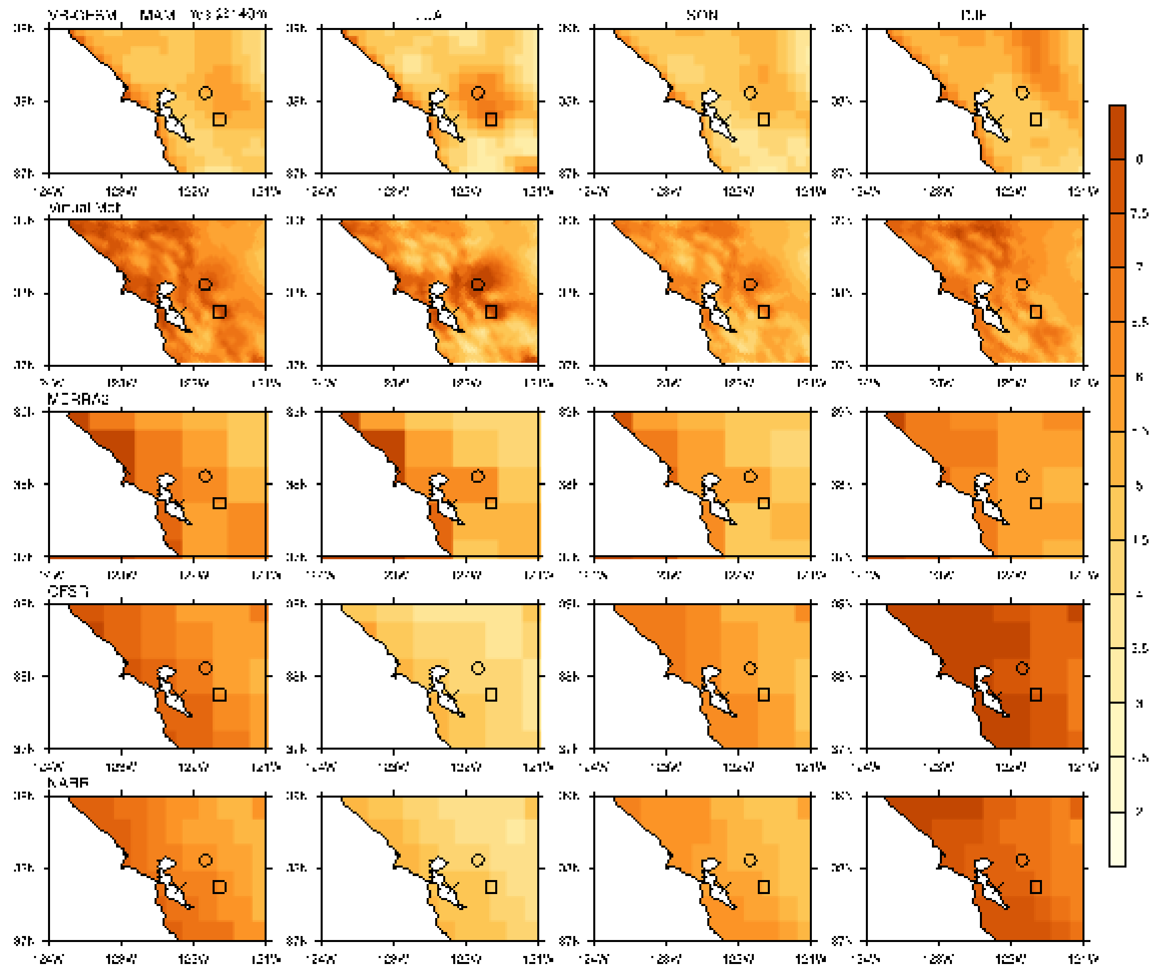

Source: Lawrence Berkeley National Laboratory

Figure A-4: Seasonal Average of Interpolated 140m Wind Speed from Each Datasets for Historical Period 1980-2000 in the Southern California Domain

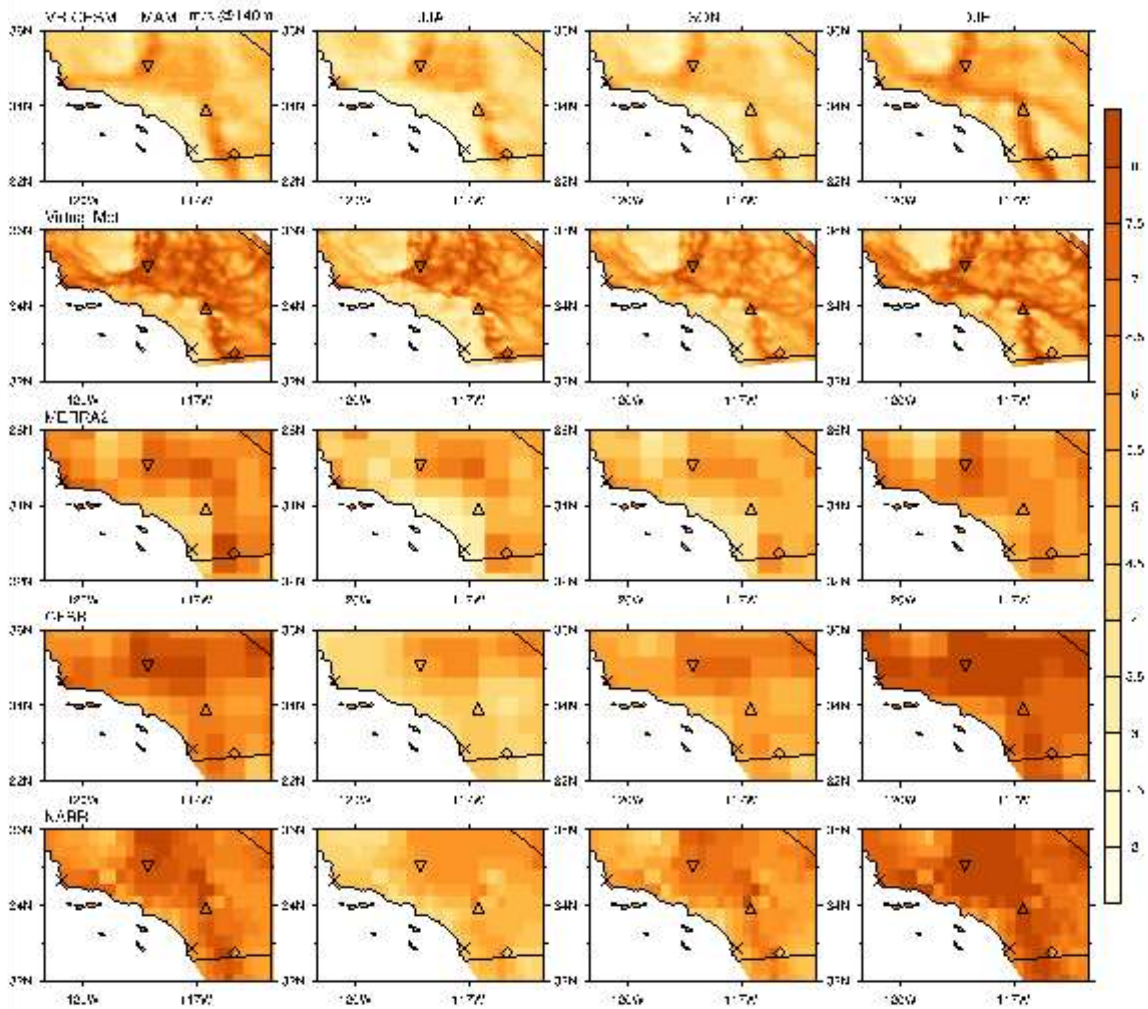

Source: Lawrence Berkeley National Laboratory

APPENDIX B: Additional Data Relating to Historical Wind Resource Variability

Table B-1: Summary Statistics of Annual Capacity Factor by Site

	Average CF	Standard deviation of annual CF	(Standard deviation of annual CF) / (Average CF)	(Top Year CF) / (Bottom Year CF)	(Top 5 years CF) / (Bottom 5 years CF)
Altamont Pass	0.40	0.020	4.9%	1.22	1.18
Shiloh	0.45	0.017	3.9%	1.24	1.13
Alta	0.57	0.024	4.2%	1.19	1.14
San Gorgonio	0.31	0.025	7.8%	1.44	1.29
Ocotillo	0.35	0.026	7.4%	1.47	1.26

Source: Lawrence Berkeley National Laboratory

Table B-2: Coefficient of Determination (R^2) Between Site Annual Capacity Factors.

	Altamont	Shiloh	Alta	San Gorgonio	Ocotillo
Altamont	1				
Shiloh	0.28	1			
Alta	0.24	0.01	1		
San Gorgonio	0.13	0.03	0.55	1	
Ocotillo	0.07	0.00	0.48	0.66	1

Source: Lawrence Berkeley National Laboratory

Table B-3: Capacity Factor and Portion of Total Annual Generation by Cluster

Cluster	Altamont CF	% Altamont Total Generation	Shiloh CF	% Shiloh Total Generation	Alta CF	% Alta Total Generation	San Gorgonio CF	% San Gorgonio Total Generation	Ocotillo CF	% Ocotillo Total Generation
C1 or S1	65.4	33.5	63.3	29.2	64.0	10.1	39.9	11.5	37.4	9.6
C2 or S2	32.4	10.3	35.3	10.1	58.1	12.0	16.7	6.3	20.6	6.9
C3 or S3	22.4	5.8	24.6	5.7	66.1	18.1	41.7	20.7	44.3	19.6
C4 or S4	21.2	5.0	43.3	9.1	36.2	9.8	15.1	7.5	19.5	8.6
C5 or S5	49.9	7.9	45.5	6.5	35.9	5.5	7.2	2.0	7.2	1.8
C6 or S6	37.4	7.5	36.0	6.5	16.5	2.7	0.9	0.3	1.7	0.5
C7 or S7	46.2	16.3	64.4	20.4	93.0	9.8	69.9	13.5	83.0	14.2
C8 or S8	45.8	5.3	40.7	4.2	83.8	11.4	71.4	17.6	81.0	17.8
C9 or S9	8.5	2.1	16.6	3.7	74.3	16.9	43.5	18.0	47.3	17.4
C10 or S10	63.6	6.1	52.6	4.5	49.9	3.3	26.8	3.3	36.7	4.0

*** (Note: These values correspond to Figure 5 in the main text).**

Source: Lawrence Berkeley National Laboratory

Table B-4: At Shiloh: Differences in Frequency, Capacity Factor, and Generation by Cluster

	Average # of days in top 5 years	Average # of days in bottom 5 years	Average CF in top 5 years	Average CF in bottom 5 years	% of total generation in top 5 years	% of total generation in bottom 5 years	(generation in top 5 years)/ (generation in bottom 5 years)
C1	80.0	69.0	64.4	60.6	30.0%	27.4%	1.23
C2	42.8	50.8	37.0	34.6	9.2%	11.5%	0.90
C3	34.2	41.4	31.2	26.5	6.2%	7.2%	0.97
C4	35.4	29.2	45.9	39.5	9.5%	7.6%	1.41
C5	20.0	23.8	50.5	40.9	5.9%	6.4%	1.04
C6	34.2	30.2	38.4	32.7	7.6%	6.5%	1.33
C7	49.0	53.0	65.0	61.2	18.5%	21.2%	0.98
C8	15.8	18.2	44.2	38.4	4.1%	4.6%	1.00
C9	39.6	36.8	17.9	16.6	4.1%	4.0%	1.16
C10	14.6	12.6	57.8	46.4	4.9%	3.8%	1.44

Source: Lawrence Berkeley National Laboratory

Table B-5: At Altamont Pass: Differences in Frequency, Capacity Factor, and Generation by Cluster

	Average # of days in top 5 years	Average # of days in bottom 5 years	Average CF in top 5 years	Average CF in bottom 5 years	% of total generation in top 5 years	% of total generation in bottom 5 years	(generation in top 5 years)/ (generation in bottom 5 years)
C1	89.8	70.6	66.6	61.5	37.9%	32.4%	1.38
C2	39.6	51.0	35.7	29.6	9.0%	11.3%	0.93
C3	38.4	38.8	24.0	24.0	5.9%	6.9%	0.99
C4	29.8	38.6	21.6	18.3	4.1%	5.3%	0.91
C5	28.2	22.0	50.5	46.1	9.0%	7.6%	1.41
C6	30.6	22.6	37.0	39.2	7.2%	6.6%	1.28
C7	38.2	55.4	44.1	41.6	10.7%	17.2%	0.73
C8	21.6	15.4	49.6	45.9	6.8%	5.3%	1.52
C9	31.8	38.0	12.8	5.8	2.6%	1.7%	1.83
C10	17.2	13.0	63.4	59.1	6.9%	5.7%	1.42

Source: Lawrence Berkeley National Laboratory

Table B-6: At Alta: Differences in Frequency, Capacity Factor, and Generation by Cluster

	Average # of days in top 5 years	Average # of days in bottom 5 years	Average CF in top 5 years	Average CF in bottom 5 years	% of total generation in top 5 years	% of total generation in bottom 5 years	(generation in top 5 years)/ (generation in bottom 5 years)
C1	42.0	27.0	69.1	57.3	13.1%	8.0%	1.88
C2	50.6	42.2	58.7	59.0	13.4%	12.8%	1.19
C3	58.4	59.0	67.3	65.0	17.8%	19.8%	1.03
C4	48.2	69.0	35.1	35.7	7.6%	12.7%	0.69
C5	26.4	37.2	35.2	36.3	4.2%	7.0%	0.69
C6	22.0	33.2	14.5	17.4	1.4%	3.0%	0.55
C7	27.0	15.6	94.1	92.4	11.5%	7.4%	1.76
C8	29.6	25.6	83.9	82.5	11.2%	10.9%	1.18
C9	50.2	40.0	75.9	69.4	17.2%	14.3%	1.38
C10	10.8	16.2	51.7	49.0	2.5%	4.1%	0.70

Source: Lawrence Berkeley National Laboratory

Table B-7: At San Gorgonio: Differences in Frequency, Capacity Factor, and Generation by Cluster

	Average # of days in top 5 years	Average # of days in bottom 5 years	Average CF in top 5 years	Average CF in bottom 5 years	% of total generation in top 5 years	% of total generation in bottom 5 years	(generation in top 5 years)/ (generation in bottom 5 years)
C1	42	29	47.2	34.0	15%	10%	2.02
C2	44	44	15.5	16.1	5%	7%	0.98
C3	56	49	43.8	36.2	19%	18%	1.38
C4	52	68	16.4	13.7	6%	9%	0.90
C5	28	34	6.7	7.2	1%	2%	0.76
C6	26	30	0.9	1.2	0%	0%	0.69
C7	31	21	73.0	66.6	17%	14%	1.64
C8	31	24	72.1	69.5	17%	16%	1.38
C9	42	51	48.2	38.3	15%	19%	1.02
C10	12	15	30.3	27.3	3%	4%	0.87

Source: Lawrence Berkeley National Laboratory

Table B-8: At Ocotillo: Differences in Frequency, Capacity Factor, and Generation by Cluster

	Average # of days in top 5 years	Average # of days in bottom 5 years	Average CF in top 5 years	Average CF in bottom 5 years	% of total generation in top 5 years	% of total generation in bottom 5 years	(generation in top 5 years)/ (generation in bottom 5 years)
C1	40	31	44.8	31.3	13%	8%	1.87
C2	42	48	19.1	21.5	6%	9%	0.77
C3	60	54	46.0	38.8	19%	19%	1.30
C4	54	67	21.0	18.0	8%	11%	0.93
C5	27	36	6.4	6.9	1%	2%	0.69
C6	30	29	1.5	2.2	0%	1%	0.71
C7	29	18	83.1	81.9	17%	13%	1.63
C8	30	20	82.4	78.7	17%	14%	1.58
C9	42	50	54.0	43.7	16%	19%	1.04
C10	12	13	39.5	33.7	3%	4%	1.14

Source: Lawrence Berkeley National Laboratory

Table B-9: The Top and Bottom Years, by Capacity Factor, at Each Site

Shiloh		Altamont Pass		Alta		Gorgonio		Ocotillo	
Top 5 Years	Bottom 5 Years	Top 5 Years	Bottom 5 Years	Top 5 Years	Bottom 5 Years	Top 5 Years	Bottom 5 Years	Top 5 Years	Bottom 5 Years
2007	2003	1983	1989	1998	1987	1998	1994	1998	1981
2012	1998	2007	1988	1996	1992	1983	2001	2010	1988
2008	2014	1981	2014	1983	2013	2010	1987	1983	1992
1996	1989	2012	1993	1981	2015	1982	1984	2011	1987
1990	1993	1982	1992	1982	1988	2011	1988	2002	1984

Source: Lawrence Berkeley National Laboratory

Table B-10: Capacity Factor by Year and Site

Year	Shiloh	Altamont Pass	Alta	San Gorgonio	Ocotillo
1980	0.45	0.41	0.58	0.33	0.36
1981	0.43	0.43	0.60	0.31	0.32
1982	0.45	0.42	0.60	0.34	0.35
1983	0.43	0.44	0.60	0.37	0.38
1984	0.44	0.41	0.55	0.27	0.29
1985	0.44	0.39	0.58	0.32	0.36
1986	0.43	0.38	0.54	0.29	0.33
1987	0.46	0.39	0.54	0.27	0.31
1988	0.45	0.37	0.53	0.27	0.32
1989	0.42	0.38	0.59	0.31	0.38
1990	0.46	0.41	0.57	0.32	0.35
1991	0.46	0.39	0.55	0.30	0.33
1992	0.43	0.36	0.53	0.29	0.31
1993	0.39	0.36	0.57	0.32	0.35
1994	0.43	0.40	0.57	0.29	0.34
1995	0.45	0.40	0.55	0.32	0.34
1996	0.47	0.41	0.62	0.33	0.38
1997	0.45	0.41	0.57	0.32	0.37
1998	0.43	0.41	0.63	0.38	0.43
1999	0.44	0.40	0.56	0.32	0.37
2000	0.44	0.40	0.58	0.31	0.37
2001	0.46	0.40	0.56	0.29	0.36
2002	0.46	0.40	0.56	0.31	0.38
2003	0.43	0.41	0.56	0.30	0.34
2004	0.46	0.42	0.56	0.31	0.34
2005	0.45	0.39	0.55	0.31	0.35
2006	0.44	0.39	0.56	0.31	0.34

Year	Shiloh	Altamont Pass	Alta	San Gorgonio	Ocotillo
2007	0.48	0.44	0.57	0.31	0.35
2008	0.47	0.42	0.57	0.31	0.35
2009	0.45	0.41	0.56	0.32	0.37
2010	0.44	0.40	0.58	0.36	0.39
2011	0.44	0.39	0.58	0.34	0.38
2012	0.48	0.43	0.57	0.30	0.35
2013	0.45	0.39	0.53	0.31	0.34
2014	0.42	0.36	0.55	0.31	0.34
2015	0.45	0.40	0.53	0.31	0.34

Source: Lawrence Berkeley National Laboratory

APPENDIX C: Characterization of the Central and Southern California Clusters

Table C-1: Basic Characteristics of the Central Californian Clusters

	% of days per year	% of days in Winter	% of days in Spring	% of days in Summer	% of days in Fall	Avg Temp (C)	Monthly Temp Anomaly (C)	Precipitation (mm/day)
C1	20.53	0.86	19.66	44.32	16.85	16.85	-0.56	0.06
C7	14.14	0.09	5.50	40.70	9.95	19.14	0.80	0.04
C2	12.76	11.98	16.15	7.25	15.66	15.97	0.88	0.07
C3	10.32	16.54	12.68	1.09	11.11	13.54	-0.14	0.38
C9	10.01	16.23	6.13	0.72	17.16	14.69	0.58	0.06
C4	9.36	16.94	9.45	1.06	10.16	13.25	-0.48	0.04
C6	8.08	9.55	12.26	2.02	8.52	13.19	-0.95	0.11
C5	6.37	13.52	7.67	0.06	4.37	13.27	0.13	1.64
C8	4.60	12.13	3.11	0.06	3.24	13.25	0.37	2.09
C10	3.83	2.16	7.40	2.72	2.99	13.52	-1.57	0.26

Source: Lawrence Berkeley National Laboratory

Table C-2: Basic Characteristics of the Southern California Clusters

	% of days per year	% of days in Winter	% of days in Spring	% of days in Summer	% of days in Fall	Avg Temp (C)	Monthly Temp Anomaly (C)	Precipitation (mm/day)
S3	15.53	6.90	11.50	30.74	12.79	24.56	0.58	0.12
S4	15.46	2.68	10.24	25.94	22.83	25.71	1.21	0.23
S9	12.90	1.02	15.46	27.60	7.23	25.56	1.16	0.07
S2	11.72	17.49	15.43	1.39	12.70	18.52	0.06	0.11
S6	9.21	20.39	4.95	0.12	11.63	17.87	0.19	0.06
S1	8.97	20.36	8.61	0.21	6.90	17.69	0.19	0.50
S5	8.71	17.71	5.95	0.39	10.99	17.53	-0.57	0.09
S8	7.70	1.05	11.41	11.84	6.35	21.18	-2.13	0.14
S7	6.01	7.73	11.59	0.60	4.12	14.99	-3.58	0.38
S10	3.79	4.68	4.86	1.18	4.46	18.63	-1.03	0.17

Source: Lawrence Berkeley National Laboratory

Figure C-1: Average Wind Vectors for the Central California Clusters

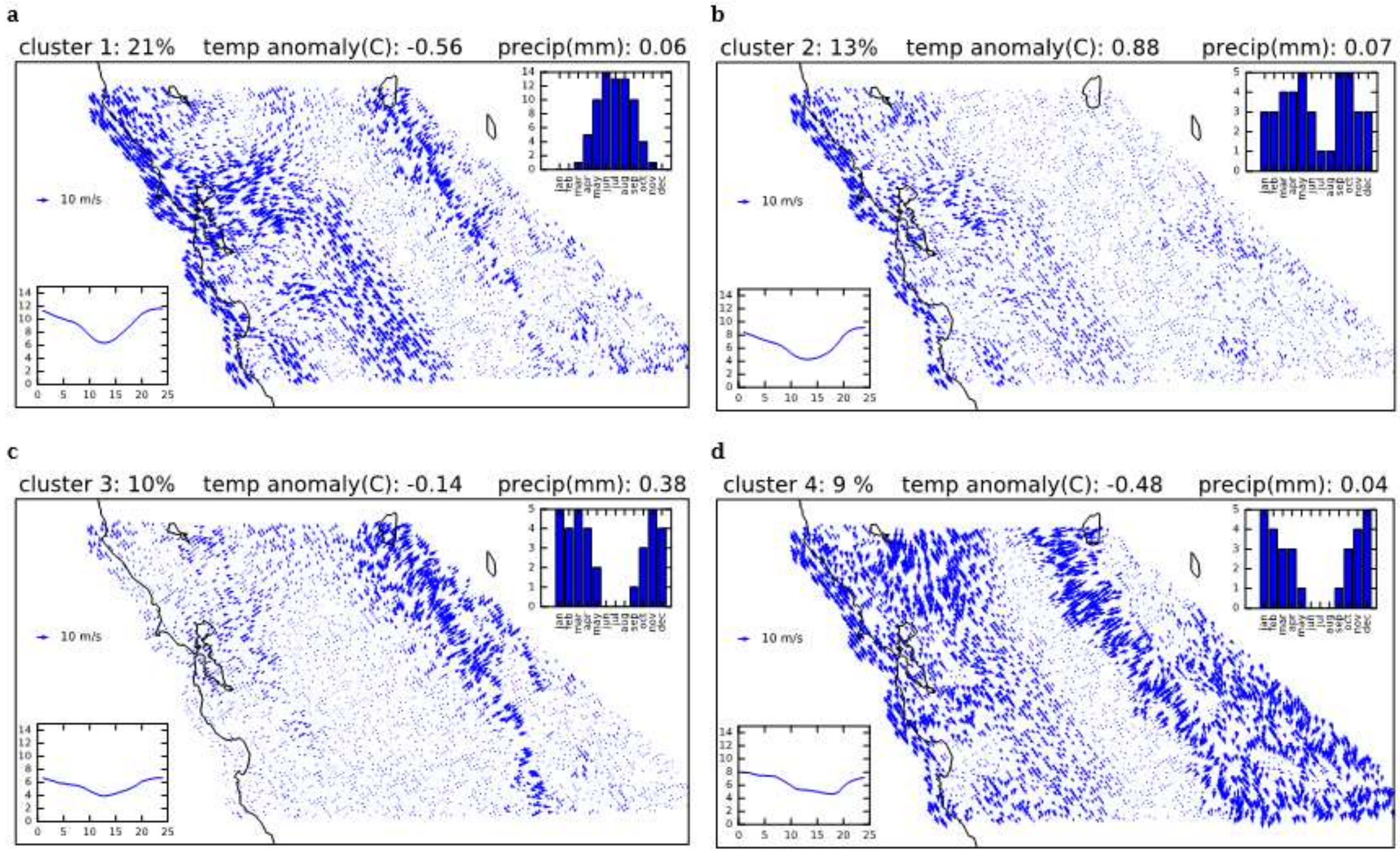

e

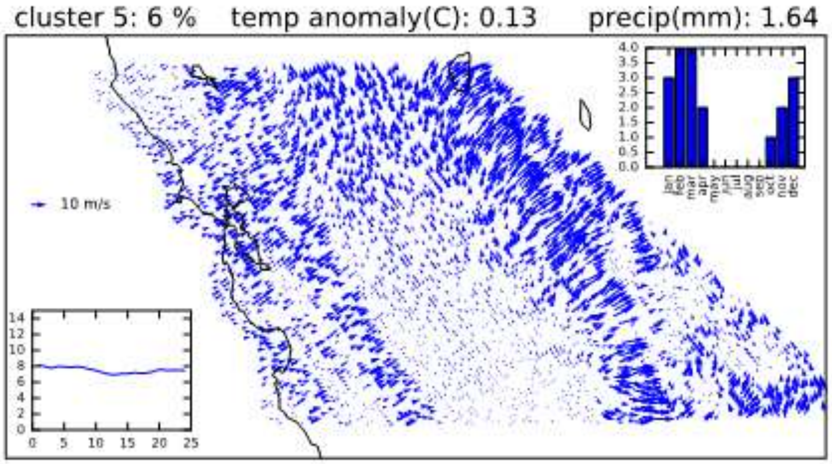
cluster 5: 6 %
temp anomaly(C): 0.13
precip(mm): 1.64
10 m/s

f

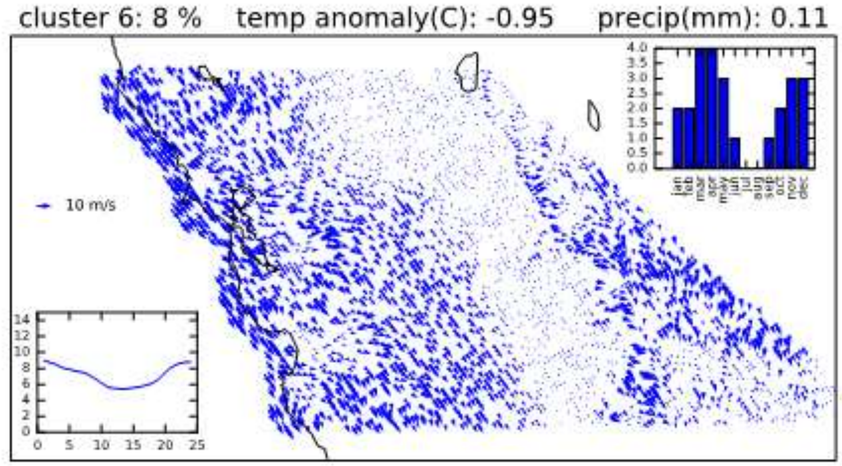
cluster 6: 8 %
temp anomaly(C): -0.95
precip(mm): 0.11
10 m/s

g

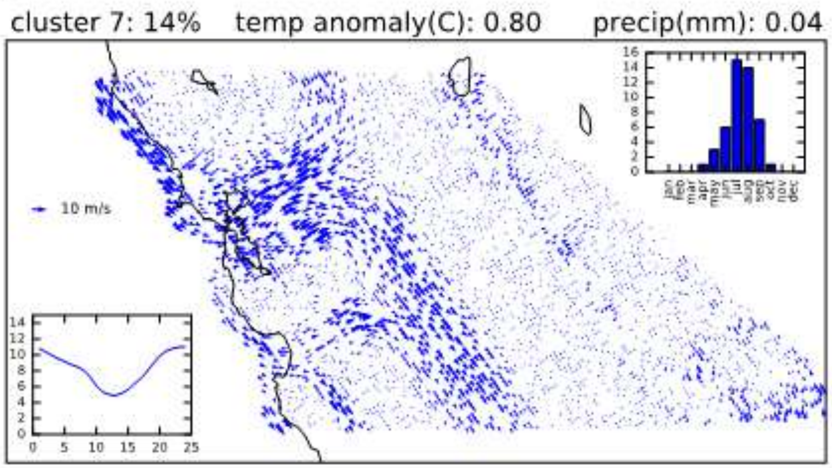
cluster 7: 14%
temp anomaly(C): 0.80
precip(mm): 0.04
10 m/s

h

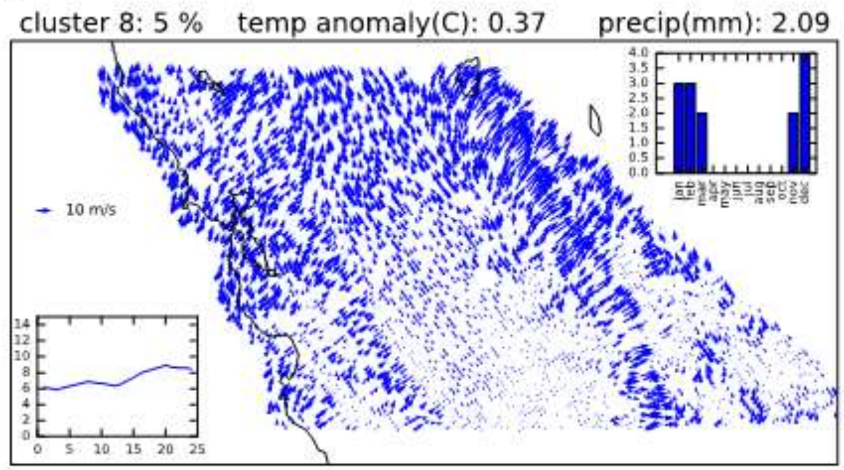
cluster 8: 5 %
temp anomaly(C): 0.37
precip(mm): 2.09
10 m/s

i

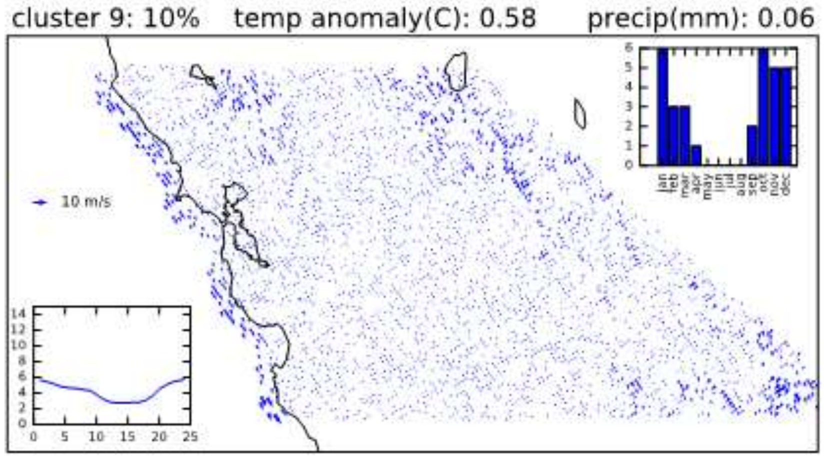

j

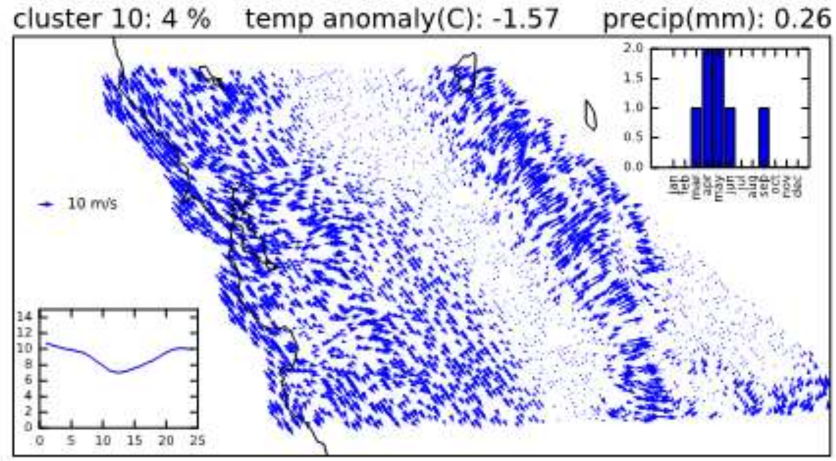

** The upper right corner inlay the average number of days per month the cluster is found. The lower left corner inlay shows the average diurnal pattern of wind speed (m s^{-1}) at the grid cells centered on the Altamont Pass and Shiloh wind farms. The information across the top of each panel includes the cluster number, the percentage of the year each cluster is found, the average temperature anomaly at the Altamont Pass and Shiloh wind farms (with the anomaly taken separately for each month and then averaged over the full-time span), and finally, the average daily precipitation.* Source: Lawrence Berkeley National Laboratory

Figure C-2: Average Wind Vectors for the Southern California Clusters

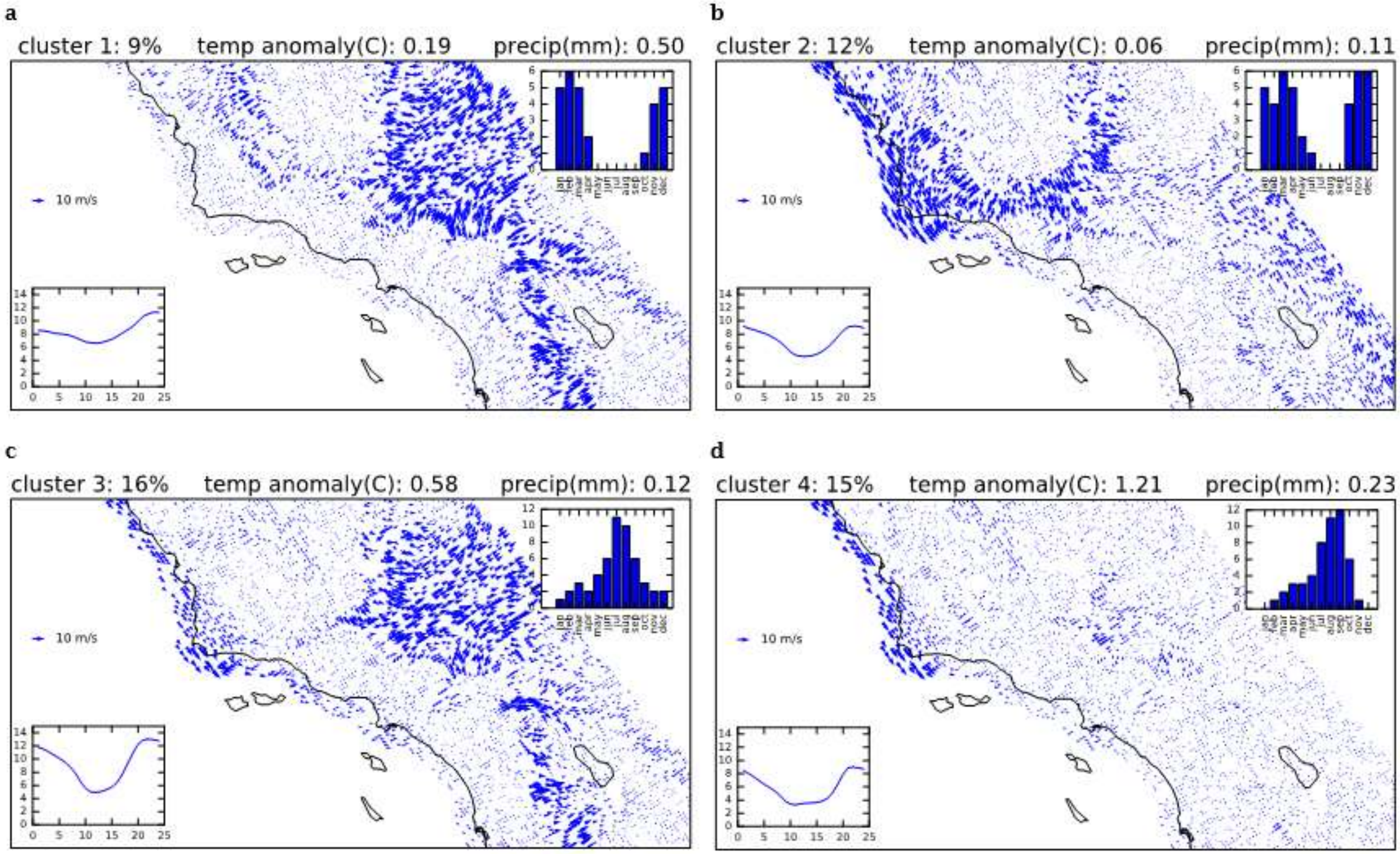

APPENDIX D: Autocorrelation

Figure D-1: Partial Autocorrelation Plots for (a) C7 and (b) C9